Direct and indirect signals of natural composite Higgs models

Christoph Niehoff, Peter Stangl and David M. Straub

Excellence Cluster Universe, TUM,
Boltzmannstr. 2, 85748 Garching, Germany

E-mail: christoph.niehoff@tum.de, peter.stangl@tum.de,
david.straub@tum.de

ABSTRACT: We present a comprehensive numerical analysis of a four-dimensional model with the Higgs as a composite pseudo-Nambu-Goldstone boson that features a calculable Higgs potential and protective custodial and flavour symmetries to reduce electroweak fine-tuning. We employ a novel numerical technique that allows us for the first time to study constraints from radiative electroweak symmetry breaking, Higgs physics, electroweak precision tests, flavour physics, and direct LHC bounds on fermion and vector boson resonances in a single framework. We consider four different flavour symmetries in the composite sector, one of which we show to not be viable anymore in view of strong precision constraints. In the other cases, all constraints can be passed with a sub-percent electroweak fine-tuning. The models can explain the excesses recently observed in WW, WZ, Wh and $\ell^+\ell^-$ resonance searches by ATLAS and CMS and the anomalies in angular observables and branching ratios of rare semi-leptonic B decays observed by LHCb. Solving the B physics anomalies predicts the presence of a dijet or $t\bar{t}$ resonance around $1\,\mathrm{TeV}$ just below the sensitivity of LHC run 1. We discuss the prospects to probe the models at run 2 of the LHC. As a side product, we identify several gaps in the searches for vector-like quarks at hadron colliders, that could be closed by reanalyzing existing LHC data.

Contents

1 Introduction

The Standard Model Higgs boson faces a severe naturalness problem since the presence of heavy states associated to a more fundamental theory would lead to enormous corrections to its mass, requiring an extreme fine-tuning to explain the observed value. This conundrum can be solved if the Higgs boson is not an elementary scalar but a bound state of some new strong interaction. The lightness of the composite Higgs with respect to the — as yet unobserved — composite resonances finds a natural explanation if the Higgs is a pseudo-Nambu-Goldstone boson (pNGB) of an approximate global symmetry of the strong sector [1, 2]. To avoid the flavour problems of technicolour theories, the mechanism of partial compositeness can be invoked to generate the masses of the SM particles [3]. This mechanism is closely related to the "geometric" generation of fermion mass hierarchies from wave function overlaps in models with warped extra dimensions [4–7], and in fact much of the progress in composite Higgs models in the last decades has been made using holographic models [8–10]. In these models, the Higgs potential becomes calculable, leading to additional predictivity. Recently, also four-dimensional models have been constructed where the Higgs potential is calculable at one-loop level [11–13].[1] These models have the advantage that they are simpler in structure than the 5D theories, but more general, as

---

[1]See [14] for an overview of the model landscape and [15] for a comprehensive review of 4D pNGB Higgs models.

they need not necessarily be the low-energy limit of a 5D holographic theory. Our aim in this paper is to study one particular implementation of the 4D pNGB Higgs, taking into account all relevant experimental constraints.

Direct and indirect constraints on composite pNGB Higgs models have already been discussed in the literature (for recent analyses see e.g. [16, 17] for electroweak precision tests, [18–20] for flavour physics, [21–25] for Higgs physics, [23, 26–34] for quark partner searches, and [27, 35–39] for vector resonance searches). However, a complete and simultaneous numerical analysis of all relevant constraints on a particular model is still lacking. This is due in part to the fact that a mere parameter scan, as is typically done in supersymmetric extensions of the SM, is not feasible since the parameter space does not "factorize" into Standard Model (SM) and new physics (NP) parameters; due to partial compositeness, the masses of SM particles and the angles and phase of the Cabibbo-Kobayashi-Maskawa (CKM) matrix are non-trivial functions of many model parameters. As a consequence, finding viable parameter points from a random set of model parameters becomes untractable. This problem becomes even more severe once the Higgs potential is taken into account, as the Higgs mass and VEV often arise from an interplay between gauge and fermion loops which again depends on many parameters. For these reasons, numerical analyses of composite Higgs models often have to rely on simplifying assumptions, e.g. only considering third generation fermions and their partners — which does not allow including flavour constraints, for instance. Full numerical studies of indirect constraints have been performed in warped extra dimensional models (without a pNGB Higgs) by making use of approximate analytical expressions for the SM parameters [40–45], but this only works for particular representations of the additional fermions.[2] We have overcome these problems by generalising a numerical method first proposed in [46] and with the help of a high-performance computing cluster. This allows us for the first time to scrutinize one specific model taking into account all relevant experimental constraints and to identify novel correlations.

In selecting a model to analyze in detail, our focus has been to maximize naturalness and predictivity, but to be as economic as possible concerning both particle content and number of parameters. The model should thus fulfill the following requirements.

- The symmetry breaking coset should contain custodial symmetry to avoid excessive contributions to the T parameter, but no extra Higgs states. This singles out SO(5)/SO(4).

- The $Zb_L\bar{b}_L$ coupling should be custodially protected from tree-level corrections. This leaves two possible choices of quark partner representations under the SO(4) symmetry [47]. We choose the one where all quark partners can be embedded in two fundamental representations, as in the MCHM5 [48].

- The Higgs potential should be calculable. This can be achieved by imposing the Weinberg sum rules [13, 49]. These are automatically fulfilled in deconstructed models

---

[2]Namely if the left-handed elementary quark doublet mixes with a single composite $SU(2)_L$ doublet, unlike in the model to be studied below.

like the 4DCHM [11] or the DCHM [12]. We choose the 4DCHM, because it features a finite one-loop effective potential already for two sites.[3]

- The contribution to $\Delta F = 2$ observables, i.e. meson-antimeson mixing, should be suppressed compared to the naive anarchic expectation to avoid the ϵ_K problem [21, 41, 44]. Several mechanisms have been proposed to address this problem (apart from invoking accidental cancellations). We focus on the assumption that the composite sector is exactly invariant under a large flavour symmetry which is only broken minimally (i.e. by the amount required to reproduce CKM mixing) by the composite-elementary mixings.[4] This arguably corresponds to one of the strongest assumptions one can make on the flavour structure of partial compositeness, which is why we view it as a natural starting point in the search for a model that passes precision tests, but is natural in the electroweak sense.

In summary, we focus on the two-site 4DCHM with quark partners in two fundamentals of SO(5), which we will call M4DCHM5 in the remainder of the paper. For the flavour structure of this model, we will consider the four different possibilities studied qualitatively already in [18]: an effective U(3)³ [59–61] or U(2)³ [18, 61] flavour symmetry with flavour-invariant composite-elementary mixings either for left- or right-handed quarks in both cases, dubbed left- or right-compositeness, respectively.

We stress that, while we aim to include as many experimental constraints as possible, our analysis is on a conceptually different level compared to analyses of weakly-coupled renormalizable extensions of the SM, e.g. the MSSM. This is because the models we are studying are non-renormalizable with a cutoff in the few-TeV region and contain a sector with strong couplings. Consequently, the models are not only less ambitious, but also less predictive since contributions from cutoff-scale operators or strong interaction effects could potentially spoil the picture obtained from naive computations in the two-site picture. Nevertheless, for the observables we are considering, the calculable effects often already lead to stringent experimental constraints and we find it unlikely that cutoff-scale physics comes to the rescue by cancelling these effects. It should however be kept in mind that many of the predictions are afflicted with considerable theoretical uncertainties.

2 Model setup

In this section, we briefly review the M4DCHM and its Lagrangian. For details, the reader is referred to the original publication [11]. The relation to similar models is discussed in [13].

2.1 Bosonic part

The M4DCHM can be understood as a deconstructed description of an extra-dimensional Gauge-Higgs-Unification model with a bulk gauge group SO(5) that is broken down by

---

[3]In the two-site DCHM, a logarithmic divergence spoils the predictivity for the Higgs VEV, but the Higgs mass can still be computed [50].

[4]For alternative mechanisms, see [51–58] .

boundary conditions on the branes to SO(4) and the SM gauge group. To make the model phenomenologically viable, the symmetries are enlarged to include a bulk colour sector and an additional $U(1)_X$ to match the hypercharge assignments of the SM. So, from a 4D point of view, there is a strongly interacting composite sector subject to a global symmetry breaking pattern[5] $(SU(3)_c \times SO(5) \times U(1)_X)/(SU(3)_c \times SO(4) \times U(1)_X)$ and an elementary SM-like sector with gauge group $SU(3)^0 \times SU(2)^0 \times U(1)^0$.

In the two-site model one considers only one level of heavy resonances, thus the spectrum contains resonances ρ_μ^A for the SO(5) as well as heavy gluons and a heavy $\rho_{X\mu}$. These resonances mix with their elementary counterparts such that the diagonal group becomes the remaining SM gauge group and hypercharge is given as[6]

$$Y = \mathsf{T}^{3_R} + X. \tag{2.1}$$

The bosonic sector of the theory contains the gauge part as well as the sigma model describing the global symmetry breaking,

$$\mathcal{L}_{\text{bosonic}} = \mathcal{L}_{\text{gauge}} + \mathcal{L}_\sigma. \tag{2.2}$$

The gauge Lagrangian,

$$
\begin{aligned}
\mathcal{L}_{\text{gauge}} = {} & -\frac{1}{4}\text{tr}\left[G^0{}_{\mu\nu}G^{0\mu\nu}\right] - \frac{1}{4}\text{tr}\left[W^0{}_{\mu\nu}W^{0\mu\nu}\right] - \frac{1}{4}B^0{}_{\mu\nu}B^{0\mu\nu} && \text{(elementary)} \\
& -\frac{1}{4}\text{tr}\left[\rho_{G\mu\nu}\rho_G{}^{\mu\nu}\right] - \frac{1}{4}\text{tr}\left[\rho_{\mu\nu}\rho^{\mu\nu}\right] - \frac{1}{4}\rho_{X\mu\nu}\rho_X{}^{\mu\nu} && \text{(composite)} \\
& + \frac{f_G^2}{4}\left(g_{03}G^0{}_\mu - g_G\,\rho_{G\mu}\right)^2 + \frac{f_X^2}{4}\left(g_{0'}B^0{}_\mu - g_X\rho_{X\mu}\right)^2, && \text{(mixing)} \quad (2.3)
\end{aligned}
$$

contains the usual kinetic terms for the elementary $SU(3)^0 \times SU(2)^0 \times U(1)^0$ gauge fields, where

$$W^0{}_\mu = W^{0a_L}{}_\mu\,\mathsf{T}^{a_L}, \tag{2.4}$$

as well as kinetic terms for the gluon-, SO(5)- and $U(1)_X$-resonances. For the ρ_μ resonances it will be useful to group them into $SU(2)_L$, $SU(2)_R$ and coset components (following [13], the latter we will call "axial resonances" in the following),

$$\rho_\mu = \rho_\mu^A\,\mathsf{T}^A = \rho_{L\mu}^{a_L}\,\mathsf{T}^{a_L} + \rho_{R\mu}^{a_R}\,\mathsf{T}^{a_R} + \mathfrak{a}_\mu^{\hat{a}}\,\mathsf{T}^{\hat{a}}. \tag{2.5}$$

We also introduce explicit mixing terms between the SU(3)- and U(1)-resonances with their elementary counterparts, which are characterized by the scales f_G and f_X.

The sigma model Lagrangian

$$\mathcal{L}_\sigma = \frac{f_1^2}{4}\text{tr}\left[(\mathcal{D}_\mu\Omega_1)^\dagger(\mathcal{D}^\mu\Omega_1)\right] + \frac{f_2^2}{2}\left[(\mathcal{D}_\mu\Omega_2)^{\text{t}}(\mathcal{D}^\mu\Omega_2)\right]_{55} \tag{2.6}$$

---

[5]The M4DCHM also contains an additional symmetry breaking $(SO(5)_L \times SO(5)_R)/SO(5)_{L+R}$ to account for the presence of heavy resonances.

[6]See appendix A for our convention for the SO(5) generators.

contains covariant derivatives acting on the sigma model fields Ω_1 and Ω_2, which are given as

$$\mathcal{D}_\mu \Omega_1 = \partial_\mu \Omega_1 - i \left(g_0 \, W^0{}_\mu + g_0{}' B^0{}_\mu \, \mathsf{T}^{3_R} \right) \Omega_1 + i \, g_\rho \, \Omega_1 \, \rho_\mu, \tag{2.7}$$

$$\mathcal{D}_\mu \Omega_2 = \partial_\mu \Omega_2 - i \, g_\rho \, \rho_\mu \, \Omega_2. \tag{2.8}$$

Note that the sigma model fields are uncharged under the global $\mathrm{U}(1)_X$ symmetry (and, of course, they do not carry colour charges).

We adopt the so-called holographic gauge for the sigma model fields, which is inspired by a convenient gauge chosen in the corresponding 5D gauge theory,

$$\Omega_1(x) = \mathcal{U} = \exp\left[i \frac{\sqrt{2}}{f_1} \sigma_{\hat{a}}(x) \, \mathsf{T}^{\hat{a}} \right], \qquad \Omega_2(x) = \mathbb{1}_5. \tag{2.9}$$

There is also the SM gauge freedom that has to be fixed. Here we adopt the SM unitary gauge, such that $\sigma_{\hat{a}}(x) = (0, 0, 0, h(x))$. In this gauge the Goldstone matrix takes the form

$$\mathcal{U} := \exp\left[i \frac{\sqrt{2}}{f_1} \sigma_{\hat{a}}(x) \, \mathsf{T}^{\hat{a}} \right] = \begin{pmatrix} 1 & & & & \\ & 1 & & & \\ & & 1 & & \\ & & & \cos\left(\frac{h(x)}{f_1}\right) & \sin\left(\frac{h(x)}{f_1}\right) \\ & & & -\sin\left(\frac{h(x)}{f_1}\right) & \cos\left(\frac{h(x)}{f_1}\right) \end{pmatrix}. \tag{2.10}$$

Writing the Lagrangian as above in holographic gauge leads to a mixing term of the form

$$\frac{1}{\sqrt{2}} \, g_\rho \, f_1 \, \mathfrak{a}_4^\mu \, \partial_\mu h. \tag{2.11}$$

One can get rid of this term by a field redefinition,

$$\mathfrak{a}_4^\mu \to \mathfrak{a}_4^\mu - \frac{\sqrt{2}}{g_\rho} \frac{f}{f_2^2} \partial^\mu h \,, \qquad\qquad h \to \frac{f_1}{f} h \,, \tag{2.12}$$

where f is given by $f^{-2} := f_1^{-2} + f_2^{-2}$. By this transformation the mixing term vanishes and the composite Higgs kinetic term is canonically normalized. As a result, all dependencies on the Higgs field are given via

$$s_h = \sin\left(\frac{h}{f}\right). \tag{2.13}$$

2.2 Fermionic part

For the fermionic part of the model, we distinguish between the quark and the lepton part,

$$\mathcal{L}_{\text{fermionic}} = \mathcal{L}_{\text{quark}} + \mathcal{L}_{\text{lepton}}. \tag{2.14}$$

As in the boson sector, the quark Lagrangian contains elementary, composite and mixing parts,

$$
\begin{aligned}
\mathcal{L}_{\text{quark}} = {} & i\bar{q}^0{}_L \slashed{D} q^0{}_L + i\overline{u^0}_R \slashed{D} u^0{}_R + i\overline{d^0}_R \slashed{D} d^0{}_R && \text{(elementary)} \\
& + i\overline{\Psi}_{\text{comp}} \slashed{D} \Psi_{\text{comp}} + i\overline{\widetilde{\Psi}}_{\text{comp}} \slashed{D} \widetilde{\Psi}_{\text{comp}} && \text{(composite)} \\
& - m_U \left(\overline{Q}_u Q_u + \overline{S}_u S_u \right) - m_{\widetilde{U}} \left(\overline{\widetilde{Q}}_u \widetilde{Q}_u + \overline{\widetilde{S}}_u \widetilde{S}_u \right) \\
& - \left(m_{Y_U} + Y_U \right) \overline{S}_{uL} \widetilde{S}_{uR} - m_{Y_U} \overline{Q}_{uL} \widetilde{Q}_{uR} \; + \; \text{h.c.} \\
& + \Delta_{u_L} \bar{\xi}_{uL} \mathcal{U} \left(Q_{uR} + S_{uR} \right) + \Delta_{u_R} \bar{\xi}_{uR} \mathcal{U} \left(\widetilde{Q}_{uL} + \widetilde{S}_{uL} \right) \; + \; \text{h.c.} && \text{(mixing)} \\
& + (u \leftrightarrow d) && (2.15)
\end{aligned}
$$

Here we have two bidoublets, Q and $\widetilde{Q}$, and two singlets, S and $\widetilde{S}$, for every flavour. For the kinetic terms we used an SO(5) notation where we combined the singlets and bidoublets into SO(5) fundamentals: $\Psi_{\text{comp}} = (Q, S)_{u,d}$, $\widetilde{\Psi}_{\text{comp}} = (\widetilde{Q}, \widetilde{S})_{u,d}$. For these the covariant derivatives are then defined as

$$
\mathcal{D}_\mu \Psi_{\text{comp}} = \left(\partial_\mu - i g_G \, \rho_{G\mu} - i g_\rho \, \rho_\mu - i q_X \, g_X \, \rho_{X\mu} \right) \Psi_{\text{comp}} \tag{2.16}
$$

and the same for $\widetilde{\Psi}_{\text{comp}}$. The $\text{U}(1)_X$ charges are assigned to match the hypercharge of the SM. Thus, the fundamentals $\Psi_{\text{comp}}^{(u)}$ and $\Psi_{\text{comp}}^{(d)}$ have $q_X^{(u)} = \frac{2}{3}$ and $q_X^{(d)} = -\frac{1}{3}$.

The elementary fields are embedded into (incomplete) SO(5) fundamentals via

$$
\xi_{uL} = \frac{1}{\sqrt{2}} \begin{pmatrix} d_L \\ -i d_L \\ u_L \\ i u_L \\ 0 \end{pmatrix} , \; \xi_{uR} = \begin{pmatrix} 0 \\ 0 \\ 0 \\ 0 \\ u_R \end{pmatrix} , \tag{2.17}
$$

$$
\xi_{dL} = \frac{1}{\sqrt{2}} \begin{pmatrix} u_L \\ i u_L \\ -d_L \\ i d_L \\ 0 \end{pmatrix} , \; \xi_{dR} = \begin{pmatrix} 0 \\ 0 \\ 0 \\ 0 \\ d_R \end{pmatrix} \tag{2.18}
$$

Since we are mainly interested in the interplay between quark flavour measurements and the Higgs potential, we do not consider effects of partial lepton compositeness in this work. Indeed, if the compositeness of the left- and right-handed lepton chiralities are comparable, they are required to be small due to the leptons' lightness and their impact on the observables to be considered below is expected to be small. Moreover, flavour-changing interactions are strongly constrained by negative searches for charged lepton flavour violating processes. In practice, we simply consider elementary leptons with direct bilinear couplings to the Higgs field,

$$
\mathcal{L}_{\text{lepton}} = i\bar{l}_L \slashed{D} l_L + i\bar{\ell}_R \slashed{D} \ell_R - \frac{m_{\text{SM}}}{v} \, \bar{l}_L \cdot \begin{pmatrix} 0 \\ h \end{pmatrix} \ell_R \; + \; \text{h.c.}, \tag{2.19}
$$

where, just as for the elementary quarks, the covariant derivatives are understood as couplings to the elementary $\mathrm{SU}(3)^0 \times \mathrm{SU}(2)^0 \times \mathrm{U}(1)^0$ gauge fields. We note however that a significant degree of compositeness for some of the leptons could be motivated experimentally, e.g. to reconcile radiative electroweak symmetry breaking (EWSB) with naturalness in the absence of light top partners [62] or to explain the hints for violation of lepton flavour non-universality in B decays [63]. These effects are beyond the scope of our present analysis.

Let us note here that many of the above model parameters are correlated if they originate from an extradimensional gauge theory, e.g. coupling constants are generated by overlap integrals of Kaluza-Klein mode functions. In our numerical analysis, we will not impose such relations but instead try to be as general as possible to explore the viability of purely 4D pNGB Higgs models, regardless of whether a dual 5D description exists.

2.3 Flavour structure

As noted in the introduction, we assume the strong sector to be invariant under a flavour symmetry, only to be broken by the composite-elementary mixings. We consider four possibilities (see [18] for a thorough comparison),

- In $\mathrm{U}(3)^3_{\mathrm{LC}}$ (LC for left-handed compositeness), the strong sector is invariant under a $\mathrm{U}(3)$ symmetry[7] that is broken by the *right-handed* composite-elementary mixings.

- In $\mathrm{U}(3)^3_{\mathrm{RC}}$ (RC for right-handed compositeness), the strong sector is invariant under a $\mathrm{U}(3) \times \mathrm{U}(3)$ which is broken by the *left-handed* composite-elementary mixings.

- The $\mathrm{U}(2)^3_{\mathrm{LC}}$ and $\mathrm{U}(2)^3_{\mathrm{RC}}$ models are analogous, but restricted to a smaller symmetry only acting on the first two generations of composite quarks.

In the $\mathrm{U}(3)^3$ models, the matrices in the composite part of the fermion Lagrangian (the 3rd and 4th lines in (2.15)) are proportional to the identity, while in the $\mathrm{U}(2)^3$ models, they are of the form $\mathrm{diag}(a, a, b)$. The main difference is the form of the composite-elementary mixings. We give their explicit forms in appendix C.

2.4 Higgs potential

The explicit breaking of the global symmetries by the mixings of the composite resonances with the elementary sector generates an effective potential for the NGB field (to be identified with the SM Higgs) at the quantum level, so that it acquires a mass and a VEV, breaking electroweak symmetry. In general, the effective potential is UV-sensitive and not necessarily calculable. In the M4DCHM it is finite at one loop, making the model predictive under the assumption that higher loop contributions are subleading with respect to the (calculable) one-loop contribution. We will rely on this assumption in the following.

At one loop, the effective potential is given in terms of all the n-point correlation functions of the Higgs and therefore contains a gauge as well as a fermion contribution. It

---

[7]The cube in $\mathrm{U}(3)^3$ refers to the fact that after the breaking, the SM quark sector is approximately invariant under a $\mathrm{U}(3)_q \times \mathrm{U}(3)_u \times \mathrm{U}(3)_d$.

can be calculated by the Coleman-Weinberg formula [64]

$$V_{\text{eff}}(h) = \sum \frac{c_i}{64\pi^2} \left(2 \operatorname{tr} \left[M_i^2(h) \right] \Lambda^2 - \operatorname{tr} \left[\left(M_i^2(h) \right)^2 \right] \log \left[\Lambda^2 \right] \right. \\ \left. + \operatorname{tr} \left[\left(M_i^2(h) \right)^2 \log \left[M_i^2(h) \right] \right] \right), \qquad (2.20)$$

where $M_i^2(h)$ denote the Higgs-dependent mass-(mixing)-matrices[8] which we give in appendix B and

$$c_i = \begin{cases} 3 \text{ for neutral gauge bosons} \\ 6 \text{ for charged gauge bosons} \\ -12 \text{ for (coloured) Dirac fermions} \end{cases}.$$

Here we explicitly showed the dependence on the cutoff of the theory. For a non-renormalizable effective theory these UV dependent terms spoil the predictivity, such that one has to demand the following relations for ensuring the calculability of the Higgs potential:

$$\operatorname{tr} \left[M_i^2(h) \right] - \operatorname{tr} \left[M_i^2(h = 0) \right] = 0, \qquad (2.21)$$

$$\operatorname{tr} \left[(M_i^2(h))^2 \right] - \operatorname{tr} \left[(M_i^2(h = 0))^2 \right] = 0, \qquad (2.22)$$

where it was taken into account that the constant term of the potential is not physical. These relations are just a reformulation of the Weinberg sum rules of the fermion and gauge sector that are usually imposed to guarantee a finite potential [13, 49]. For the quark sector, these relations represent a generalisation of the Weinberg sum rules to the three family case.

In deconstructed models the Higgs potential is usually protected by the higher dimensional gauge symmetry, such that the Weinberg sum rules are automatically satisfied. This is the case for the M4DCHM as well [11, 13]. Note that in this case also the scale dependence cancels from the effective potential. Then the expression for the potential simplifies to

$$V_{\text{eff}}(h) = \sum_{\text{all particles}} \frac{c_i}{64\pi^2} m_i^4(h) \log(m_i^2(h)), \qquad (2.23)$$

where $m_i(h)$ denote the masses in the mass basis, i.e. the singular values of the mass matrices.

3 Experimental constraints

In this section, we discuss all the experimental constraints that we impose in our analysis. Since approximate analytical expressions for most of the observables have already been provided elsewhere (see in particular [18, 19, 46, 57]), we focus on discussing the numerical computation and on specifying our treatment of theoretical and experimental uncertainties. Section 3.1 specifies how we compute the masses and couplings of the SM states, including among others the Higgs mass and VEV as well as the CKM matrix, section 3.2 discusses

---

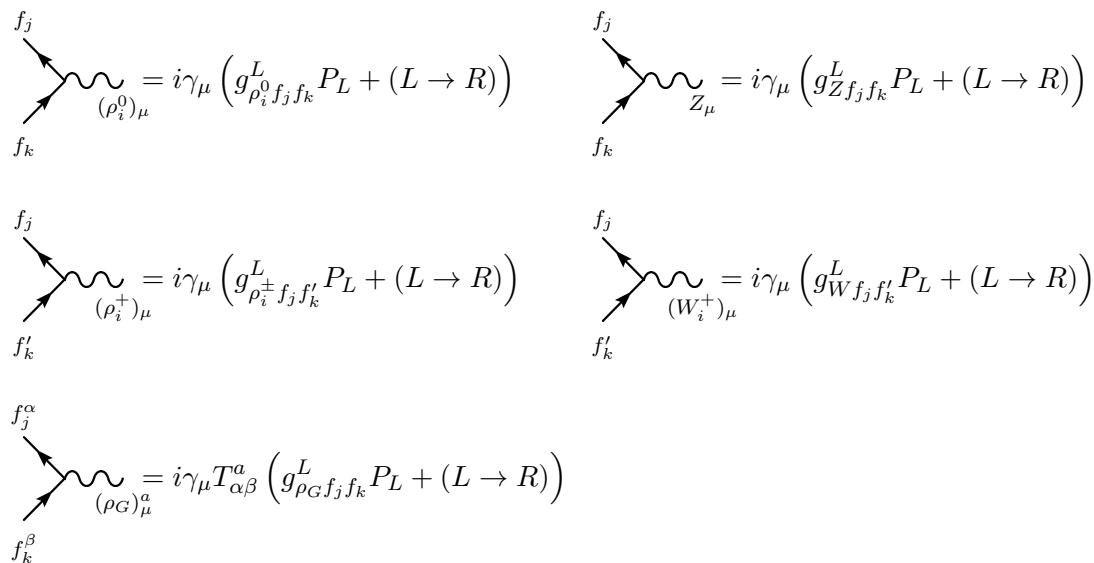[8]For fermions these are given by $M^2(h) = M(h)^\dagger M(h)$.

Figure 1. Notation for Feynman rules used in this work.

indirect constraints, including electroweak precision observables and flavour physics, while section 3.3 deals with the direct bounds on fermion and vector resonances.

Since the numerical computation of the observables involves masses and couplings in the mass eigenstate basis (mb), we fix our notation for the couplings by specifying the Feynman rules in figure 1. In the gauge basis (gb) the Lagrangian contains non-diagonal mass matrices for vector bosons and fermions as well as interaction terms connecting both kinds of fields, which are (schematically) given as follows

$$\mathcal{L} \supset [M_{\mathrm{g}}]_{ij} A_{\mu\, i} A_j^\mu - [M_\psi]_{ij} \overline{\Psi}_i \Psi_j + [g_{\mathrm{gb}}]_{ijk} \overline{\Psi}_i \gamma_\mu \Psi_j A_k^\mu. \tag{3.1}$$

After EWSB one can go to the mass basis by unitary transformations,

$$\Psi_{L,R\, i}^{(\mathrm{gb})} = \left[V_\psi^{(L,R)} \right]_{ij} \Psi_{L,R\, i}^{(\mathrm{mb})}, \qquad A_{\mu\, i}^{(\mathrm{gb})} = [V_g]_{ij}\, A_{\mu\, i}^{(\mathrm{mb})}, \tag{3.2}$$

such that the couplings as defined in figure 1 can be calculated as

$$\left[g^{(\mathrm{mb})} \right]_{abc} = [V_\psi^\dagger]_{ai}\, [V_\psi]_{jb}\, [V_g]_{kc}\, \left[g^{(\mathrm{gb})} \right]_{ijk}. \tag{3.3}$$

3.1 Standard model masses and couplings

3.1.1 Higgs VEV and masses of SM states

The tree-level masses for fermions and gauge bosons are obtained by diagonalizing the mass matrices given in appendix B after EWSB. Since the interaction terms of the Goldstone bosons generate mixing terms between elementary fields and the composite resonances, all masses of fields with SM-like quantum numbers will depend on the VEV taken by the pNGB, i.e. they depend on $s_h^* = \sin(\langle h \rangle / f)$. In the model used in this work this quantity is not a free parameter, but it is calculable as the minimum of the loop-generated effective potential.

In practice, we calculate the s_h-dependent masses of all particles and use (2.23) to calculate the effective Higgs potential. Then, the correct value of s_h^* is obtained by numerically minimizing the potential. We also explicitly demand that the found minimum is non-trivial, otherwise we discard the parameter point.

The value of s_h^* is fixed in our numerical analysis by imposing the tree-level value of the Fermi constant in muon decay as a constraint,

$$G_\mu^{\text{tree}} = \frac{1}{\sqrt{2}v_{\text{SM}}^2} = \frac{1}{\sqrt{2}(s_h^*)^2 f^2} \,, \tag{3.4}$$

which is valid up to negligible vector resonance exchange contributions. Since we only include the tree-level G_μ, we add a relative theoretical uncertainty of 1%. Loop corrections to G_μ are effectively included in terms of the T parameter, see section 3.2.1.

Once s_h^* is known, the Higgs mass can be calculated as the curvature of the effective potential at its minimum,

$$m_h^2 = \partial_h^2 V_{\text{eff}}(h)\big|_{h=\langle h \rangle} = \frac{1 - s_h^2}{f^2} \, \partial_{s_h}^2 V_{\text{eff}}(s_h)\big|_{s_h=s_h^*} \,. \tag{3.5}$$

For the W, Z, and top masses, we directly interpret the masses obtained from diagonalizing the mass matrices as $\overline{\text{MS}}$ running masses at the scale m_t. We add a relative theory uncertainty of 5% to account for this crude assumption. In principle, we could compute the one-loop matching corrections to the masses to get a more reliable estimate. In practice, this is not feasible because the composite-elementary mixing means that the numerical computation of a large self-energy matrix, e.g. 27×27 in the case of the top quark, would be necessary which quickly leads to excessive computing times.

For the light quark masses, we also interpret the tree-level masses as $\overline{\text{MS}}$ running masses at m_t; then we use RunDec [65] to run them to the relevant scales where they can be compared to the PDG averages [66].

3.1.2 CKM matrix

In the SM, CKM elements are determined from a global fit to weak decays mediated by tree-level W exchange as well as loop-induced meson-antimeson mixing observables. In the presence of NP, the latter are susceptible to NP contributions as will be discussed below in section 3.2.4. But even the tree-level processes receive corrections in a composite Higgs framework that lead to relevant constraints. The reason is that the 3×3 quark mixing matrix is no longer unitary in the presence of composite-elementary mixing, but becomes part of a larger (27×27) mixing matrix among quarks and quark partners. Deviations from CKM unitarity, predicted by the SM, can thus be used to constrain quark compositeness.

To compare to the absolute values of CKM elements measured in experiments, one can define effective CKM elements from ratios of W couplings,

$$|V_{ij}| = \frac{|g_{W u_i d_j}^L|}{|g_{W \ell \nu}^L|} \,. \tag{3.6}$$

The $|V_{ij}|$ obtained in this way can be directly compared to the elements extracted in experiments assuming the SM as long as right-handed W couplings and contributions from

tree-level heavy resonance exchange can be neglected. We do take these two effects into account in our numerics, although they turn out to be negligible.

In our numerical analysis, we include five CKM elements that are directly measured in tree-level processes.

- $|V_{ud}|$ from superallowed nuclear beta decays,

- $|V_{us}|$ from $K \to \pi \ell \nu$ decays,

- $|V_{ub}|$ from inclusive $B \to X_u \ell \nu$ and exclusive $B \to \pi \ell \nu$ decays,

- $|V_{cb}|$ from inclusive $B \to X_c \ell \nu$ and exclusive $B \to D^* \ell \nu$ decays,

- $|V_{tb}|$ from the cross-section of t-channel single top production at LHC.

The measured values and references are given in table 1. In the case of $|V_{ub}|$ and $|V_{cb}|$, there are long standing discrepancies between the determinations from inclusive vs. exclusive B decays. Since these tensions cannot be resolved in our model, we use the PDG prescription [66] to rescale the discrepant measurements. We multiply the uncertainties of $|V_{ub}|$ by a factor of 1.9 compared to the ones given in table 1, and a factor of 2.9 in the case of $|V_{cb}|$.

$|V_{ud}|$ and $|V_{us}|$ are important because in the SM, they are constrained by the unitarity condition on the first row of the CKM matrix,

$$1 = |V_{ud}|^2 + |V_{us}|^2 + |V_{ub}|^2 \approx |V_{ud}|^2 + |V_{us}|^2 \,, \tag{3.7}$$

where $|V_{ub}|$ is numerically negligible. The smallness of $|V_{ub}|$ and $|V_{cb}|$ is also why, in the SM, $|V_{tb}| \approx 1$ holds up to a permille level correction. Partial compositeness can lead to a deviation from both relations (see e.g. [16, 18, 60]).

Finally, we also include the CKM angle γ that is measured via the interference of $b \to c\bar{u}s$ and $b \to u\bar{c}s$ amplitudes in $B \to DK$ decays. Again in the case where right-handed W couplings and direct vector resonance contributions can be neglected, γ can be computed from the tree-level W couplings as

$$\gamma = \arg \left(-\frac{g^L_{Wud} \, g^{L*}_{Wub}}{g^L_{Wcd} \, g^{L*}_{Wcb}} \right) \,. \tag{3.8}$$

This expression is independent of phase conventions. For the experimental value in table 1, we symmetrize the value obtained by the CKMfitter collaboration from a fit to all experiments.

3.2 Indirect constraints

3.2.1 S and T parameters

By construction, the T parameter does not receive a contribution at tree level in pNGB models based on the $SO(5)/SO(4)$ coset. At one loop, the dominant contribution typically comes from fermion loops involving, in particular, the top partners. In addition, the modification of the gauge boson couplings to the Higgs and the electroweak would-be

R_b	0.21629(66)	[67]	$\lvert V_{ud}\rvert$	0.97417(21)	[68]
R_c	0.1721(30)	[67]	$\lvert V_{us}\rvert$	0.2249(8)	[69]
R_h	20.804(50)	[67]	$\lvert V_{ub}\rvert_{\rm ex}$	$(3.72 \pm 0.16) \times 10^{-3}$	[70]
μ_{WW}^{gg}	0.86 ± 0.17	[71, 72]	$\lvert V_{ub}\rvert_{\rm in}$	$(4.33 \pm 0.28) \times 10^{-3}$	[73]
μ_{ZZ}^{gg}	1.18 ± 0.39	[71, 72]	$\lvert V_{cb}\rvert_{\rm ex}$	$(3.904 \pm 0.075) \times 10^{-2}$	[74]
μ_{gg}^{gg}	1.12 ± 0.22	[71, 72]	$\lvert V_{cb}\rvert_{\rm in}$	$(4.221 \pm 0.078) \times 10^{-2}$	[75]
$\mu_{\tau^+\tau^-}^{gg}$	0.97 ± 0.39	[71, 72]	$\lvert V_{tb}\rvert$	0.998 ± 0.041	[76]
ΔM_K	$3.483(6) \times 10^{-15}\,\mathrm{GeV}$	[66]	$\lvert \epsilon_K\rvert$	$2.228(11) \times 10^{-3}$	[66]
ΔM_d	$0.510(3)\,\mathrm{ps}^{-1}$	[77]	$S_{\psi K_S}$	0.682(19)	[77]
ΔM_s	$17.761(22)\,\mathrm{ps}^{-1}$	[77]	ϕ_s	-0.010 ± 0.039	[78]
S	0.05 ± 0.11	[79]	γ	$(72.9 \pm 6.7)°$	[80]
T	0.09 ± 0.13	[79]			

Table 1. Values of the experimental constraints used in the numerical analysis. For details and the treatment of theoretical uncertainties, see main text.

Goldstone bosons leads to an "infrared-log" contribution [81, 82]. Finally, also loops involving the heavy spin-1 resonances can contribute (see [17] for a recent discussion). For simplicity, in our analysis we restrict ourselves to the fermion contribution, which is finite and gauge-independent. It can be computed numerically as

$$\alpha_{\rm em} T = \frac{\Pi_{WW}^T}{m_W^2} - \frac{\Pi_{ZZ}^T}{m_Z^2} \tag{3.9}$$

where the masses are tree-level masses, and

$$-16\pi^2 \Pi_{VV}^T = \sum_{f_i, f_j} H\left(m_{f_i}^2, m_{f_j}^2\right) \left(\lvert g_{Vf_if_j}^L\rvert^2 + \lvert g_{Vf_if_j}^R\rvert^2\right)$$
$$+ 4 m_{f_i} m_{f_j} B_0\left(m_{f_i}^2, m_{f_j}^2\right) \mathrm{Re}\left(g_{Vf_if_j}^{L*} g_{Vf_if_j}^R\right) \tag{3.10}$$

is the fermion contribution to the transverse part of the vacuum polarization. The sum runs over all SM fermions and quark resonances. The Passarino-Veltman function is defined as in [83] and the function H can be found e.g. in [84].

In contrast to T, the S parameter arises already at tree level, effectively leading to a lower bound on the mass scale of the spin-1 resonances. In models where $T = T_{\rm SM}$ at tree level, the NP contribution to S can be obtained numerically as

$$\alpha_{\rm em} S\,|_{T=0} = \frac{1}{4}\left(s_W^2 - \sin^2\theta_{\rm eff}\right), \tag{3.11}$$

where $s_W^2 = 1 - m_W^2/m_Z^2$ and the effective weak mixing angle is defined via the leptonic forward-backward asymmetry,

$$x = \frac{g_{Zee}^R + g_{Zee}^L}{g_{Zee}^R - g_{Zee}^L}, \qquad\qquad \sin^2\theta_{\rm eff} = \frac{1+x}{4}. \tag{3.12}$$

Experimentally, a recent global fit of electroweak precision data finds [79]

$$S = 0.05 \pm 0.11 \,, \qquad\qquad T = 0.09 \pm 0.13 \,, \qquad\qquad (3.13)$$

with a correlation coefficient of $+0.9$. Since we neglect gauge contributions to T and all loop contributions to S, in our numerical analysis we further assume uncorrelated theory uncertainties of 0.05 for S and 0.10 for T, which we combine with the correlated experimental uncertainties. The size of these theory uncertainties is chosen to encompass the typical size of the neglected "IR-log" contributions to S and T.

3.2.2 Z decays

Due to the large degree of compositeness required for the left-handed top quark (and thus also b quark), the partial width of the Z into b quarks measured at LEP provides a powerful constraint on models with partial compositeness. While our model features a custodial protection of this coupling, the observable is still important to constrain the subleading composite-elementary mixing of the b_L. In the flavour-symmetric models, also the partial widths into lighter quarks lead to constraints. We include the following observables in our analysis,

$$R_b = \frac{\Gamma(Z \to b\bar{b})}{\Gamma(Z \to q\bar{q})} \,, \qquad R_c = \frac{\Gamma(Z \to c\bar{c})}{\Gamma(Z \to q\bar{q})} \,, \qquad R_h = \frac{\Gamma(Z \to q\bar{q})}{\Gamma(Z \to \ell\bar{\ell})} \,, \qquad (3.14)$$

where $\Gamma(Z \to q\bar{q})$ implies a sum over all quarks but the top. We compute only the tree-level corrections at zero momentum to these observables (see [16] for a discussion of effects beyond this limit). We add the higher-order SM contributions (see [85]) numerically to reproduce the correct SM predictions in the absence of NP contributions. The experimental measurements are listed in table 1.

A comment is in order on the loop corrections to $Z \to \bar{b}_L b_L$, which we have not taken into account. Although corrections are already generated at tree level in the M4DCHM5, these are suppressed by the custodial protection mechanism, which however is not active at loop level. In [81, 86, 87] it was shown that in similar models as the ones we are studying, there is a correlation between fermionic loop corrections to the T parameter and the loop correction to $Z \to \bar{b}_L b_L$. For a heavy new physics scale, this can be understood as being due to renormalization-group mixing of dimension-6 operators invariant under the SM gauge symmetries. Considering the operators (in the notation of [88] and in the basis where the down-type quark mass matrix is diagonal)

$$Q_{\phi q}^{(1)} = (\phi^\dagger i \overleftrightarrow{D}_\mu \phi)(\bar{q}_3 \gamma^\mu q_3) \,, \qquad Q_{\phi q}^{(3)} = (\phi^\dagger i \overleftrightarrow{D}_\mu^a \phi)(\bar{q}_3 \tau^a \gamma^\mu q_3) \,, \qquad (3.15)$$

the correction to the left-handed Z coupling to bottom quarks δg_{Zbb}^L satisfies

$$\delta g_{Zbb}^L \propto \left(C_{\phi q}^{(3)} + C_{\phi q}^{(1)} \right) \,. \qquad (3.16)$$

Custodial protection implies $C_{\phi q}^{(1)} \approx -C_{\phi q}^{(3)}$ up to subleading mixing effects, implying a vanishing correction δg_{Zbb}^L at the matching scale. Since the two Wilson coefficients run

differently [89–91], a non-zero correction is induced at the electroweak scale which is proportional to the matching scale value of $C_{\phi q}^{(3)}$.[9] The quantum corrections leading to this running induce at the same time a non-zero T parameter which is also proportional to the matching scale value of $C_{\phi q}^{(3)}$ and thus correlated to δg_{Zbb}^L. For a positive contribution to the T parameter, the sign of this correlation leads to a negative contribution to R_b that is disfavoured by experiment [81, 86, 87]. Thus, parameter points with a large positive contribution to the T parameter might be excluded by taking into account the one-loop corrections to δg_{Zbb}^L. A challenge of taking this loop contribution into account is that it involves Passarino-Veltman functions at non-zero external momentum with three propagators. Due to the large number of states in the M4DCHM5, this would significantly increase computing time, so we are not able to take this effect into account. It should thus be kept in mind that our results might be optimistic in the sense that we might keep points that are possibly excluded. A dedicated analysis of the impact of higher order corrections to δg_{Zbb}^L would be worthwhile. We also note that the tension between the constraints on the T parameter and δg_{Zbb}^L might be relaxed by including an additional level of resonances [87].

3.2.3   Higgs production and decay

We compute the modification of the Higgs partial widths $r_X = \Gamma(h \to X)/\Gamma(h \to X)_{\rm SM}$ at tree level for $X = WW$, ZZ, $b\bar{b}$, and $\tau^+\tau^-$, and at one-loop level for $X = gg$ and $\gamma\gamma$. We take into account the loop contributions from all SM and heavy fermions and vector bosons. The signal strength in a particular final state, assuming pure gluon fusion production, can then be obtained as

$$\mu_X^{gg} = \frac{r_X \, r_{gg}}{r_{\rm tot}} \,, \tag{3.17}$$

where $r_{\rm tot} = \Gamma_h/\Gamma_h^{\rm SM}$ is the modification of the total width.

We use ATLAS and CMS measurements to constrain the signal strength. In the case of ATLAS, the gluon fusion result is given explicitly. In the case of CMS, we use the "0/1 jet" result for WW, ZZ, and $\tau^+\tau^-$, and the "untagged" result for $\gamma\gamma$. We naively combine the ATLAS and CMS results for each final state, using the PDG prescription to enlarge the error in the case of poor agreement. The resulting constraints are listed in table 1. We neglect the correlations between individual measurements. Since the $h \to b\bar{b}$ signal strength is only measured in the case of vector boson associated production, we do not include it in our numerical analysis.

3.2.4   Meson-antimeson mixing

The meson-antimeson mixing amplitude for the neutral meson M^0 ($= K^0$, B_s, B_d, or D^0) can be written as

$$M_{12}^M = \frac{1}{2m_M}\langle \bar{M}^0|\mathcal{H}^{\Delta F=2}|M^0\rangle = \left(M_{12}^M\right)_{\rm SM} + \sum_a C_a^{q_i q_j}(\mu_l)\langle\bar{M}^0|Q_a^{q_i q_j}(\mu_l)|M^0\rangle \tag{3.18}$$

---

[9]The Wilson coefficient $C_{\phi u}$ associated with the Operator $Q_{\phi u} = (\phi^\dagger i \overleftrightarrow{D}_\mu \phi)(\bar{u}_3\gamma^\mu u_3)$ that also enters the RGE induced contributions to δg_{Zbb}^L vanishes due to custodial protection.

with $q = u$ or d. The loop-induced SM contribution is discussed e.g. in [92]. The sum contains NP contributions due to tree-level vector resonance exchange that are encoded in the Wilson coefficients of the following $\Delta F = 2$ operators.

$$Q_{VLL}^{q_i q_j} = (\bar{q}_L^i \gamma^\mu q_L^j)(\bar{q}_L^i \gamma^\mu q_L^j), \qquad Q_{VRR}^{q_i q_j} = (\bar{q}_R^i \gamma^\mu q_R^j)(\bar{q}_R^i \gamma^\mu q_R^j), \qquad (3.19)$$

$$Q_{VLR}^{q_i q_j} = (\bar{q}_L^i \gamma^\mu q_L^j)(\bar{q}_R^i \gamma^\mu q_R^j), \qquad Q_{SLR}^{q_i q_j} = (\bar{q}_R^i q_L^j)(\bar{q}_L^i q_R^j), \qquad (3.20)$$

that can be written in terms of the Feynman rules defined in figure 1 as

$$C_{VLL}^{q_i q_j} = -\frac{1}{2} \sum_k \left(\frac{g_{\rho_k^0 q_i q_j}^L}{m_{\rho_k^0}}\right)^2 - \frac{1}{6} \left(\frac{g_{\rho_G q_i q_j}^L}{m_{\rho_G}}\right)^2, \qquad (3.21)$$

$$C_{VRR}^{q_i q_j} = C_{VLL}^{q_i q_j}\big|_{L \to R}, \qquad (3.22)$$

$$C_{VLR}^{q_i q_j} = -\sum_k \frac{g_{\rho_k^0 q_i q_j}^L g_{\rho_k^0 q_i q_j}^R}{m_{\rho_k^0}^2} + \frac{1}{6} \frac{g_{\rho_G q_i q_j}^L g_{\rho_G q_i q_j}^R}{m_{\rho_G}^2}, \qquad (3.23)$$

$$C_{SLR}^{q_i q_j} = \frac{g_{\rho_G q_i q_j}^L g_{\rho_G q_i q_j}^R}{m_{\rho_G}^2}. \qquad (3.24)$$

These expressions are valid at the matching scale of NP and SM, while (3.18) depends on the values at the hadronic scale μ_l that is chosen conventionally as m_b for $B_{d,s}$ mixing, $3\,\text{GeV}$ for D^0 mixing, and $2\,\text{GeV}$ for K^0 mixing. In principle, the correct matching scale is set by the mass scale of the heavy resonances. However, in our numerical scan, we often encounter vastly different scales for the different resonances. Consequently, we have decided to simply match the tree-level Wilson coefficients to the SM at the scale m_t and to neglect the RG evolution above m_t. A more complete treatment, including intermediate thresholds, is beyond the scope of our present work. We note that the RG evolution typically makes the NP effects larger at low scales. In that sense, our treatment leads to more conservative bounds. All relevant anomalous dimensions for the evolution below m_t can be found in [93].

The matrix elements in (3.18) depend on meson decay constants and bag parameters, both of which can be determined from lattice QCD. They can be written as

$$\langle \bar{M}^0 | Q_a^{q_i q_j}(\mu_l) | M^0 \rangle = m_M f_M^2 \mathcal{B}_a^M(\mu_l), \qquad (3.25)$$

where

$$\mathcal{B}_{VLL}^M = \mathcal{B}_{VRR}^M = \frac{1}{3} B_1^M(\mu_l), \qquad (3.26)$$

$$\mathcal{B}_{VLR}^M = -\frac{1}{6}\left(\frac{m_M}{m_{q_i} + m_{q_j}}\right)^2 B_5^M(\mu_l), \qquad \mathcal{B}_{SLR}^M = \frac{1}{4}\left(\frac{m_M}{m_{q_i} + m_{q_j}}\right)^2 B_4^M(\mu_l). \qquad (3.27)$$

For the lattice predictions of the decay constants as well as the bag parameters B_i for B_d and B_s mixing, we use ref. [69], for the kaon bag parameters we use ref. [94], and for the charm bag parameters ref. [95].

We use the following observables sensitive to NP in the meson-antimeson mixing amplitude.

- The mass differences in the B_d and B_s systems,

$$\Delta M_{d,s} = 2|M_{12}^{B_{d,s}}|. \tag{3.28}$$

For the theoretical uncertainties, which are dominated by lattice uncertainties, we take 10.2% relative uncertainty for ΔM_d and 7.6% for ΔM_s. Note that we do not have to account for uncertainties due to CKM elements as these are allowed to vary in our scan. We further take these lattice uncertainties to be correlated with a coefficient of 0.17, since the ratio of the relevant lattice parameters is known more precisely than for the individual systems.

- The mixing-induced CP asymmetry in $B_d \to J/\psi\, K_S$,

$$S_{\psi K_S} = \sin\left(\arg\left(M_{12}^{B_d}\right)\right), \tag{3.29}$$

which in the SM measures $\sin 2\beta$. We add a theory uncertainty of 0.01 to account for possible penguin pollution [96].

- The sine of the B_s mixing phase as obtained from an average of the mixing-induced CP asymmetries in $B_s \to J/\psi\, K^+ K^-$ and $B_s \to J/\psi\, \pi^+\pi^-$ decays,[10]

$$\sin\phi_s = \sin\left(\arg\left(M_{12}^{B_s}\right)\right). \tag{3.30}$$

In this case, we add a theory uncertainty due to penguin pollution of 0.017 [96].

- The parameter for indirect CP violation in K^0 mixing,

$$|\epsilon_K| = \kappa_\epsilon \frac{\mathrm{Im}\left(M_{12}^{K^0}\right)}{\sqrt{2}\Delta M_K} \tag{3.31}$$

where the experimental value for ΔM_K can be used. For the (non-CKM) theory uncertainty on $|\epsilon_K|$, we take a relative uncertainty of 11%.

- The mass difference in K^0 mixing,

$$\Delta M_K = 2\mathrm{Re}\left(M_{12}^{K^0}\right). \tag{3.32}$$

The SM contribution to ΔM_K is plagued by large uncertainties due to long-distance contributions. Although first results are available from lattice calculations [99], these are still for unphysical kinematics. Thus we conservatively allow the NP contribution to saturate the experimental central value at 1σ (i.e. at 3σ, we allow points where the NP contribution is three times the experimental central value, implying a necessary cancellation with the SM contribution).

We do not impose D^0 mixing observables as constraints, as they are expected to receive small NP contributions in models with minimally broken U(2)^3 [61], but we will discuss predictions for them in section 4 below.

---

[10]Here we have used the average performed by the LHCb collaboration. Very recently, a measurement with comparable precision has been presented by CMS [97]. The observable has also been measured by ATLAS [98].

3.2.5 Rare B decays

The $b \to s\gamma$ transition arises first at the one-loop level; approximate analytical results as well as generic formulae that can be used in a numerical analysis have been presented in [19]. We include the constraint from the $B \to X_s\gamma$ branching ratio, that agrees well between SM prediction [100] and experimental world average [77],

$$\mathrm{BR}(B \to X_s\gamma)_{\mathrm{SM}} = (3.36 \pm 0.23) \times 10^{-4} \,, \tag{3.33}$$

$$\mathrm{BR}(B \to X_s\gamma)_{\mathrm{WA}} = (3.43 \pm 0.22) \times 10^{-4} \,. \tag{3.34}$$

For the NP contribution, we use the following formula (cf. [101]),

$$\frac{\mathrm{BR}(B \to X_s\gamma)}{\mathrm{BR}(B \to X_s\gamma)_{\mathrm{SM}}} = \frac{1}{\left(|C_7^{\mathrm{eff}}(m_b)^{\mathrm{SM}}|^2 + N_\gamma\right)} \left(|C_7^{\mathrm{eff}}(m_b)|^2 + |C_7'(m_b)|^2 + N_\gamma\right) \,, \tag{3.35}$$

where $N_\gamma = 3.6 \times 10^{-3}$.

The imaginary part of the Wilson coefficients and the relative size of the left- and right-handed Wilson coefficients can be constrained by other processes, most notably $B \to K^* \mu^+ \mu^-$ angular observables. We do not impose these additional observables as constraints, but will discuss predictions for them in section 4.

NP contributions to semi-leptonic FCNC decays of B and K mesons arise already at tree level, mediated by the Z boson that can obtain flavour-changing couplings to quarks at tree level as well as by heavy neutral vector resonances (for a thorough discussion of these effects in composite Higgs models, see [46]. Similar effects are obtained in models with a warped extra dimension [42, 44]). Writing the four-fermion operators as

$$Q_{VAB}^{d_i d_j \ell\ell} = (\bar{d}_A^j \gamma^\mu d_A^i)(\bar{\ell}_B \gamma^\mu \ell_B) \,, \tag{3.36}$$

with $A, B = L, R$, the Wilson coefficients are obtained in analogy with section 3.2.4 as

$$C_{VAB}^{d_i d_j \ell\ell} = -\frac{g_{Zd_j d_k}^A g_{Z\ell\ell}^B}{m_Z^2} - \sum_i \frac{g_{\rho_i^0 d_j d_k}^A g_{\rho_i^0 \ell\ell}^B}{m_{\rho_i^0}^2} \,. \tag{3.37}$$

Here we have explicitly included the Z contribution as it contributes formally at the same level in v/f as the heavy resonance exchanges. The smallness of the flavour-changing coupling (which only arises after EWSB and is of order v^2/f^2) is compensated by the absence of the suppression by the heavy resonance mass in the propagator.

One can map the coefficients (3.37) onto the traditional operator basis for $d_i \to d_j \ell^+ \ell^-$ transitions as

$$C_9^{d_i d_j} = \Lambda_{ij}^2 \left(C_{VLR}^{d_i d_j \ell\ell} + C_{VLL}^{d_i d_j \ell\ell}\right) \,, \qquad C_{10}^{d_i d_j} = \Lambda_{ij}^2 \left(C_{VLR}^{d_i d_j \ell\ell} - C_{VLL}^{d_i d_j \ell\ell}\right) \,, \tag{3.38}$$

$$C_9'^{d_i d_j} = \Lambda_{ij}^2 \left(C_{VRR}^{d_i d_j \ell\ell} + C_{VRL}^{d_i d_j \ell\ell}\right) \,, \qquad C_{10}'^{d_i d_j} = \Lambda_{ij}^2 \left(C_{VRR}^{d_i d_j \ell\ell} - C_{VRL}^{d_i d_j \ell\ell}\right) \,, \tag{3.39}$$

where

$$\Lambda_{ij}^2 = \frac{\pi}{\sqrt{2} G_F \alpha_{\mathrm{em}} V_{ti} V_{tj}^*} \,. \tag{3.40}$$

The primed coefficients are only generated at a very suppressed level in the flavour-symmetric models we consider. Since we are assuming leptons to be elementary, all Wilson coefficients are lepton flavour universal. Relaxing this assumption, the recent hint for lepton flavour non-universality can potentially be explained as well [63], but we are not considering this possibility here. Since the lepton-Z couplings are SM-like to an excellent precision in our setup, the Z-mediated contributions fulfill the well-known relation $C_9 = (4s_w^2 - 1)C_{10}$, i.e. they mostly contribute to C_{10}.

Concerning the resonance-mediated contributions, as mentioned above, they formally contribute at the same order in v/f as the Z contributions. Their couplings to elementary leptons however only arise through mixing of the composite and elementary vectors, so the resonance-mediated contributions are expected to be parametrically suppressed compared to the Z-mediated ones by a factor $g_{\text{el}}^2/g_{\text{co}}^2$, where $g_{\text{el,co}}$ are generic elementary and composite gauge couplings. Still, there are parts of parameter space where these contributions can be relevant. To understand their impact, it is instructive to work in a basis where instead of the three electrically neutral electroweak resonances ρ_L^0, ρ_R^0, and ρ_X^0, one works with three linear combinations that, before EWSB, couple to the same quantum numbers as the Z, the photon, and one which does not couple to the leptons at all. The first two states are analogous to the KK Z and the KK photon in Randall-Sundrum models (cf. [43, 102]). This basis is relevant because the "KK Z" contribution leads to $C_9 = (4s_w^2 - 1)C_{10}$ just as the Z-mediated one, while the "KK photon" contribution affects only C_9 and not C_{10}. In addition, the part of the "KK Z" contribution that involves the composite-elementary mixings Δ_{u_L} is forbidden by the same custodial protection that protects the $Zb_L\bar{b}_L$ coupling, while a similar protection is absent for the "KK photon" contribution. This is particularly relevant in U(3)$_{\text{RC}}^3$, where the correction involving Δ_{d_L} is flavour diagonal in the mass basis [18], cf. (C.4). As a consequence, the Z-mediated as well as the "KK Z" contribution to the $\Delta F = 1$ operators vanish, while the "KK photon" contribution can be nonzero.

Recently, a number of tensions between measurements and SM expectations have appeared in several observables in rare $b \to s$ decays. This includes in particular

- A suppression of the angular observable P_5' in $B \to K^*\mu^+\mu^-$ [103–105];

- A suppression of the branching ratio of $B_s \to \phi\mu^+\mu^-$ [105, 106];

- A suppression of R_K, the ratio of branching ratios of $B^+ \to K^+\mu^+\mu^-$ and $B^+ \to K^+e^+e^-$ [107].

While the first two of these anomalies could be due to unexpected hadronic effects (see e.g. [108, 109]) and the last one due to a statistical fluctuation, all of them could be explained consistently by a negative NP contribution to the Wilson coefficient C_9^{bs} (a positive contribution to C_{10}^{bs} is allowed in addition) with muons only [110–115]. In composite Higgs models, such lepton flavour non-universal contribution was shown by us to arise if muons carry a significant degree of compositeness [63].[11] In the present setup, since we are considering elementary leptons only, all effects are lepton flavour universal. Although in this case,

---

[11]Another possibility is to introduce composite leptoquarks [116].

the deviation in R_K cannot be explained, the overall agreement with the data could still be significantly improved compared to the SM if there are (lepton flavour universal) NP contributions in C_9^{bs} (and possibly C_{10}^{bs}), which can resolve the tensions in $B \to K^* \mu^+ \mu^-$ angular observables and various branching ratios and give a good fit to the data [115]. As discussed above, such contribution can arise from "KK photon"-like resonance exchanges.

In view of these tensions, we do not impose semi-leptonic $b \to s$ transitions as constraints in our numerical analysis, but rather consider the predictions for them *a posteriori*.

We do however include the branching ratio of $B_s \to \mu^+ \mu^-$ as a constraint. This branching ratio, which has reduced theoretical uncertainties compared to the semi-leptonic decays, was recently observed by LHCb and CMS [117] in agreement with the SM expectation [118],

$$\mathrm{BR}(B_s \to \mu^+ \mu^-)_{\mathrm{SM}} = (3.65 \pm 0.23) \times 10^{-9}\,, \tag{3.41}$$

$$\mathrm{BR}(B_s \to \mu^+ \mu^-)_{\mathrm{exp}} = (2.8^{+0.7}_{-0.6}) \times 10^{-9}\,. \tag{3.42}$$

In the presence of new physics, the branching ratio is modified as

$$\frac{\mathrm{BR}(B_s \to \mu^+ \mu^-)}{\mathrm{BR}(B_s \to \mu^+ \mu^-)_{\mathrm{SM}}} = \frac{|C_{10}^{bs} - C_{10}'^{\,bs}|^2}{|(C_{10}^{bs})_{\mathrm{SM}}|^2}\,. \tag{3.43}$$

Again, the imaginary parts and the chirality structure can be constrained by other observables in exclusive and inclusive semi-leptonic decays.

3.2.6 Contact interactions

Four-quark contact interactions are constrained by measurements of the dijet angular distribution at LHC. These constraints become relevant when some of the first-generation quark fields have a significant degree of compositeness. This is unavoidable in the $U(3)^3$ models, but also occurs in part of the parameter space of the $U(2)^3$ models. The relevant four-quark operators involve only the first generation quarks as the contribution from the other generations is PDF-suppressed. The Wilson coefficients are computed analogously to the $\Delta F = 2$ ones in section 3.2.4. Experimental bounds are usually quoted on operators in an $SU(2) \times U(1)_Y$ gauge-invariant basis. Using the notation of [119], their Wilson coefficients can be related to the ones in the low-energy basis as

$$c_{qq}^{(1)} = C_{VLL}^{uu} + \frac{1}{6} C_{VLL}^{uddu}\,, \qquad\qquad c_{qq}^{(8)} = C_{VLL}^{uu}\,, \tag{3.44}$$

$$c_{qu}^{(1)} = C_{VLR}^{uu} - \frac{1}{6} C_{SLR}^{uu}\,, \qquad\qquad c_{qu}^{(8)} = -\frac{1}{6} C_{SLR}^{uu}\,, \tag{3.45}$$

$$c_{uudd}^{(1)} = C_{VRR}^{uudd} + \frac{1}{3} C_{VRR}^{uddu}\,, \qquad\qquad c_{uudd}^{(8)} = 2 C_{VRR}^{uddu}\,, \tag{3.46}$$

$$c_{uu}^{(1)} = C_{VRR}^{uu}\,, \qquad\qquad c_{dd}^{(1)} = C_{VRR}^{dd}\,, \tag{3.47}$$

and with the appropriate replacement $u \to d$ for $c_{qd}^{(1,8)}$. In addition to the operators in (3.19), (3.20) and the ones with $d \to u$, we have defined

$$Q_{VLL}^{uddu} = (\bar{u}_L \gamma^\mu d_L)(\bar{d}_L \gamma^\mu u_L)\,, \qquad\qquad Q_{VLL}^{uudd} = (\bar{u}_L \gamma^\mu u_L)(\bar{d}_L \gamma^\mu d_L)\,, \tag{3.48}$$

as well as $L \to R$.

The Wilson coefficients of the four-quark operators in the low-energy basis can be computed analogously to the $\Delta F = 2$ Wilson coefficients in section 3.2.4. However, an important difference is that the measurement of the dijet angular distribution at LHC involves processes at much higher energies compared to meson decays. The EFT approach is only valid if the exchanged resonances are much heavier than the typical energy scale of the process in question. In [120], it has been shown that for resonance masses below about 5 TeV, the contact interaction bounds become much weaker than a naive application of the EFT would suggest. To account for this fact in an approximate way, we follow a prescription advocated in this paper and multiply every individual contribution to the four-quark operators arising from exchange of a resonance with mass m_{ρ_i} by a correction factor $(1 + C^2/m_{\rho_i}^2)^{-2}$, adopting $C = 1.3$ TeV as a rough estimate based on a numerical analysis of the full mass dependence in two benchmark scenarios [120].

ATLAS and CMS have presented constraints on contact interactions using the full run-1 data set. However, the constraints are only quoted for a single operator (in the case of ATLAS) or for individual operators, but only allowing one at a time (in the case of CMS). In our case, multiple operators might be present simultaneously, and the operators with right-handed quarks typically differ for up- and down-type quarks. The full dependence of the dijet angular distribution on all operators has been discussed in [119] and simple formulae for the impact of the operators in specific rapidity bins have been presented there for the 7 TeV LHC. We use these results, updated to the 8 TeV LHC, to obtain the relative contributions of individual operators to the differential cross section, while we use the bound on the Wilson coefficient $c_{qq}^{(1)}$ quoted by the experimentalists for the normalization. Details on the procedure are discussed in appendix D.

3.3 Direct searches

In addition to the *indirect* searches, i.e. precision constraints from flavour, electroweak, and Higgs physics, composite Higgs models are also subject to increasingly strong *direct* constraints from searches for composite resonances at the LHC. Since we are focusing on a model with a minimal Higgs sector and we are ignoring partial compositeness of leptons, in our case the relevant searches are the ones for quark partners, to be discussed in section 3.3.1, and for spin-1 resonances, to be discussed in section 3.3.2.

3.3.1 Quark partners

Pair production of heavy quarks and subsequent decay to SM quarks and weak bosons has been searched for at Tevatron and LHC. Recently, also final states involving the Higgs have been included in the searches. In the simplest case where only decays to third generation quarks and a W, Z or Higgs are allowed, these channels can be combined to obtain stringent bounds on the masses of vector-like 3rd generation quark partners. In our numerical analysis, we aim to be more general since in principle, a quark partner can have several relevant decay modes involving SM or partner quarks, 3rd or light generation quarks. To this end, we compute the production cross section times branching ratio of each quark partner in each experimentally relevant decay mode, and compare it directly to the upper bounds on this quantity provided in the experimental analysis.

Decay	Experiment	$\sqrt{s}$ [TeV]	Luminosity [fb^{-1}]	Analysis	
$Q \to tW$	CMS	7	5	B2G-12-004	[121]
$Q \to jW$	ATLAS	7	1.04	EXOT-2011-28	[122]
	CDF	1.96	4.6		[123]
$Q \to qW$	CMS	8	19.7	B2G-12-017	[124]
$Q \to jZ$	CDF	1.96	1.055		[125]
$U \to tZ$	CMS	7	5	B2G-12-004	[121]
	CMS	7	1.1	EXO-11-005	[126]
$D \to bH$	ATLAS	8	20.3	CONF-2015-012	[127]
	CMS	8	19.8	B2G-12-019	[128]
	CMS	8	19.5	B2G-13-003	[129]
	CMS	8	19.7	B2G-14-001	[130]
$D \to bZ$	CMS	7	5	EXO-11-066	[131]
	CMS	8	19.8	B2G-12-019	[128]
	CMS	8	19.5	B2G-13-003	[129]
	CMS	8	19.6	B2G-12-021	[132]
$D \to tW$	ATLAS	8	20.3	EXOT-2013-16	[133]
	CMS	8	19.8	B2G-12-019	[128]
	CMS	8	19.5	B2G-13-003	[129]
	CDF	1.96	2.7		[134]
$Q \to bW$	CMS	7	5	EXO-11-050	[135]
	CMS	7	5	EXO-11-099	[136]
	ATLAS	7	4.7	EXOT-2012-07	[137]
	ATLAS	8	20.3	CONF-2015-012	[127]
	CMS	8	19.7	B2G-12-017	[124]
$Q_{5/3} \to tW$	ATLAS	8	20.3	EXOT-2013-16	[133]
	ATLAS	8	20.3	EXOT-2014-17	[138]
	CMS	8	19.6	B2G-12-012	[139]
$U \to tH$	CMS	8	19.7	B2G-12-004	[140]

Table 2. Experimental analyses included in our numerics for heavy quark partner decay. Q stands for any quark partner where the decay in question is allowed by electric charges, j stands for a light quark or b jet, and q for a light quark jet.

For the pair production cross section, we simply take the model-independent NNLO QCD production cross section for a heavy quark computed in Hathor [141]. This means we neglect

- Single production, that is relevant for quarks that have a significant degree of compositeness, and in this case dominates at higher masses [26–30, 142];

- Contributions to the pair production cross section from heavy resonance exchange [143, 144].

Taking into account these two effects is beyond the scope of our study, as it cannot be implemented efficiently in a fast parameter scan. The bounds we obtain should thus be considered conservative.

Since the experimental analyses typically quote bounds on the pair production cross section assuming a 100% branching ratio to the desired final state, we correct for the branching ratio $\mathrm{BR}(Q \to f)$ of the quark partner to final state f by multiplying the production cross section with

- $\mathrm{BR}(Q \to f)^2$ in case the experimental analysis requires both partners to decay to f;

- $(1-(1-\mathrm{BR}(Q \to f))^2)$ in case the experimental analysis requires one or both of the partners to decay to f.

In the M4DCHM5, there are in total 24 heavy charge-2/3 quarks (denoted with U in the following), 24 charge-$(-1/3)$ quarks (D), as well as 6 exotic charge-5/3 quarks ($Q_{5/3}$) and 6 charge-$(-4/3)$ quarks ($Q_{-4/3}$). The decay modes always involve one SM quark or quark resonance plus one W, Z, Higgs, or vector resonance. In our numerical analysis, we can only impose constraints on decays involving SM particles only. This is not a strong restriction since the lightest quark partners are always required to decay to SM states for kinematic reasons. In table 2, we list all the experimental searches that we include in our numerical analysis for the individual decay modes. In this table, Q stands for any quark partner where the decay in question is allowed by electric charges, j stands for a light quark or b jet, and q for a light quark jet. Note that there are no dedicated searches for the $Q_{-4/3}$, but searches of the type $Q \to (bW, jW, qW)$ are also sensitive to these states.

An important point concerning the experimental coverage of parameter space is that the experiments typically employ a hard p_T cut to reduce backgrounds. This maximizes the sensitivity to heavy states, but misses out on the low end of the mass spectrum. In fact, combining all existing analyses in table 2, we have identified a number of gaps in the coverage of quark partner masses. This is illustrated by the plots in figure 2. They show the 95% C.L. upper bound on the branching ratio in the decay modes to W or Z bosons as a function of the quark partner mass. We make the following observations.

- When kinematically allowed, there is a gap between the LEP bound of $100\,\mathrm{GeV}$ and the lower end of the Tevatron bounds. This should however not be taken seriously as quark partners with mass comparable to the top quark would very likely have shown up already.
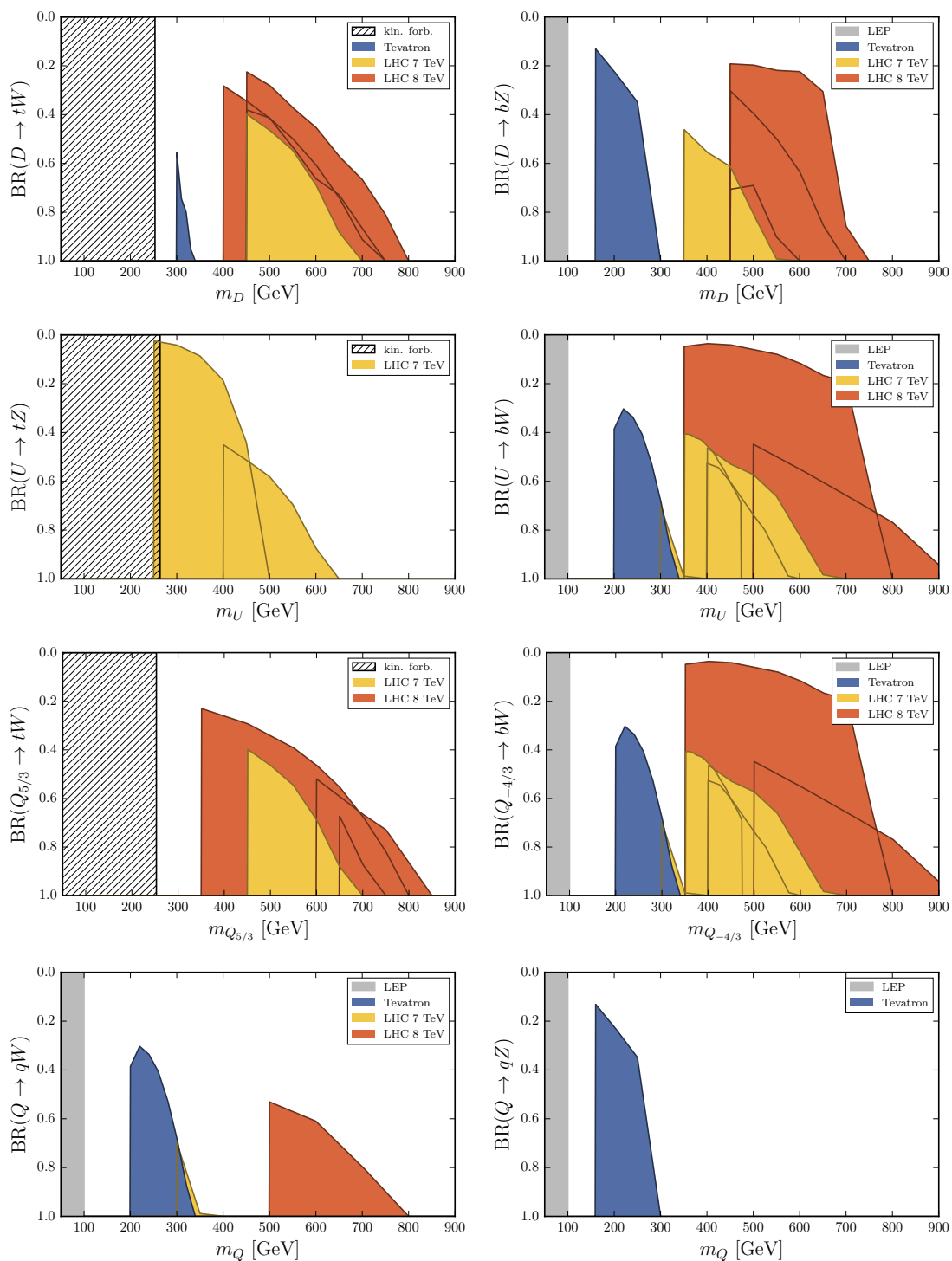
Figure 2. Upper bounds on the branching ratios of quark partners decaying to SM states from individual Tevatron and LHC searches. QCD pair production is assumed. Q stands for any quark partner where the decay is allowed by the electric charges. q stands for a light quark (excluding the b).

- More seriously, there are gaps between the upper end of the Tevatron exclusions and the lower end of the LHC exclusions. This leaves a window between about 300 and 350–500 GeV not covered by existing searches.[12] The only exception is the mode $U \to tZ$, but quark partners around 300 GeV would have a very small phase space to decay to tZ, making it plausible that the branching ratio is smaller than in the other channels.

- Bounds on light quark partners are weak, with no existing LHC search for the decay mode involving the Z boson. This is problematic since, depending on their quantum numbers, some of the light generation partners have very small branching ratio into qW as will be demonstrated in section 4.5.1 below.

Concerning the gaps mentioned in the second item, they could very likely be closed by a reanalysis of existing run-1 data (this is also indicated by recasting of some existing new physics searches, see e.g. [145]). We call upon the experimental collaborations to perform such a reanalysis, given the importance of the partner mass scale for naturalness and radiative electroweak symmetry breaking in the models at hand. In our numerical analysis, in order not to be biased by these low-mass regions for quark partners, we have imposed a hard lower bound of 500 GeV on all quark partner masses, in addition to the LHC 7 and 8 TeV searches that are sensitive to higher masses (while the Tevatron searches become irrelevant).

3.3.2 Spin-1 partners

Spin-1 resonances can be pair-produced in a Drell-Yan like process. If narrow enough, they would show up as a peak in the dilepton, dijet, $t\bar{t}$, VV, or Vh final state, depending on the branching ratios. In the models considered by us, the spin-1 and spin-1/2 resonances are strongly coupled to each other. Consequently, if the decay to two fermion resonances is kinematically allowed, the resonances become very broad and are not captured by the experimental analyses anymore.[13] Still, we expect that they are sufficiently narrow in part of the parameter space, so we include the experimental constraints.

The hadronic production cross section of a spin-1 resonance can be written as

$$\sigma(pp \to \rho + X) = \sum_{q_1 q_2} \frac{\Gamma(\rho \to q_1 \bar{q}_2)}{s \, m_\rho} \frac{4\pi^2}{3} \mathcal{L}_{q_1 \bar{q}_2} c_\rho \,, \tag{3.49}$$

where $q_{1,2} = u$ or d, c_ρ is the colour multiplicity of the resonance ($c_\rho = 1$ for electroweak resonances and $c_\rho = 8$ for ρ_G), s is the hadronic center-of-mass energy squared and $\mathcal{L}_{i_1 i_2}$ is the parton-parton luminosity of the relevant initial state defined as

$$\mathcal{L}_{q_1 \bar{q}_2}(s, \hat{s}) = \int_{\hat{s}/s}^1 \frac{dx}{x} f_{q_1}(x, \mu) f_{\bar{q}_2}\left(\frac{\hat{s}}{xs}, \mu\right) \,. \tag{3.50}$$

For the Tevatron, (3.49) is valid with the appropriate replacements.

---

[12]The presence of a gap between Tevatron and LHC 7 TeV searches has already been noticed in [23].

[13]They would however still constitute a contribution to the pair production cross section of the fermion resonances, see the comment in section 3.3.1.

Decay	Experiment	$\sqrt{s}$ [TeV]	Lum. [fb^{-1}]	Analysis	
$\rho^\pm \to \ell^\pm \nu$	ATLAS	7	4.7	EXOT-2012-02	[146]
$\rho^\pm \to W^\pm h$	ATLAS	8	20.3	EXOT-2013-23	[147]
	CMS	8	19.7	EXO-14-010	[148]
$\rho^\pm \to W^\pm Z$	ATLAS	8	20.3	EXOT-2013-01	[149]
	ATLAS	8	20.3	EXOT-2013-07	[150]
	ATLAS	8	20.3	EXOT-2013-08	[151]
	CMS	8	19.7	EXO-12-024	[152]
$\rho^\pm \to tb$	CMS	8	19.5	B2G-12-010	[153]
$\rho^0 \to W^+ W^-$	ATLAS	8	20.3	EXOT-2013-01	[149]
	CMS	8	19.7	EXO-13-009	[154]
$\rho^0 \to Zh$	ATLAS	8	20.3	EXOT-2013-23	[147]
	CMS	8	19.7	EXO-13-007	[155]
$\rho^0 \to \ell^+ \ell^-$	ATLAS	8	20.3	EXOT-2012-23	[156]
	CMS	8	20.6	EXO12061	[157]
$\rho^0/\rho_G \to t\bar{t}$	ATLAS	8	20.3	CONF-2015-009	[158]
	CMS	8	19.5	B2G-12-008	[159]

Table 3. Experimental analyses included in our numerics for heavy vector resonance decay.

The M4DCHM5 contains 3 charged and 5 neutral electroweak vector resonances, plus the colour-octet gluon resonance. As in the spin-$\frac{1}{2}$ case, we can only impose constraints on decays to SM states. We include all the analyses listed in table 3. The only relevant final state that we have not included is the decay to dijets. The reason is that the experimental bounds on the dijet resonance cross section depend on an acceptance factor that is model dependent and that is not easy to take into account in a parameter scan.

In our numerical analysis, we employ a cut of 5% on the relative total width Γ_ρ/m_ρ, above which all bounds are ignored for an individual resonance. While several of the analyses are actually sensitive to broader resonances, it is not possible to include this dependence in a parameter scan. As in the case of fermion resonances, our bounds should thus be considered as conservative.

3.3.3 LHC excesses

Interestingly, several of the searches for spin-1 resonances we include as constraints contain an excess of events around 2 TeV. The most significant deviation is in the ATLAS search for $\rho^\pm \to WZ$, corresponding to a local significance of 3.4σ, but an excess around the same mass appears also in the corresponding CMS search, and, to a lesser extent, in searches for WW or Wh final states. This is particularly interesting in the context of composite Higgs

models as the resonances associated to $SU(2)_L$ (denoted $\rho_{L\mu}$ in the gauge eigenstate basis in section 2) form a triplet of a charged and a neutral vector that are almost degenerate, have approximately equal branching ratios to WZ, WW, Wh, and Zh final states, and can have a production cross section in the right ballpark to explain these excesses [36, 37, 160–164].

4 Numerical analysis and predictions

This section contains the main results of our paper. After describing the numerical analysis procedure in section 4.1, we will discuss fine-tuning in all models in section 4.2.2, the numerical results of signals in indirect searches in $U(2)^3_{LC}$ in section 4.3, for indirect searches in $U(2)^3_{RC}$ and $U(3)^3_{RC}$ in section 4.4, and for direct LHC searches in all models in section 4.5.

4.1 Strategy

4.1.1 Scanning procedure

Our aim is to sample the parameter space of the M4DCHM with four different flavour structures while satisfying all the experimental constraints discussed in section 3. This is particularly challenging because partial compositeness implies that all SM masses and couplings are relatively complicated functions of the model parameters and the additional requirement of correct radiative EWSB is even harder to control analytically. To cope with these challenges, we have improved a method first employed in [46]. We construct a χ^2 function depending on all the theoretical predictions for all constraints discussed in section 3 as well as the corresponding experimental measurements. We then proceed in four steps.

1. We randomly generate a set of input parameters that only fulfills the most rudimentary consistency conditions (e.g. composite gauge couplings being greater than 1, effective potential possesses a minimum away from zero).

2. We use brute-force numerical minimization (with `NLopt` [165]) to "burn-in" into a region of parameter space not too far from viability.

3. We use a Markov Chain Monte Carlo (MCMC, with `pypmc` [166]) to sample the viable parameter space.

4. We filter the Markov chains so that only points remain where each individual constraint is satisfied at the 3σ level.

After the burn-in phase, the generation of viable parameter points is very efficient, as the MCMC is adaptive and has an acceptance rate around 23%. The downside of the method is that adjacent points have high autocorrelation, implying that very long chains are needed to obtain a reasonable coverage of the parameter space. Furthermore, the parameter space can contain several disconnected minima. For these reasons, we run a large number of chains (around 500 for each model) starting at different (random) initial points.

We stress that we do not interpret the outcome of the Markov Chain statistically, in the sense of a posterior probability distribution for the model parameters. Apart from the problem of reaching sufficient coverage of the parameter space, this would be problematic

due to dependence on the choice of priors. Instead, we use the MCMC algorithm as a shortcut to generate a sufficient number of valid points. In our final sample, these points approximately follow a normal distribution peaked around 30–40, for 48 individual contributions to the χ^2. We also find that model-independently for nearly all points only ≤ 5 individual constraints are violated by more than 2σ at a time. Consequently, the hard 3σ cut only removes a small fraction of extreme points. The largest deviations are typically found for m_t, $\mathrm{BR}(B \to X_s\gamma)$, the inclusive values of V_{ub} and V_{cb}, and for the Higgs signal strengths.

4.1.2 Model parameters

Below, we specify the model parameters and any relations we have imposed among them in our scan.

- f, f_1, f_X, f_G.

  We have imposed $1 < f_1/f < \sqrt{3}$, where the lower bound corresponds to a decoupling of the axial resonances and the upper bound is motivated by the partial unitarization of Goldstone boson scattering [13]. We have not assumed f_1, f_X, and f_G to be degenerate, but we have restricted them to be within a factor of two, i.e. $\frac{1}{2} \leq f_{X,G}/f_1 \leq 2$, to prevent the fit from completely decoupling one of the resonances.

- g_ρ, g_X, g_G.

  We have varied these couplings completely independently, only imposing $1 < g_{\rho,X,G} \leq 4\pi$ to have a strong but semi-perturbative coupling (in the case of the gluon resonance, we also imposed $g_G > g_{s0}$). We further imposed $f_{1,X,G}\, g_{\rho,X,G}/\sqrt{2} < 4\pi f$, to not have resonance masses above the (naive) cutoff of the theory.

- g_0, g_0', g_{s0}.

  These parameters are fixed by the known gauge couplings once the composite gauge couplings are specified.

- m_Q, $m_{\widetilde{Q}}$, m_{Y_Q}, $m_{Y_Q} + Y_Q$ where $Q = U$ or D, in the case of U(2)^3 different for the first two and the third generation.

  In our numerical analysis described above, we have treated the *logarithms* of these parameters as scan parameters, in order not to get a bias towards heavier masses. The only relation (apart from the ones forced by the flavour symmetries) we have imposed is that all these parameters are $< 4\pi f$. Note that this implies that the above parameters can only take positive values in our scan, but this can always be arranged by a suitable choice of phases for the fermion fields.

- Quantities parametrizing the composite-elementary mixings, see appendix C for details.

  Again, we have scanned dimensionful parameters logarithmically and require them to be $< 4\pi f$, but otherwise we impose no restrictions (many relations among these parameters are fixed by the requirement to have the correct quark masses and CKM mixing).

With these assumptions, the total number of real parameters or phases is 44 for $U(2)^3_{LC}$ and $U(2)^3_{RC}$ and 30 for $U(3)^3_{LC}$ and $U(3)^3_{RC}$. To compare these parameters to the SM, it should be noted that we do not treat lepton masses as free parameters, have massless neutrinos and set the QCD $\bar{\theta}$ term to zero, but the Higgs mass and VEV are predictions rather than inputs.

4.2 General fit results and fine-tuning

4.2.1 Failure of $U(3)^3_{LC}$

In the case of $U(3)^3_{LC}$, our scans have not been able to find a single viable parameter point, even for a large number of chains. This is not surprising as already a qualitative analysis of the relevant constraints on $U(3)^3_{LC}$ [18] has revealed that there are extremely strong constraints on the model from electroweak precision test and CKM unitarity. It seems to be impossible to reconcile these constraints with the need for correct radiative EWSB. We will thus not consider $U(3)^3_{LC}$ any further.

4.2.2 Fine-tuning

Before discussing predictions for physical observables, let us address the degree to which the viable model points we have found can address the electroweak hierarchy problem. To this end, we have computed the Barbieri-Giudice fine-tuning measure [167]

$$\Delta_{BG} = \max_i \left| \frac{\partial \ln m_Z}{\partial \ln x_i} \right| \tag{4.1}$$

that quantifies the sensitivity of the weak scale to variations in the model parameters x_i. In composite Higgs models, Δ_{BG} can be obtained directly from derivatives of the potential [168]. Still, given the large parameter space, the computation turns out to be more time-consuming than for the physical observables, so we have computed Δ_{BG} only for a subset (2%) of all our points. The results for the three viable models are shown in figure 3.[14] Not surprisingly, the lowest Δ_{BG} is obtained for low f and a sub-percent fine-tuning is possible in all models as long as $f \lesssim 1\,\text{TeV}$. This is compatible with earlier analyses in similar models [168, 169]. The points with the lowest tuning measure, highlighted by stars in the plot, have

- $\Delta_{BG}^{\min} = 33$ for $U(2)^3_{LC}$,

- $\Delta_{BG}^{\min} = 55$ for $U(2)^3_{RC}$,

- $\Delta_{BG}^{\min} = 73$ for $U(3)^3_{RC}$.

Two comments are in order here. First, we reiterate that we define viability for a point as fulfilling all individual constraints at 3σ. Since we assume a 5% relative uncertainty on m_t and m_h (see section 3.1), the known tendency of the model to have a too heavy Higgs and a too light top means that the points with lowest tuning typically have the Higgs and

---

[14]Note that the individual "speckles" — visible in many of the scatter plots — correspond to different Markov chains.

top mass 15% away from their central values. Second, we stress that there are variants of the model considered by us that have lower fine-tuning since the M4DCHM5 suffers from a "double tuning" by an accidental enhancement of the Higgs mass due to the structure of the potential, see [168] for a discussion and alternatives.

To get a better understanding of the tuning in the Higgs potential, we adopted an expansion of the potential in terms of s_h (as also used e.g. in [13]),

$$V_{\text{eff}} \approx -\gamma \, f^4 \, s_h^2 + \beta \, f^4 \, s_h^4, \tag{4.2}$$

where we have explicitly defined the γ and β parameters as dimensionless by factoring out their typical scale f^4 and we have neglected terms of $\mathcal{O}(s_h^6)$. In this notation, the Goldstone VEV and the Higgs mass are given as

$$s_h^* = \sqrt{\frac{\gamma}{2\beta}}, \qquad m_h^2 = 4\gamma \left(1 - \frac{\gamma}{2\beta}\right) f^2. \tag{4.3}$$

The requirement to fulfill EWPT's (and therefore to have a not too large s_h^*) together with the hierarchy $m_h \ll f$ forces γ to take a rather small value. As already mentioned in [13, 168], this requires a cancellation between the fermion and gauge contributions to a large degree.

In our framework, we can extract the γ and β parameters for each contributing field by simply fitting the numerical values of (2.23) to the parametrization (4.2). We indeed find that the fit prefers highly correlated gauge and fermion contributions that are large individually but almost completely compensate each other. We also find large cancellations between the up- and down-quark sector and also between individual contributions in each sector.

4.3 Left-handed compositeness: indirect searches

As discussed in section 4.2.1, we have not found any viable points for $\mathrm{U}(3)_{\mathrm{LC}}^3$. We will thus restrict ourselves to $\mathrm{U}(2)_{\mathrm{LC}}^3$ in this section.

4.3.1 Light quark compositeness

Compositeness of the first two generation quarks is mainly constrained by

- First-row CKM unitarity, see section 3.1.2;

- The hadronic Z width, see section 3.2.2;

- The dijet angular distribution at LHC, see section 3.2.6.

The predictions for these quantities are shown in figure 4. The left-hand plot shows the effective CKM elements $|V_{us}|$ vs. $|V_{ud}|$ and demonstrates that large deviations from the SM relation $|V_{us}|^2 + |V_{ud}|^2 \approx 1$ (shown as a black line) are possible. The solid gray lines show the current experimental 2σ bounds. At 3σ, the points stop because of our procedure described above. On the right, we show the predictions for the hadronic Z width as defined in (3.14) (the SM central value is shown as a black line) vs. the $pp \to jj$ cross section in
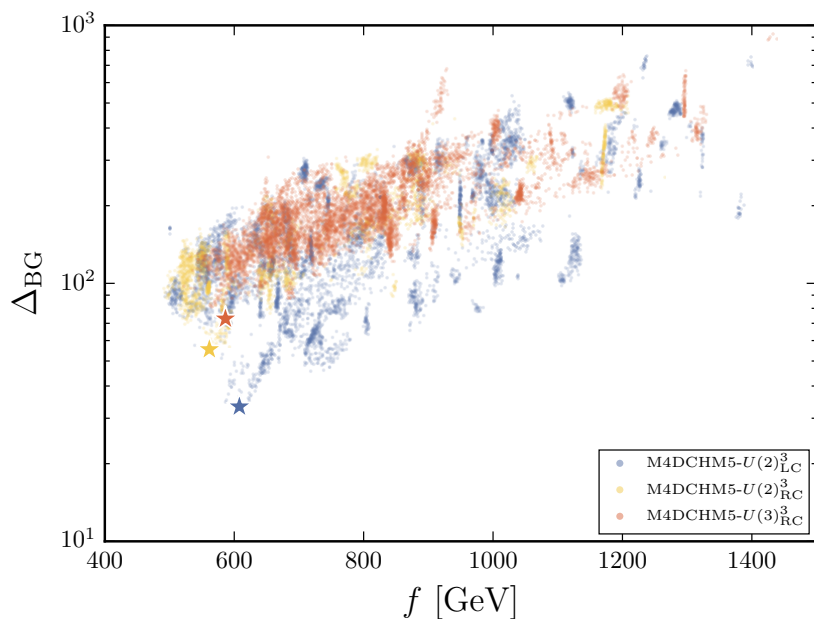
Figure 3. Barbieri-Giudice fine-tuning measure vs. f for the three viable models for a thinned-out sample of all our viable parameter points. The stars show the points with lowest fine-tuning measure for each model.
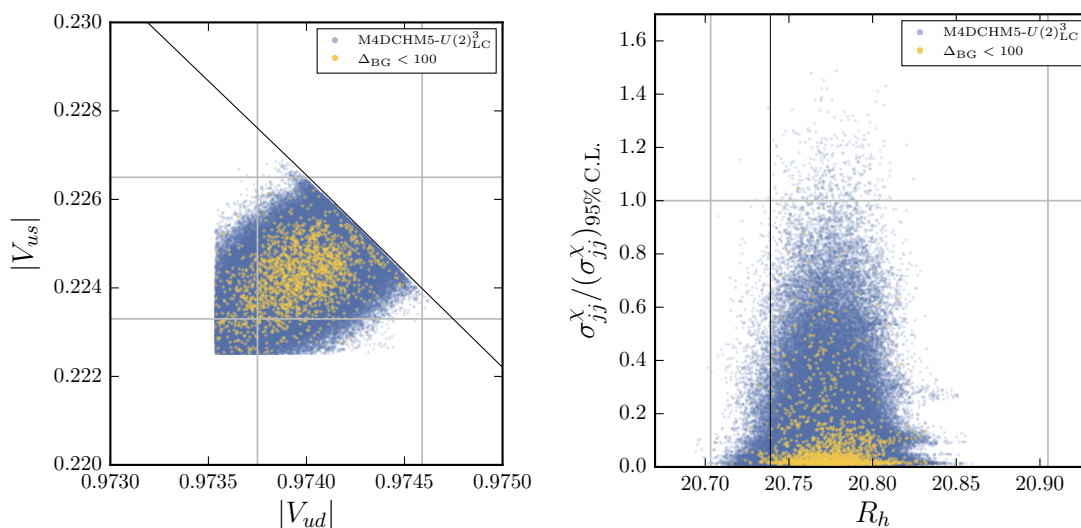
Figure 4. Observables sensitive to light quark compositeness in $U(2)^3_{LC}$. Left: first-row effective CKM elements. The black line corresponds to the SM limit of a unitary CKM matrix. Right: hadronic Z width (normalized to $Z \to e\bar{e}$) vs. the $pp \to jj$ cross section in the rapidity bin described in appendix D, normalized to the 95% C.L. limit extracted from the ATLAS analysis. The black line corresponds to the central value of the SM prediction.

the bin described in appendix D, normalized to the 95% C.L. limit extracted from the ATLAS analysis. This plot shows that sizable effects are possible in these observables as well, but almost all points lie within the 2σ region for both observables (shown as solid

gray lines), demonstrating that CKM unitarity is by far the strongest constraint on light quark compositeness in $U(2)^3_{LC}$ at present.

In these plots (as in almost all the plots of this section), on top of all the viable points in blue, we show points that have a fine-tuning measure $\Delta_{BG} < 100$ in yellow. The rationale is to demonstrate in which part of the viable space for the observables in question the most "natural" parameter points lie. We warn the reader however that these points do *not* correspond to *all* viable points with $\Delta_{BG} < 100$ — as mentioned in section 4.2.2, we have only computed Δ_{BG} for a subset of the points. One should also keep in mind that, simply due to their smaller number, these points typically cluster in the region with the highest point density.

4.3.2 Higgs production and decay

The left-hand plot in figure 5 shows the signal strengths of the Higgs produced in gluon fusion and decaying to ZZ (which equals the one to WW due to custodial symmetry), $\gamma\gamma$, and $b\bar{b}$. Most of the points lie on the curves that are expected from analytical considerations of coupling modifications (see e.g. [170]). This is even true for $h \to \gamma\gamma$ and $gg \to h$, since in pNGB Higgs models, the loop contribution of heavy resonances to these processes almost entirely cancels with the coupling modification of the top quark, leaving the Higgs non-linearities as the dominant effect [22].

However the plot also shows deviations from these relations. These can be understood to be caused by light quark compositeness, spoiling the above mentioned cancellation [171]. In this way, the signal strength can be closer to (or further away from) their SM values than naively expected for small f. Nevertheless, we find this effect to be mild, given the strong constraints on light quark compositeness discussed in the previous section.[15]

Concerning the $h \to b\bar{b}$ signal strength, we note that the figure shows the signal strength in the case of gluon fusion production, while the experimental bounds are currently based on the associated production with vector bosons, that we do not include in our analysis.

4.3.3 Oblique parameters

The right-hand plot in figure 5 shows the predictions for the S and T parameters. We show the region allowed by experiment at 2σ as a gray dashed ellipse, while the gray solid ellipse takes into account also the additional theory uncertainty discussed in section 3.2.1. The tree-level contribution to S is strictly positive, while the fermionic loop contribution to T can have either sign, but is preferred to be positive by experiment for positive values of S and indeed large positive contributions are possible for our choice of fermion representations, which is important as it helps to alleviate the bound from S.

4.3.4 Meson-antimeson mixing

Figure 6 shows the predictions for $\Delta F = 2$ observables in $U(2)^3_{LC}$. In the left-hand column, we directly show the correlation between observables. In this case, it is important to

---

[15]The fact that almost all points lie on the same curve and only a few individual Markov chains have strayed away from it explains the frayed appearance of the plot.
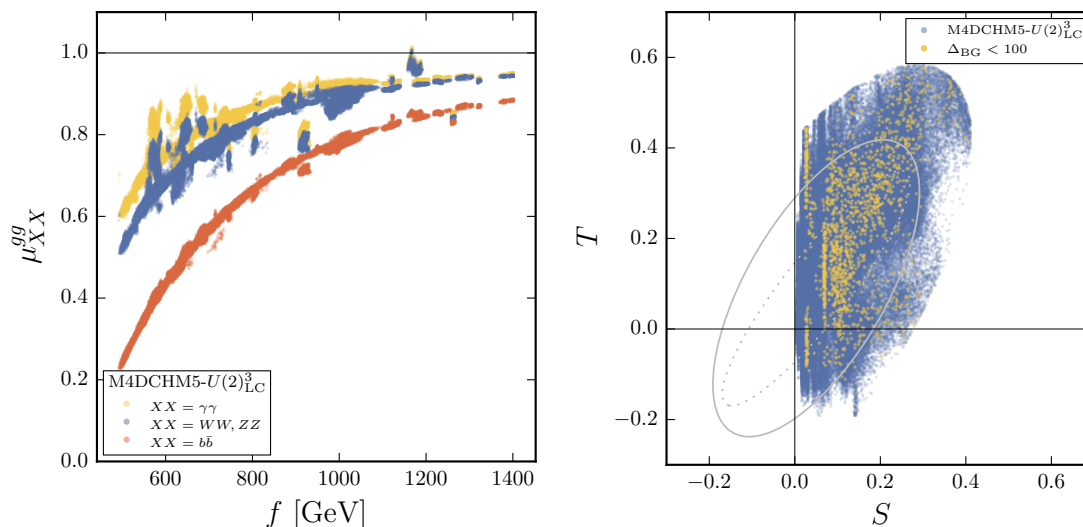
Figure 5. Left: Higgs signal strength for gluon fusion production and decay to final states ZZ (equal to WW by custodial symmetry), $\gamma\gamma$, and $b\bar{b}$ in $\mathrm{U}(2)^3_{\mathrm{LC}}$. The SM corresponds to $\mu = 1$, shown as a horizontal line. Right: oblique parameters S and T in $\mathrm{U}(2)^3_{\mathrm{LC}}$, defined to be 0 in the SM.

notice that the CKM parameters themselves are varied in our fit and are not fixed to their SM central values (as is often done in parameter scans of, e.g., SUSY models). As a consequence, any correlations among (tree-level) NP contributions are washed out by the spread in the allowed values for the CKM parameters. The dashed gray lines in these plots show the allowed regions with merely the experimental 2σ uncertainties, while the solid gray contours take into account additionally the (correlated) theory uncertainties at 2σ. As discussed in section 3.2.4, we only need to account for the non-CKM (i.e., lattice) theory uncertainties, as for a given point, the CKM parameters are predictions.

While these plots are more directly related to the experimental measurements, the variation of CKM parameters obscures the relation to the NP contributions. This is why in the right-hand column of figure 6 we show the ratios (or phase differences) of the observables and the SM W-loop contribution for each parameter point. In this way, the correlations valid at leading order in the $\mathrm{U}(2)^3$ spurion expansion, $\Delta M_d / \Delta M_d^{\mathrm{SM}} = \Delta M_s / \Delta M_s^{\mathrm{SM}}$ and $\phi_s - \phi_s^{\mathrm{SM}} = \phi_d - \phi_d^{\mathrm{SM}}$ (where $S_{\psi K_S} = \sin\phi_d$), shown by solid black lines in the plots, become apparent. In the bottom right plot, the black line corresponds to the MFV limit of equal relative modification in the B_d and K^0 mixing amplitudes, while no such correlation is expected in $\mathrm{U}(2)^3$. We make the following observations.

- The mass differences in the B_d and B_s systems can receive corrections up to $+60\%$, but negative NP contributions are disfavoured. This can be understood from the fact that the tree-level Wilson coefficient of $Q_{VLL}^{d_i b}$, cf. (3.21), involves the square of a coupling that carries a small phase.

- The B_s mixing phase can saturate the experimental lower bound, but positive values for $\sin\phi_s$ are only predicted for a small number of points. This is due to the correlation
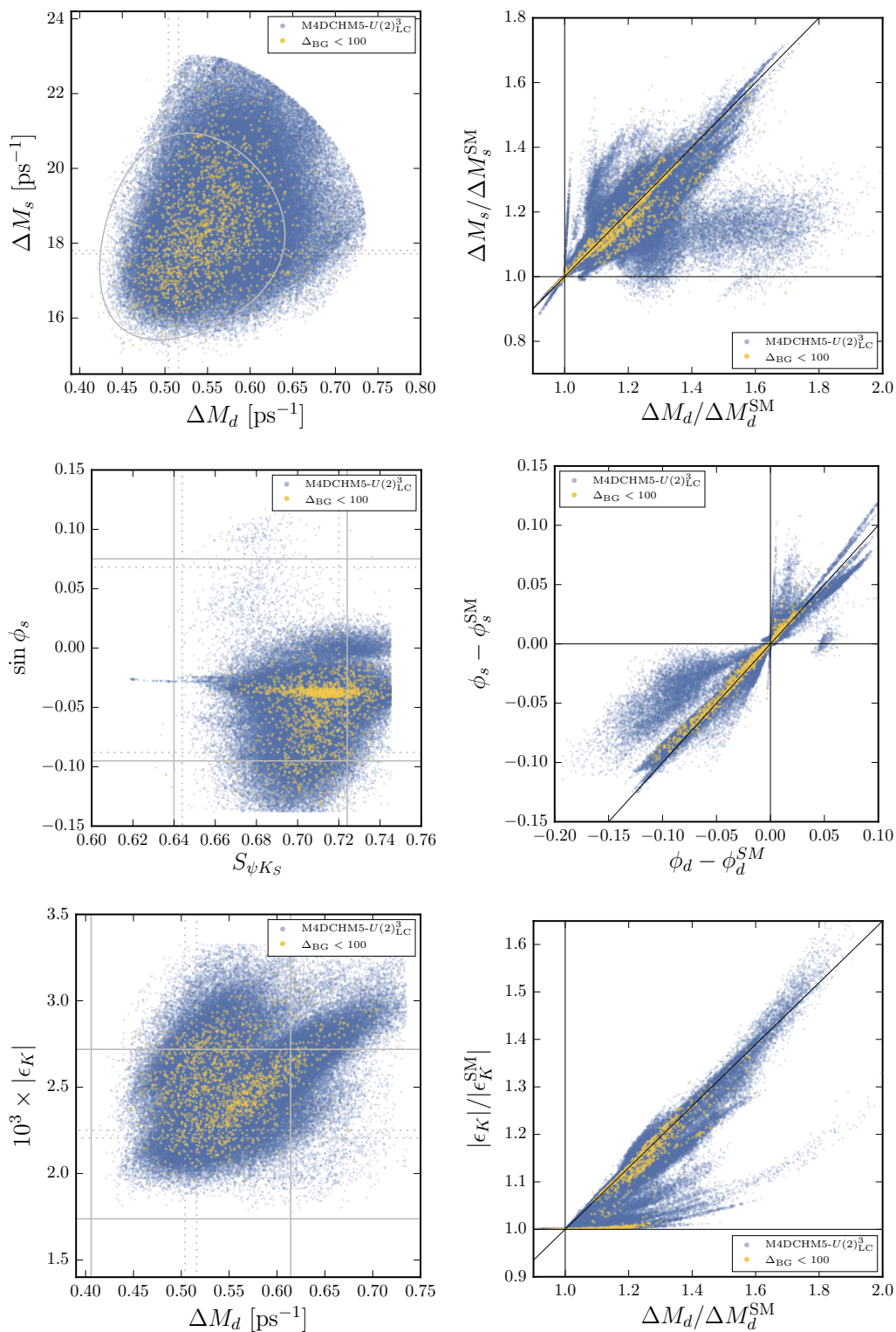
Figure 6. $\Delta F = 2$ observables in U(2)$^3_{\mathrm{LC}}$.

with ϕ_d and the preference for a negative NP contribution to the latter, that is also visible in global CKM fits [80, 172, 173].

- Both for the mass differences and for the phases in the B_d and B_s systems, the leading-order $U(2)^3$ correlations are broken for a significant fraction of the points, seen as a deviation from the black diagonal lines. This is due to non-negligible contributions from left-right operators. We have identified two reasons for why these effects are larger than expected from a general EFT analysis [61].

  1. The Wilson coefficients of these operators are RG-enhanced;
  2. Due to partial compositeness and the possibility to have a hierarchy even among the (diagonal) left-handed composite-elementary mixings, the spurion hierarchies in the right-handed mixings can be milder than the Yukawa hierarchies, effectively enhancing subleading terms in the spurion expansion.

  A similar effect has already been noted in the context of the MSSM with a $U(2)^3$ symmetry [172] (where it was mostly due to an accidental enhancement of a loop function) and we find the effect to be even more pronounced in the composite Higgs case. We stress nevertheless that the majority of parameter points does fulfill the $U(2)^3$ relations to a good precision, corresponding to a large density of points around the black lines in the plots.

- The relative modification of ϵ_K compared to the SM is always equal[16] to or smaller than the relative modification of ΔM_d. This confirms the general expectation for $U(2)^3_{\rm LC}$ in [18].

So far, we have not discussed D^0-$\bar{D}^0$ mixing. On the one hand, the D^0 system is plagued by large theoretical uncertainties due to poorly known long-distance contributions; on the other, the effects in $U(2)^3$ models are expected to be small on general grounds [61]. To investigate whether this expectation is correct, we have computed the tree-level NP contribution to the D^0 mixing amplitude in $U(2)^3_{\rm LC}$. Since the SM contribution is expected to be real to a good accuracy, the most promising NP effect would be a CP violating one. A global fit to data from the D system [174] allows to directly constrain the absolute value and the phase of the mixing amplitude. At 2σ, this constrains the imaginary part of the mixing amplitude to be

$$-0.5 \text{ ns}^{-1} \gtrsim \text{Im } M_{12}^D \lesssim 1.6 \text{ ns}^{-1} \,. \tag{4.4}$$

Numerically, we have found that the NP contributions to $\text{Im } M_{12}^D$ are always negative in $U(2)^3_{\rm LC}$ and can reach at most -0.5 ns^{-1}. We conclude that CP violation in D^0 mixing is currently not a relevant constraint on the model, but future improvements of the bound by factors of a few would start to cut into its parameter space. We have further found that the NP contributions to $\text{Im } M_{12}^D$ are strongly anticorrelated with ϵ_K: sizable NP contributions to the former never occur simultaneously with sizable NP contributions to the latter. However, the NP contributions to both observables can be small simultaneously.

---

[16]With a small correction factor stemming from the SM charm contribution.

4.3.5 Rare B decays

The Wilson coefficient C_7^{bs} of the electromagnetic dipole operator, cf. section 3.2.5, receives NP contributions, but only to the extent that is allowed by the strong constraint from the branching ratio of $B \to X_s \gamma$. We find these contributions to be aligned in phase with the SM to a high degree, such that CP violating effects, e.g. in the direct CP asymmetry in $B \to K^* \gamma$, are expected to be small. Contributions to the chirality-flipped coefficient $C_7'^{bs}$ are small by $U(2)^3$ symmetry.

The most interesting effects in rare B decays stem from the tree-level contributions to the semi-leptonic Wilson coefficients C_9^{bs} and C_{10}^{bs}. As discussed in section 3.2.5, there are Z-mediated and resonance-mediated effects that dominantly contribute to C_{10}^{bs}, but also resonance-mediated effects that contribute only to C_9^{bs}. We remind the reader that in our numerical analysis, the only observable sensitive to these Wilson coefficients that we have imposed as a constraint is the branching ratio of $B_s \to \mu^+\mu^-$, essentially limiting the absolute value of C_{10}^{bs}. All points passing this constraint are shown in the left-hand plot of figure 7. We observe that large NP effects in C_{10}^{bs} — saturating the experimental bound on $B_s \to \mu^+\mu^-$ — are possible, but also sizable effects in C_9^{bs}. Interestingly, the largest effects allowed in C_9^{bs} correspond to a negative sign that is preferred by the anomalies in $B \to K^*\mu^+\mu^-$ angular observables discussed in section 3.2.5. The gray ellipse in figure 7 left corresponds to the 2σ preferred region in a global fit to $b \to s\mu^+\mu^-$ observables [115], which shows a clear tension with the SM point $(0,0)$. The figure clearly shows that if these tensions are due to NP, the M4DCHM5-U(2)$_{\text{LC}}^3$ can explain them. This is also demonstrated by the right-hand plot in figure 7, which shows the predictions for two of the observables that currently show the biggest tensions with the SM, namely the low-q^2 branching ratio of $B_s \to \phi\mu^+\mu^-$ and the angular observable P_5' in $B \to K^*\mu^+\mu^-$. In this plot, the black star shows the central value of the SM predictions (taken from [105, 115]), the gray dashed line the values allowed at 2σ by experiment, and the gray solid lines the 2σ allowed values taking into account also the theoretical uncertainties.

We have found that all of the points that have $C_9^{bs} \lesssim -0.5$ — and could thus account for the tensions in angular observables and branching ratios — correspond to a small value (between 1 and 2) of the composite coupling g_X and a correspondingly small mass (below 1 TeV) of the mass eigenstate that is dominantly the ρ_X resonance. This can be understood from the discussion in section 3.2.5: in the limit $g_X \ll g_\rho$, the "KK photon"-like state is dominantly the field ρ_X. In addition, since g_X is not much larger than the elementary gauge coupling, the parametric suppression of the resonance-mediated contribution is lifted. It is also important to notice that this linear combination of gauge fields does not contribute to the S parameter and thus is allowed to be lighter than the other vector resonances. Sizable contributions to B_s-$\bar{B}_s$ mixing are also generated by the exchange of the light resonance, but we find that the shift in ΔM_s is below 20% relative to the SM. We have also computed the LHC production cross section and decay branching ratios of the light resonance for the points with sizable NP effects in C_9. For most of the points, the dominant decay mode is $t\bar{t}$ and the cross-section is just below the ATLAS and CMS searches for resonances in this mode that we have imposed as a constraint in our scan (see section 3.3.2). The width of the
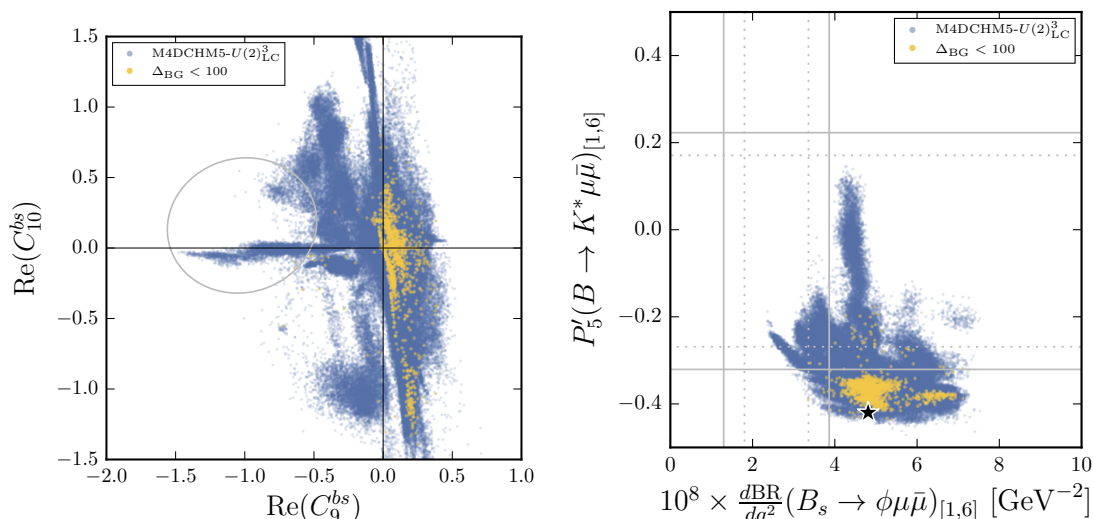
Figure 7. Left: new physics contributions to the Wilson coefficients C_9^{bs} and C_{10}^{bs} in U(2)$^3_{\text{LC}}$. Right: predictions for the angular observable P_5' in $B \to K^* \mu^+ \mu^-$ and the branching ratio of $B_s \to \phi \mu^+ \mu^-$, both in the low-q^2 bin from 1 to 6 GeV^2. The star corresponds to the central values of the SM predictions.

resonance is small enough to show up in a "bump hunt". Prospects for vector resonances will be discussed in more detail in section 4.5.3 below.

In the left-hand plot of figure 8, we finally show the predictions for the correlation between the branching ratios of $B_s \to \mu^+ \mu^-$ and $B_d \to \mu^+ \mu^-$, which is fixed by U(2)^3 to be equal relative to the respective SM predictions (but is again slightly washed out by the variation in CKM elements). The current 3σ upper bound on $B_s \to \mu^+ \mu^-$ can be saturated, but also a significant suppression can occur. This is in contrast to, e.g., the Littlest Higgs model with T-parity, where this branching ratio can only be enhanced with respect to the SM [175].

4.3.6 Top decays

A significant degree of compositeness of the left-handed top quark can lead to a reduction of the single top production cross section at LHC, corresponding to a reduced value for the effective CKM element V_{tb} as discussed in section 3.1.2. In addition, in this case there can be sizable flavour-changing couplings of the top quark to the Z boson, since the left-handed couplings are not custodially protected, in contrast to the right-handed ones.

These two effects manifest themselves in a correlation between the deviation of V_{tb} from 1 and the branching ratio of the FCNC top decay $t \to cZ$ as shown in the right-hand plot of figure 8. Both effects are quite moderate after imposing all the bounds. The deviation in V_{tb} is always within the current 2σ experimental constraint and percent-level experimental accuracy will be necessary to find a significant deviation. The branching ratio of the FCNC top decay can reach at most 10^{-5}, which will be challenging to see at the LHC [20, 176].
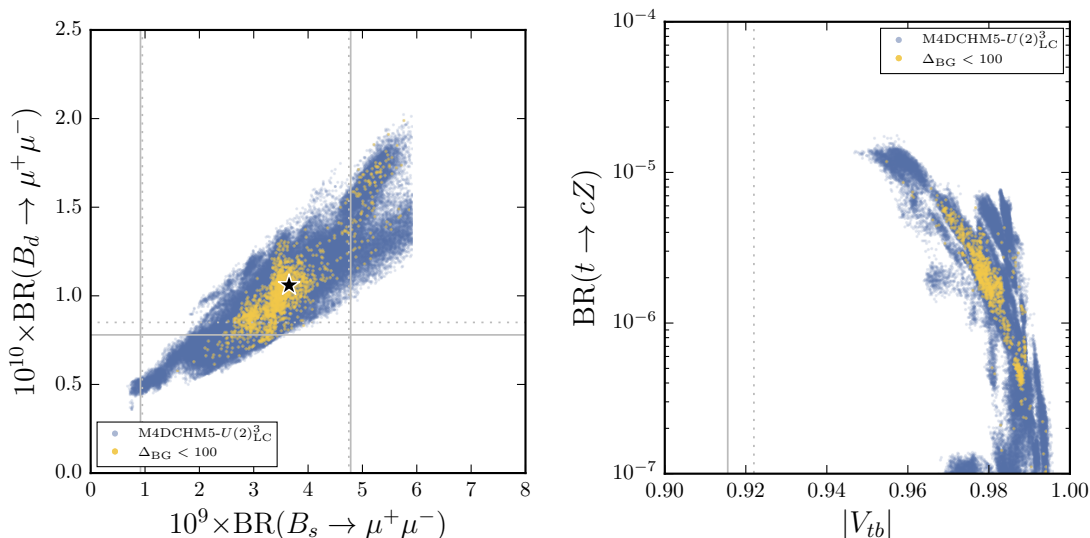
Figure 8. Left: predictions for the branching ratios of $B_s \to \mu^+\mu^-$ and $B_d \to \mu^+\mu^-$ in $\mathrm{U}(2)^3_{\mathrm{LC}}$. Right: predictions for the deviation of the effective CKM element V_{tb} from 1 vs. the branching ratio of the FCNC top decay $t \to cZ$ in $\mathrm{U}(2)^3_{\mathrm{LC}}$.

4.3.7 Other processes

So far, we have not discussed rare K decays. While these processes are important constraints on many NP models, we find the effects in $\mathrm{U}(2)^3_{\mathrm{LC}}$ to be rather small. For instance, the branching ratios of $K^+ \to \pi^+\nu\bar{\nu}$ and $K_L \to \pi^0\nu\bar{\nu}$ are modified by at most $\pm 20\%$ with respect to the SM (and are perfectly correlated due to $\mathrm{U}(2)^3$). The short-distance contribution to the branching ratio of $K_L \to \mu^+\mu^-$ is always below 2×10^{-9}.

4.4 Right-handed compositeness: indirect searches

In contrast to $\mathrm{U}(3)^3_{\mathrm{LC}}$, we do find a viable parameter space for the $\mathrm{U}(3)^3_{\mathrm{RC}}$ model. Since $\mathrm{U}(3)^3_{\mathrm{RC}}$ is a limiting case of the more general $\mathrm{U}(2)^3_{\mathrm{RC}}$ (the limit in which the composite sector mass parameters and the right-handed composite-elementary mixings for the first two and the third generation coincide), it is natural to discuss them together. We will proceed as in the case of left-handed compositeness in section 4.3.

4.4.1 Light quark compositeness

In the case of right-handed compositeness, it is typically the right-handed light quarks that can carry a sizable degree of compositeness. Consequently, in contrast to left-handed compositeness, first-row CKM unitarity does not constitute a relevant constraint and the main constraint is given by the hadronic Z width and the dijet angular distribution. The predictions for these quantities are shown in figure 9 that is the analogue of figure 4 right. We make the following observations.

- In both models, R_h is within the 2σ bounds for almost all the points.
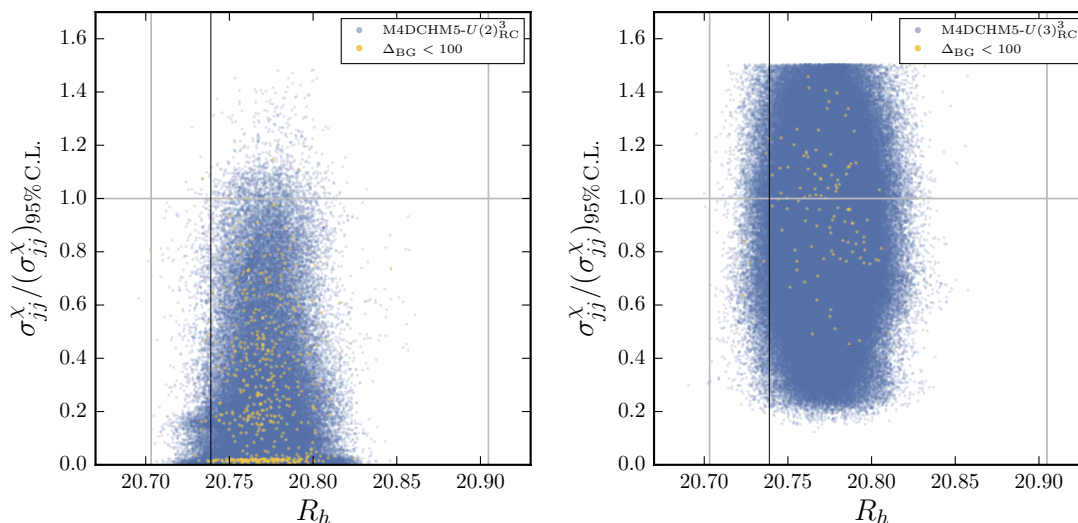
Figure 9. Hadronic Z width (normalized to $Z \to e\bar{e}$) vs. the $pp \to jj$ cross section in the rapidity bin described in the text, normalized to the 95% C.L. limit extracted from the ATLAS analysis. The black line corresponds to the central value of the SM prediction. Left: $U(2)^3_{RC}$, right: $U(3)^3_{RC}$.

- In both models[17], large effects relative to the experimental constraints are obtained in the dijet angular distribution. This is the strongest bound on light-quark compositeness in the right-handed compositeness models.

- In the case of $U(3)^3_{RC}$, we see that there is even a *lower* bound on the modification of the dijet angular distribution. Improved experimental measurements in the future could help to disfavour this scenario.

4.4.2 Higgs production and decay

Figure 10 shows the Higgs signal strengths for right-handed compositeness in analogy to figure 5. As discussed in section 4.3.2, the leading dependence on f is modified by light quark compositeness, which is more pronounced in $U(3)^3_{RC}$ due to the requirement to have a large degree of compositeness for all right-handed up-type quarks.

4.4.3 Meson-antimeson mixing

Figure 11 shows the predictions for $\Delta F = 2$ observables in $U(2)^3_{RC}$, in analogy to figure 6. We first point out the similar features,

- Sizable enhancements at the level of 60% with respect to the SM are possible in the B_d and B_s mass differences, but a suppression is strongly disfavoured.

---

[17]The alert reader may have noticed that in $U(3)^3_{RC}$, many points saturate the experimental upper bound, while in $U(2)^3_{RC}$, this does not seem to be the case, even though we have stated that $U(3)^3_{RC}$ is a subset of the $U(2)^3_{RC}$ model. The reason is a volume effect in the high-dimensional parameter space: one would need a huge number of points in the $U(2)^3_{RC}$ model to get a reasonable coverage of the subspace corresponding to $U(3)^3_{RC}$. This effect is visible in many of the plots in this section and justifies the separate analysis of $U(3)^3_{RC}$.
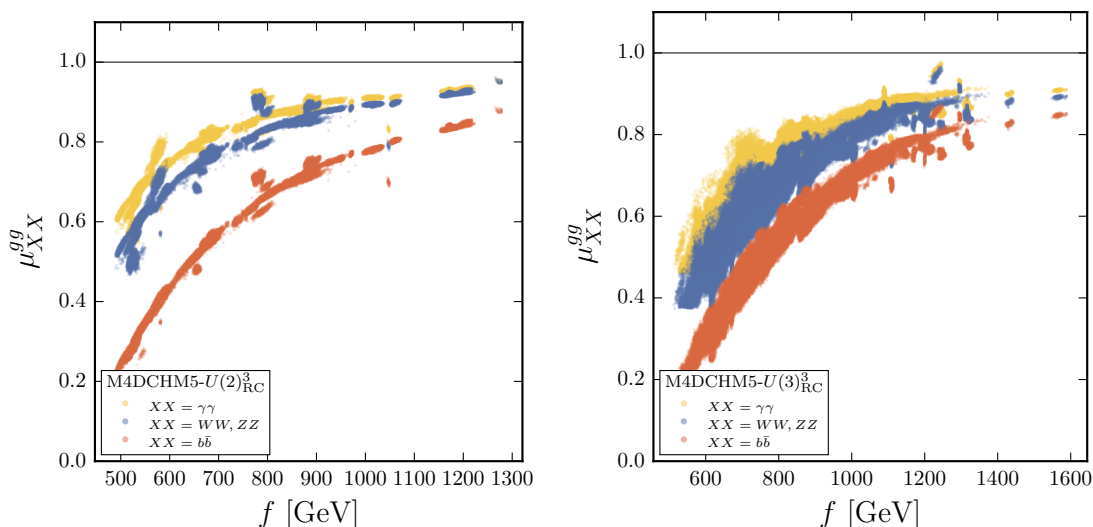
Figure 10. Higgs signal strength for gluon fusion production and decay to final states ZZ (equal to WW by custodial symmetry), $\gamma\gamma$, and $b\bar{b}$ in U(2)$^3_{\rm RC}$ (left) and U(3)$^3_{\rm RC}$ (right). The SM corresponds to $\mu = 1$, shown as a horizontal line.

- The leading-order U(2)^3 relation between ΔM_d and ΔM_s (shown as a black line) is violated by LR operators.

But there are also important differences between U(2)$^3_{\rm LC}$ and U(2)$^3_{\rm RC}$.

- There is no new phase in B_d mixing, as was already pointed out in [18].

- In B_s mixing, on the other hand, there can be a new phase roughly at the level of the current experimental uncertainties. This phase stems from the subleading terms in the spurion expansion and thus violates the leading order U(2)^3 relation (implying equal phase shifts in B_d and B_s mixing).

- The enhancement of ϵ_K relative to the SM is *always larger* than the one in ΔM_d. This is the opposite of what happened in U(2)$^3_{\rm LC}$, where the relative enhancement was *always smaller* in ϵ_K, cf. figure 6 bottom-right. In the future, this could serve as a way to distinguish the two models based on $\Delta F = 2$ observables alone.

In U(3)$^3_{\rm RC}$, we only directly show the observables normalized to their SM values in figure 12. In this case, the MFV relations, shown by black lines, are fulfilled exactly and there is no new phase, neither in B_d nor in B_s mixing.

Concerning D^0-$\bar{D}^0$ mixing, in U(2)$^3_{\rm RC}$, similarly to U(2)$^3_{\rm LC}$ discussed at the end of section 4.3.4, the NP effects are quite small and we find that the imaginary part of the mixing amplitude is always between -0.4 and $+0.2$ ns^{-1}, which is not relevant at the current experimental precision, but will become relevant when the experimental bound improves by an order of magnitude. In U(3)$^3_{\rm RC}$, there is no new phase and thus no NP contribution to the imaginary part of the mixing amplitude.
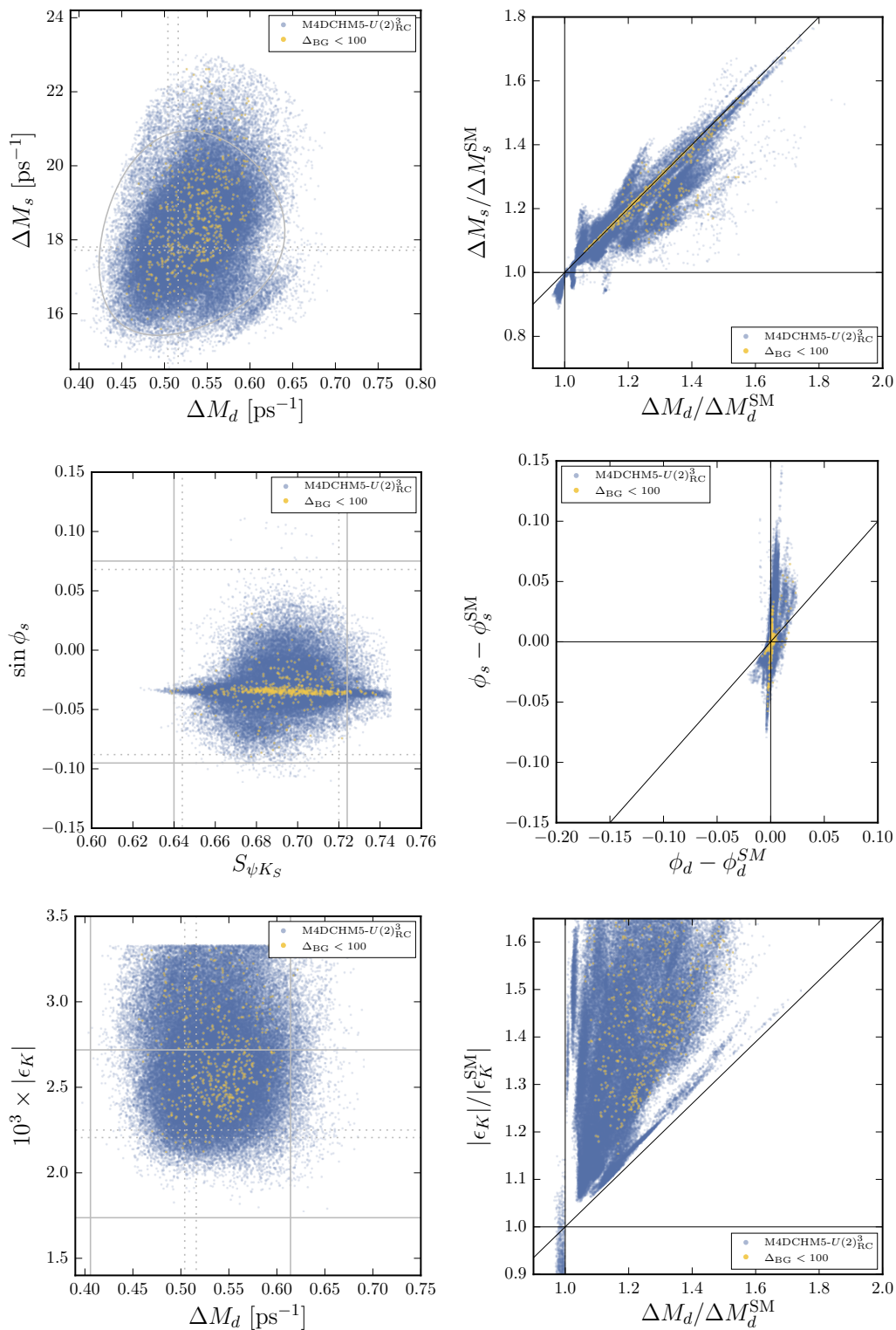
Figure 11. $\Delta F = 2$ observables in U(2)$^3_{\rm RC}$.
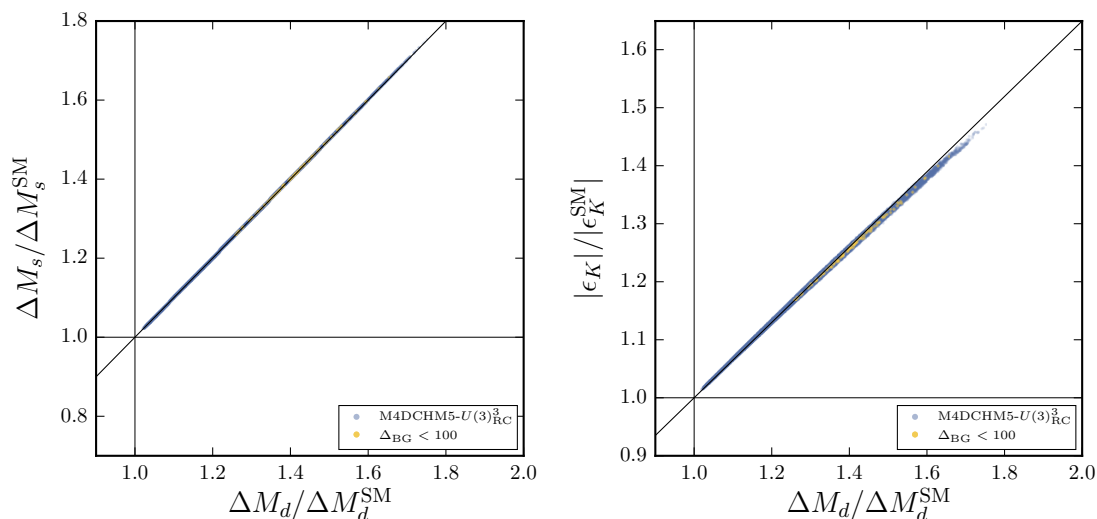
Figure 12. $\Delta F = 2$ observables in $\mathrm{U(3)}_{\mathrm{RC}}^3$.
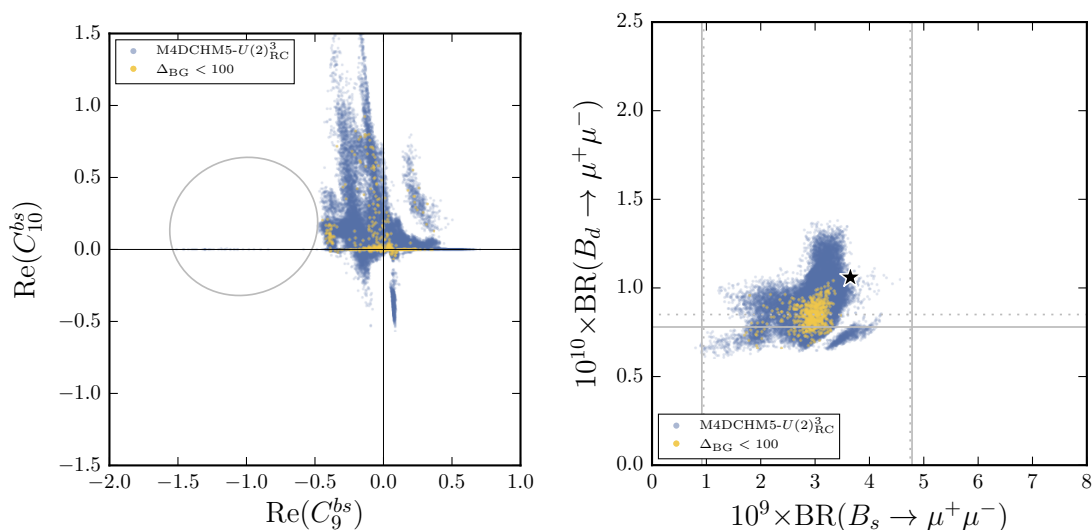
Figure 13. Left: new physics contributions to the Wilson coefficients C_9^{bs} and C_{10}^{bs} in $\mathrm{U(2)}_{\mathrm{RC}}^3$. Right: predictions for the branching ratios of $B_s \to \mu^+\mu^-$ and $B_d \to \mu^+\mu^-$ in $\mathrm{U(2)}_{\mathrm{RC}}^3$.

4.4.4 Rare B decays

In $\mathrm{U(2)}_{\mathrm{RC}}^3$, similarly to the case of left-handed compositeness discussed in section 4.3.5, the largest contribution to the Wilson coefficients of the semi-leptonic $b \to s\ell\ell$ transition occurs in the Wilson coefficient C_{10}^{bs}, but there are also contributions to the Wilson coefficient C_9^{bs}, as shown in figure 13 left. In this case, we only find a small number of points with sizably negative C_9^{bs} that populate the region preferred by a global fit to $b \to s\ell\ell$ data, indicated by a gray ellipse. These points then predict a significant suppression in absolute value of the angular observable P_5' in $B \to K^*\mu^+\mu^-$ at low q^2, see the points around $P_5' \approx -0.1$ in figure 14 left. A distinguishing feature compared to $\mathrm{U(2)}_{\mathrm{LC}}^3$ is that the contributions to C_{10}^{bs} are almost always positive, implying that the branching ratio of $B_s \to \mu^+\mu^-$ is almost always suppressed, as shown in figure 13 right.
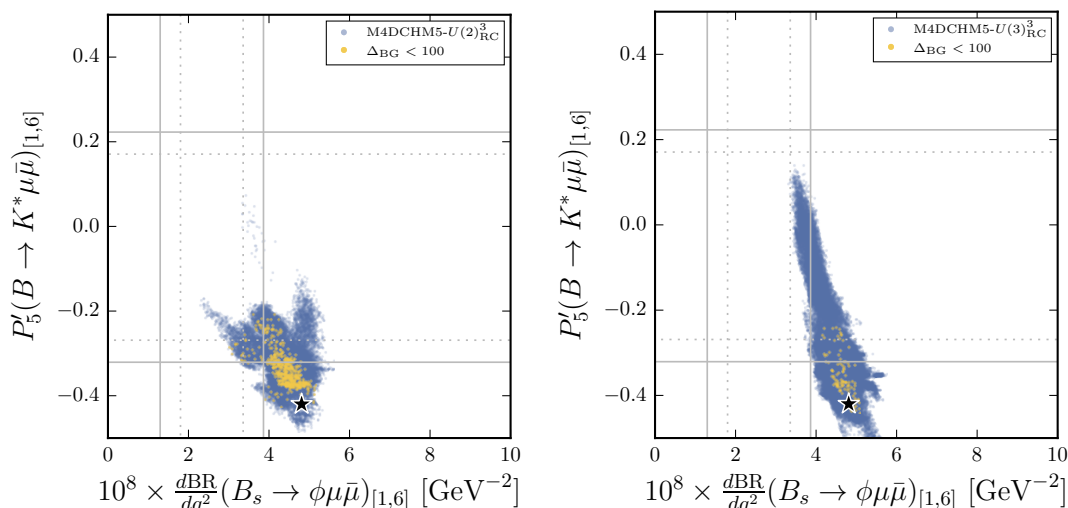
Figure 14. Predictions for the angular observable P_5' in $B \to K^* \mu^+ \mu^-$ and the branching ratio of $B_s \to \phi \mu^+ \mu^-$, both in the low-q^2 bin from 1 to $6 \, \text{GeV}^2$ in $\text{U}(2)^3_{\text{RC}}$ (left) and $\text{U}(3)^3_{\text{RC}}$ (right). The star corresponds to the central values of the SM predictions.

In $\text{U}(3)^3_{\text{RC}}$, the contributions to C^{bs}_{10} are forbidden by an interplay between custodial protection and the flavour structure as discussed in section 3.2.5. However, the resonance-mediated contributions to C^{bs}_9 are still present and we find viable points in the range $-1.7 \lesssim C^{bs}_9 \lesssim 0.9$. Consequently, also $\text{U}(3)^3_{\text{RC}}$ can explain the anomalies in $b \to s\ell\ell$ angular observables and branching ratios. For the observable P_5' and the branching ratio of $B_s \to \phi \mu^+ \mu^-$, this is illustrated in figure 14 right. Finally, we remind the reader again the $\text{U}(3)^3_{\text{RC}}$ is actually a limiting subset of $\text{U}(2)^3_{\text{RC}}$, so the fact that in $\text{U}(3)^3_{\text{RC}}$ there are much more points with sizable NP effects in C^{bs}_9 compared to $\text{U}(2)^3_{\text{RC}}$ is simply a statistical effect since the $\text{U}(3)^3_{\text{RC}}$ parameter space is more restricted.

As in $\text{U}(2)^3_{\text{LC}}$ discussed in section 4.3.5, the solution of the B physics anomalies by a negative NP contribution to C^{bs}_9 implies the presence of a light, narrow neutral vector resonance below about 1 TeV. In $\text{U}(2)^3_{\text{RC}}$, the dominant decay mode of this resonance is $t\bar{t}$ or two light quark jets, while in $\text{U}(3)^3_{\text{RC}}$ the dominant decay mode is always dijets.

4.4.5 Other processes

We have not discussed the oblique parameters as the predictions in both models with right-handed compositeness are analogous to the effects in $\text{U}(2)^3_{\text{LC}}$ shown in figure 5 right, so the same comments as in section 4.3.3 apply.

In rare K decays, the effects both in $\text{U}(2)^3_{\text{RC}}$ and in $\text{U}(3)^3_{\text{RC}}$ are even smaller than in $\text{U}(2)^3_{\text{LC}}$ discussed in section 4.3.7.

In contrast to left-handed compositeness, the branching ratio of the FCNC top decay $t \to cZ$ is always below 10^{-6} in $\text{U}(2)^3_{\text{RC}}$ and even below 10^{-8} in $\text{U}(3)^3_{\text{RC}}$ and thus negligible.

4.5 Direct searches in left- and right-handed compositeness

4.5.1 Prospects for quark partner searches

The direct bounds on quark partner masses discussed in section 3.3.1 are among the most important constraints in our analysis. It is thus clear that future searches for quark partners

will be instrumental in probing these models. Since in our numerical analysis, the lightest vector resonances are always found to be heavier than the lightest quark partners, which is due to electroweak precision tests and the other indirect bounds discussed in section 3.2, the lightest quark partners always decay to SM states. To judge which of the search channels will be most promising at run 2 of the LHC, let us first discuss the dominant decay modes of the lightest resonances.

Exotic charge quarks. The charge-5/3 and charge-(−4/3) quarks always decay to a W boson and a SM quark or quark resonance. In $U(2)^3_{LC}$, we find that there is a significant number of points where the $Q_{5/3}$ can decay to both Wt and Wq ($q = u, c$) with significant branching ratio, and similarly for the $Q_{-4/3}$ decaying into final states with bottoms vs. light quarks. In the right-handed compositeness models, we find in contrast that for any given exotic quark partner, only the decay to 3rd generation *or* the one to light quarks is relevant. This can be understood from the fact that the decay of the exotic charge quarks always involves right-handed composite-elementary mixings, and these are flavour-diagonal in right-handed compositeness, but involve flavour mixing in left-handed compositeness. In figure 15, we show the predictions for the branching ratios as a function of the mass for the exotic charged quark partners for a subset of all viable points in all three models. An interesting feature of these plots is that there is a significant number of points with branching ratios different from zero or one in a given channel. Apart from flavour mixing, this is due to the competition with decays involving a fermion resonance in the final state. For heavier masses, the branching ratios into SM-only states decrease, as can be seen from the plots as well.

Up- and down-type quark partners. When decaying to SM states, these quark partners can decay to a W, Z, or h plus a SM quark. In figures 16 and 17, we show predictions for the masses and branching ratios in the most important channels for quark partners in the three viable models.

In summary, the plots show that searches for pair-produced quark partners, both with exotic and with SM-like charges, are very promising, with masses and branching ratios just above what LHC has excluded in run 1 being viable in all models.

4.5.2 LHC excesses

As discussed in section 3.3.3, several excesses with significances up to around 3σ have been observed by ATLAS and CMS in resonance searches in Wh, WZ, and WW final states around a resonance mass of $2\,\mathrm{TeV}$. To investigate whether the models studied by us could account for these anomalies, we have computed the production cross sections of charged and neutral electroweak vector resonances times the branching ratios to the relevant final states. In figures 18 and 19, we show these predictions in the relevant mass region for all three viable models, compared to the expected (dashed) and observed (solid) limits in some of the relevant ATLAS and CMS searches (for a total list of searches included, see section 3.3.2). In these plots, to be conservative we only show points where the decaying resonance has a narrow width, namely $\Gamma/m < 0.05$, because, as discussed in section 3.3.2, we have not imposed any LHC constraints on broader resonances. We note however that
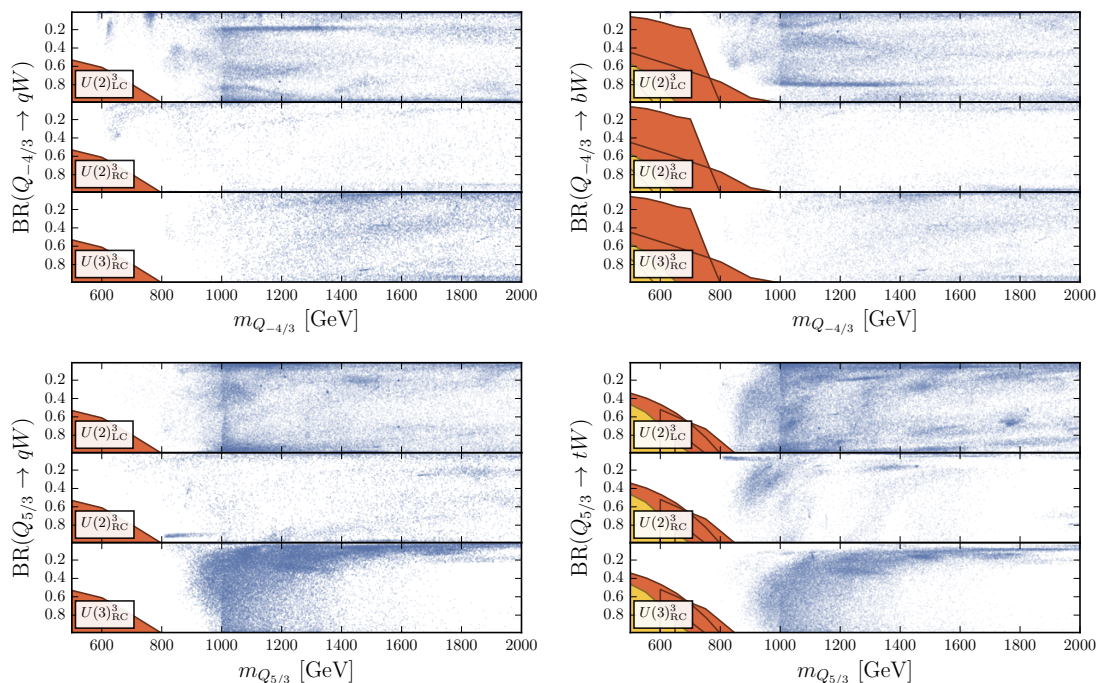
Figure 15. Branching ratios of charge-$(-4/3)$ (first row) and charge-5/3 (second row) quarks to light (left) and third-generation (right) quarks as function of their mass for all three models. The coloured regions are the same as in figure 2.

there are a significant number of more points in the same region where the width is slightly larger than 5%. But even with this strong condition, we do find points in all three models where there are resonances with mass around 2 TeV and with cross sections of the order of 5 fb in the case of $\rho^\pm \to W^\pm h$ and $\rho^\pm \to W^\pm Z^0$, which is the right ballpark to explain the excesses (see e.g. [160–164]). In the case of $\rho^0 \to W^\pm W^\mp$, the predicted cross section is roughly a factor of two smaller due to the PDF suppression, but this agrees at least qualitatively with the less pronounced excess in the CMS analysis, as seen in the upper plot of figure 19.

Interestingly, a slight excess around 2 TeV has also been observed in a CMS dilepton resonance search [157]. Our predictions for this channel are shown in the lower plot of figure 19. Also here, we find a significant number of points with cross section times branching ratio of the order of 0.1 fb, which could account for this excess. Also in this plot, we are only showing resonances with a narrow width. This is also why there are few points in the region of interest for the U(3)$_{\mathrm{RC}}^3$ model. In this model, the electroweak resonances are typically broader than 5% due to the stronger coupling to light quarks compared to the U(2)^3 models.[18]

Given figures 18 and 19, the question arises whether the points explaining the excesses in the individual plots are actually the same points, i.e. the question whether the models can explain all excesses simultaneously. For the final states involving bosons, this is obviously

---

[18]This does not mean that this model cannot explain the excesses, but a detailed analysis of the impact of broad resonances is beyond the scope of our study.
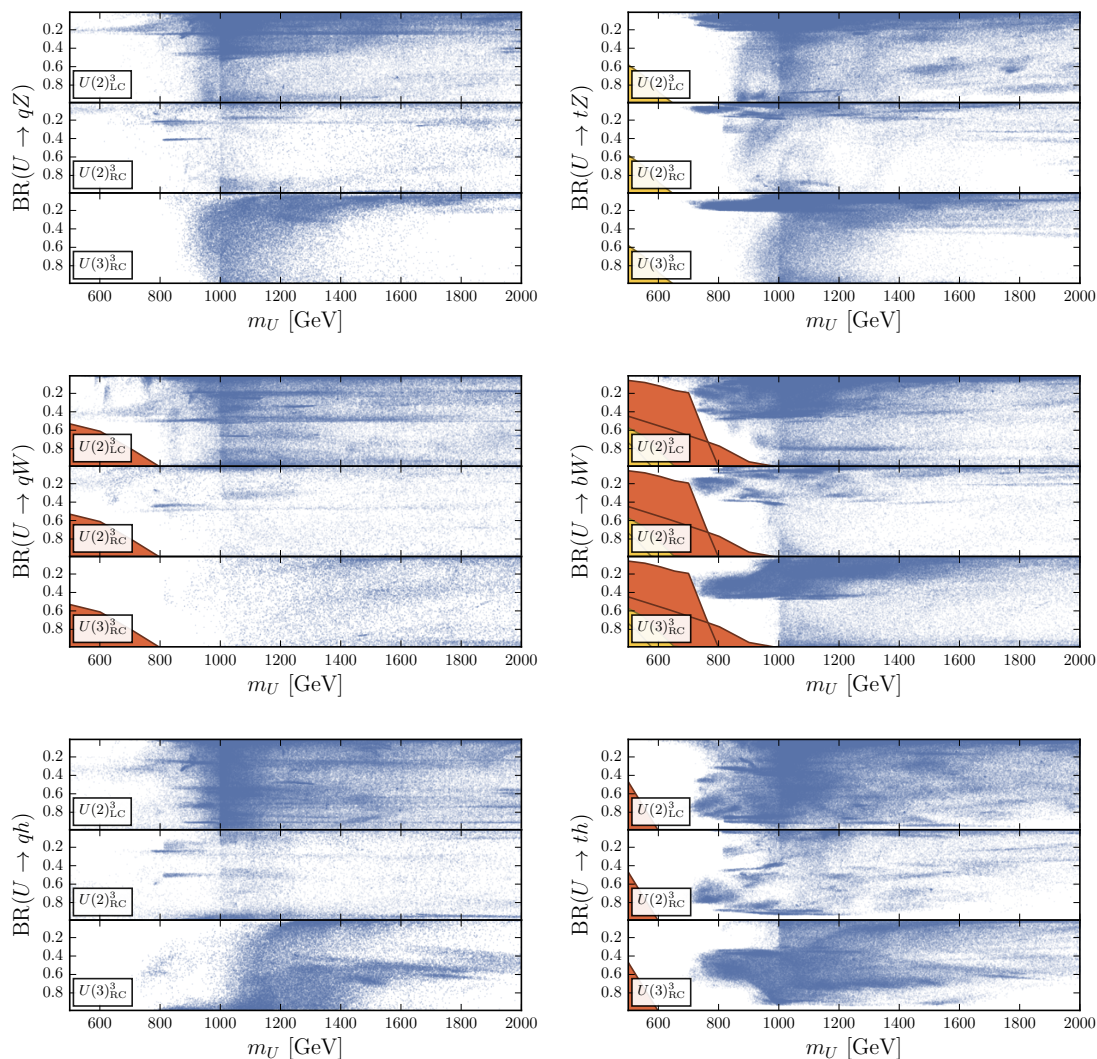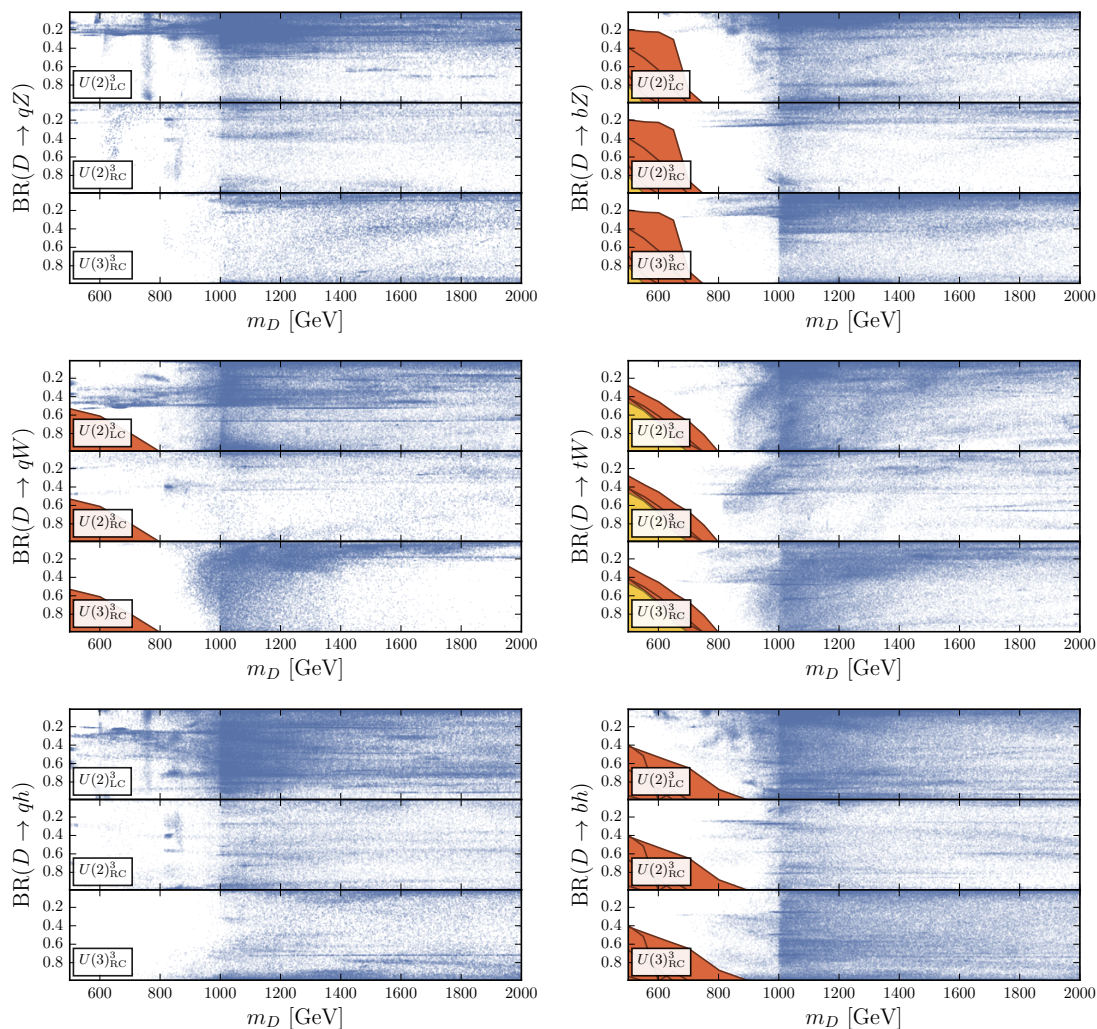
Figure 16. Branching ratios of up-type quark partners to final states involving light (left) and third generation (right) quarks as function of their mass for all three models. The coloured regions are the same as in figure 2.

the case as the branching ratios are sizable only for the composite $\mathrm{SU}(2)_L$ triplet, for which the branching ratios into WW, WZ, and Wh final states are expected to be the same (see section 3.3.3). For the diboson vs. dilepton final states, this is not obvious, so in figure 20, we compare the cross sections times branching ratios of neutral vector resonances decaying to dileptons vs. WW in all cases where the mass is between 1.7 and 2.2 TeV and the Γ/m is at most 5%. We observe that the points with production cross section times branching ratio into WW of order 1 fb typically lead to a signal in dileptons that is one to three orders of magnitude smaller. Comparing this to figure 19, we conclude that if the excesses in diboson final states are due to composite resonances, the excess in dileptons could be explained as well, but could also be absent.

Figure 17. Branching ratios of down-type quark partners to final states involving light (left) and third generation (right) quarks as function of their mass for all three models. The coloured regions are the same as in figure 2.

4.5.3 Prospects for vector resonance searches

The discussion in the previous section has already shown that the diboson and dilepton final states are promising channels to look for vector resonances in the models studied by us. It should however be stressed that the vector resonances are not required to be light enough to be probed at LHC, even at $\sqrt{s} = 13\,\mathrm{TeV}$. In all three models, we have found viable points with moderate fine-tuning where all vector resonances are heavier than $6\,\mathrm{TeV}$. In the following, we discuss the most promising search channels for the vector resonances if they are light enough.

Gluon resonance. ρ_G can only decay to fermion pairs and usually has the largest branching fraction into quark partners because it couples to them through the strong coupling g_G. In that case, the most promising experimental strategy is to look for the quark partner
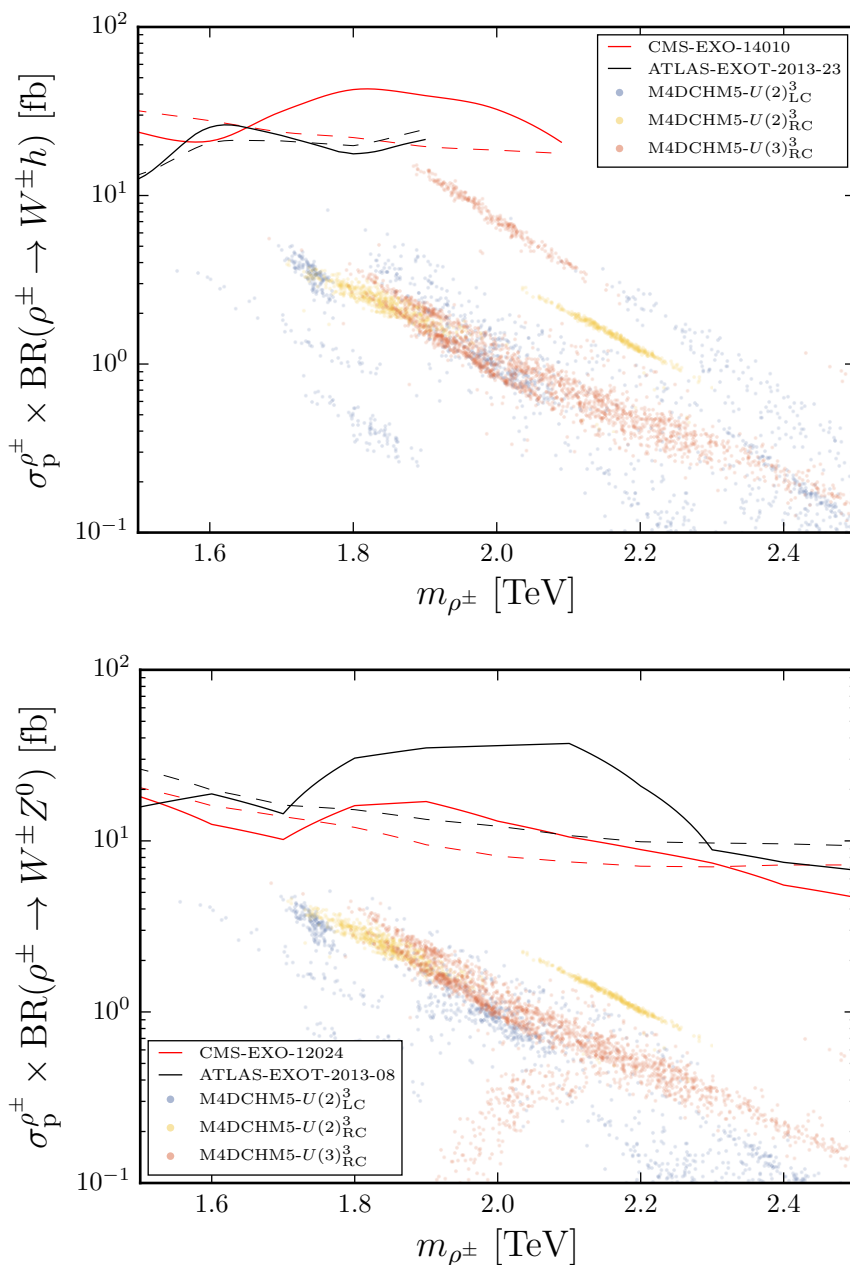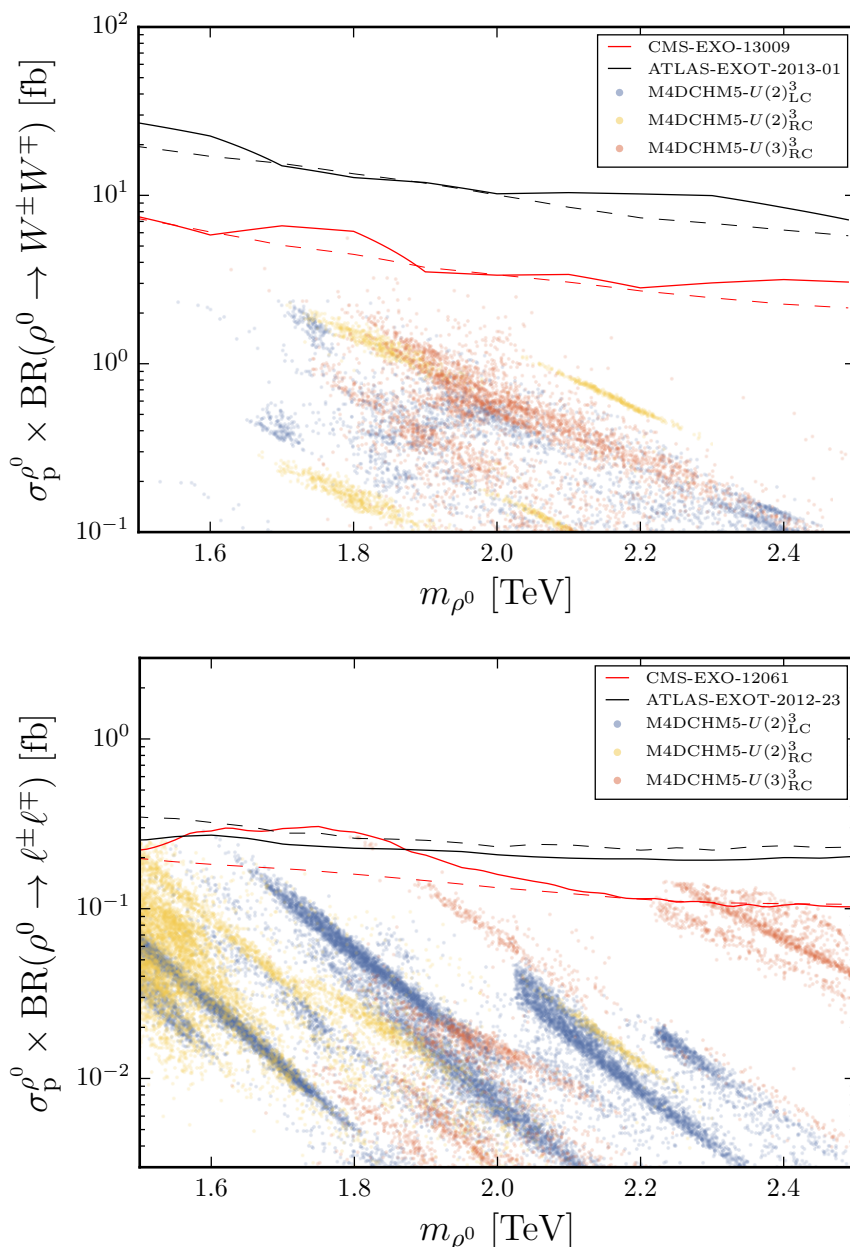
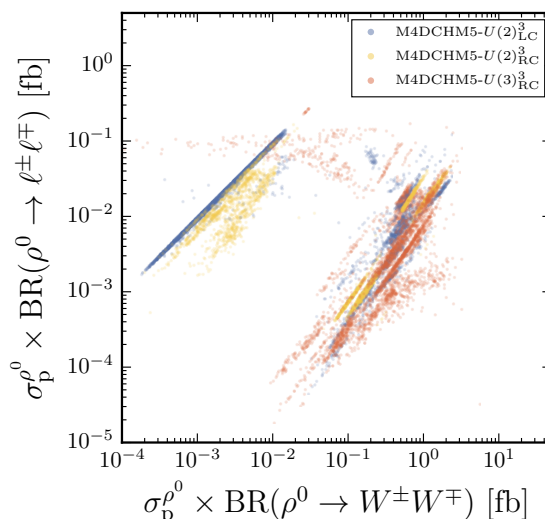**Figure 18**. Predictions for the production cross sections times branching ratios of charged electroweak vector resonances decaying to Wh or ZW final states in all three models. Only points with narrow resonances ($\Gamma/m < 0.05$) are shown. The dashed and solid curves show the expected and observed 95% C.L. experimental limits.

pair decaying to SM particles [143, 144]. If the decay to quark partners is kinematically disfavoured or forbidden, ρ_G can also decay to SM quark pairs. In the U(2)^3 models, we find that the decays to $t\bar{t}$ or $b\bar{b}$ can be up to 50% and to light quarks up to 30% (summing over the four light quark flavours). In U(3)$^3_{\rm RC}$, due to the large degree of compositeness of light right-handed quarks, the dominant SM decay mode are light quark pairs, with a

Figure 19. Predictions for the production cross sections times branching ratios of neutral electroweak vector resonances decaying to WW or dilepton final states in all three models. Only points with narrow resonances ($\Gamma/m < 0.05$) are shown. The dashed and solid curves show the expected and observed 95% C.L. experimental limits.

branching ratio up to 40%, while the $t\bar{t}$ and $b\bar{b}$ final states have branching ratios below 10% each. The relative width of ρ_G is around 10–50% when the decays to SM states are relevant, with U(3)$^3_{\rm RC}$ closer to the upper end of this range.[19]

---

[19]Note that this means that in our numerical analysis, there are effectively no direct bounds on ρ_G due to our requirement of a narrow width in the LHC searches, see section 3.3.2.

Figure 20. Predictions for the production cross sections times branching ratios of neutral electroweak vector resonances decaying to WW vs. dilepton final states in all three models. Only points with narrow resonances ($\Gamma/m < 0.05$) are shown.

Charged resonances. Among the three charged resonances, the lighter two are always nearly degenerate, with the lighter one being mostly the $\rho_R^\pm$ and the heavier one mostly the $\rho_L^\pm$, while the third charged resonance can be heavier and is mostly the axial vector resonance $\mathfrak{a}^\pm$. The most important state for collider phenomenology is the second one since it is the only one with an appreciable Drell-Yan production cross section. Since its couplings to SM quarks are even weaker compared to the gluon resonance, it typically decays to quark partners, if kinematically allowed. If not, it decays to WZ and Wh with roughly equal branching ratios (cf. the discussion in sections 3.3.3 and 4.5.2). The branching ratio into tb is typically small but can reach 20% in corners of the parameter space. The branching ratio to $\ell\nu$ is always below a percent. The other two states could be produced via vector boson fusion that we have neglected in our analysis since it is expected to be very small at the LHC (see [177] for a recent discussion). We note that the axial vector resonance typically decays to WZ and Wh with the largest branching ratios and we find $\mathrm{BR}(\rho_3^\pm \to W^\pm Z) \approx 3\,\mathrm{BR}(\rho_3^\pm \to W^\pm h)$.

Neutral electroweak resonances. Among the five neutral uncoloured resonances, the two heaviest are usually mostly the axial vector resonances that have a small production cross section in quark-antiquark collisions and (if produced via vector boson fusion) would decay with the largest branching ratios to WW and Zh with $\mathrm{BR}(\rho_{4,5}^0 \to W^\pm W^\mp) \approx 3\,\mathrm{BR}(\rho_{4,5}^0 \to Zh)$. Concerning the other three resonances, which are linear combinations of the ρ_L^0, ρ_R^0, and ρ_X^0, they again preferably decay to a pair of quark partners. If this is kinematically disfavoured, they can decay to pairs of SM quarks, leptons, or W bosons, or to Zh. In the latter two cases, one typically has $\mathrm{BR}(\rho_i^0 \to W^\pm W^\mp) \approx \mathrm{BR}(\rho_i^0 \to Zh)$, as expected for an $\mathrm{SU}(2)_L$ triplet (cf. the discussion in sections 3.3.3 and 4.5.2). We find the branching ratios into electron or muon pairs to always be below 2%, which can however be
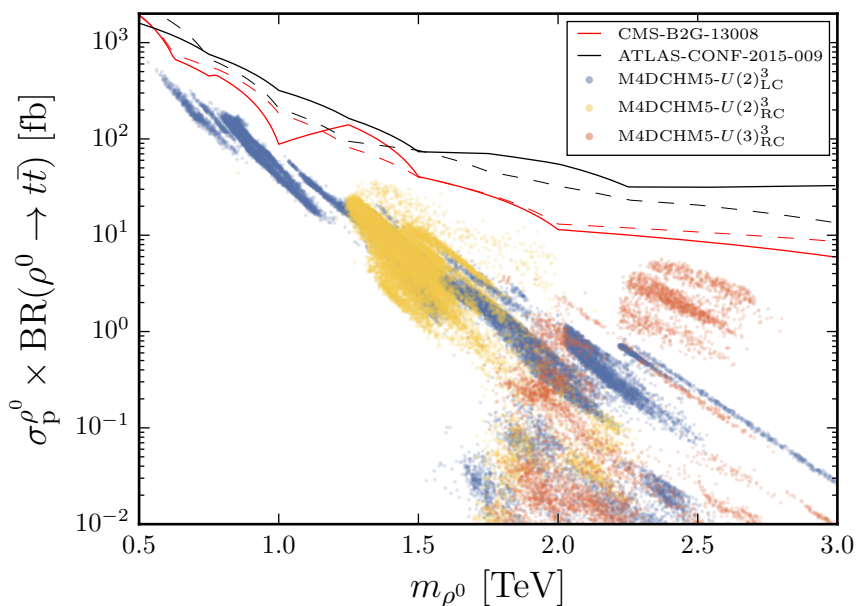
Figure 21. Predictions for the production cross sections times branching ratios of neutral electroweak vector resonances decaying to top quarks in all three models. Only points with narrow resonances ($\Gamma/m < 0.05$) are shown. The dashed and solid curves show the expected and observed 95% C.L. experimental limits.

overcome by the higher experimental sensitivity, cf. figure 19 bottom. The branching ratio to light jets can be up to 30% in the U(2)^3 models and up to 70% in U(3)$^3_{\rm RC}$, while the one to $b\bar{b}$ can be up to 40% in all models. In the U(2)^3 models, the decay to $t\bar{t}$ can come close to 100% in parts of the parameter space.

In sections 4.3.5 and 4.4.4, we have already discussed that sizable NP contributions to the rare B decay Wilson coefficient C_9^{bs}, as is required if one wants to solve the anomalies in B physics discussed in section 3.2.5 in terms of new physics, requires a light, narrow neutral vector resonance with a large branching ratio to $t\bar{t}$. In figure 21, we show the predictions for the production cross section times branching ratio of the neutral electroweak resonances decaying to $t\bar{t}$ at LHC with $\sqrt{s} = 8\,\mathrm{TeV}$, compared to existing ATLAS and CMS analyses. As in the previous plots, we only show points with narrow resonances ($\Gamma/m < 0.05$). At masses below 1 TeV, the U(2)$^3_{\rm LC}$ points correspond to the ones generating sizable NP effects in C_9^{bs}. The points in right-handed compositeness only start at higher masses because the relative width is typically larger than 5%. The plot shows that cross sections not far from what LHC has probed in run 1 are attainable in all models. We conclude that this channel remains a promising probe at run 2, and discoveries are possible both for low and high masses.

5 Summary

In this paper, we have performed a comprehensive numerical analysis of a four-dimensional pNGB Higgs model based on the symmetry breaking coset SO(5)/SO(4) with quark

partners transforming as fundamentals of SO(5). The model features a calculable one-loop Higgs potential and a custodial protection of the $Zb_L\bar{b}_L$ coupling. We have included constraints from electroweak precision tests, flavour physics, Higgs production and decay, contact interaction searches, as well as direct searches for quark and vector resonances. We have considered three different flavour symmetries, all of them exact in the composite sector and broken only by the composite-elementary mixing terms, namely $U(2)^3$ or $U(3)^3$ with left- or right-handed compositeness. Below, we summarize our main findings.

- Model-independently, we have pointed out that there are holes in existing experimental searches for quark partners decaying to W or Z plus a top or bottom quark, particularly for quark partners around $350\,\mathrm{GeV}$ which are not covered by Tevatron or LHC searches, see figure 2. We call on the experimental collaborations to close these holes by reanalyzing existing data. Quark partners decaying to a boson and a light quark are still weakly constrained.

- In our numerical analysis, we have not found a single valid parameter point for the $U(3)^3_{\mathrm{LC}}$ flavour structure. Although not a formal proof, we think this is a strong indication that this flavour structure is not compatible with electroweak precision tests and radiative EWSB in the model setup considered by us.

- We have shown that the three other flavour structures can be made compatible with all relevant constraints with a fine tuning $\Delta_{\mathrm{BG}} \lesssim 100$, see figure 3.

- We have demonstrated that first-row CKM unitarity is the most sensitive probe of light-quark compositeness in $U(2)^3_{\mathrm{LC}}$, while in right-handed compositeness the dijet angular distribution is most sensitive to it, cf. figures 4 and 9.

- Higgs signal strengths are the cleanest observables to constrain the pNGB decay constant f, with small corrections due to light-quark compositeness, cf. figures 5 and 10.

- In meson-antimeson mixing in the $U(2)^3$ models, the relations between B_d and B_s mixing that are expected from a leading-order spurion analysis are strongly violated for some of the valid points by terms that are formally of higher order in the spurion expansion.

- In both $U(2)^3$ models, all observables in B, B_s and K mixing can saturate their current experimental limits, while in $U(3)^3$, this is true for the mass differences and ϵ_K, while CP violation in the B and B_s systems is SM-like. The best means to experimentally distinguish the models based on $\Delta F = 2$ observables alone can be read off figures 6, 11, and 12:
  - In $U(2)^3_{\mathrm{LC}}$, the relative NP effect in ϵ_K compared to ΔM_d is always smaller (or equal), in $U(2)^3_{\mathrm{RC}}$ it is always larger (or equal), while in $U(3)^3_{\mathrm{RC}}$ it is always equal.
  - In $U(2)^3_{\mathrm{LC}}$, there can be large NP effects in ϕ_s which are typically correlated with an equal effect in ϕ_d; in $U(2)^3_{\mathrm{RC}}$ NP effects can be only in ϕ_s and not in ϕ_d; in $U(3)^3_{\mathrm{RC}}$ both phases are free from NP.

- In the U(2)^3 models, CP violation in D^0-$\bar{D}^0$ mixing is small compared to the current experimental sensitivity, but could become relevant if the sensitivity improves by an order of magnitude.

- The FCNC top decay $t \to cZ$ can reach a branching ratio of up to 10^{-5} in U(2)$^3_{\rm LC}$ but is negligible in the other models.

- Rare B decays of the type $b \to s\ell^+\ell^-$ can not only receive Z-mediated contributions, but also resonance-mediated contributions that can affect the Wilson coefficient C_9^{bs} which is required for a NP explanation of various anomalies in B physics data. These anomalies can be explained in all three models. In U(3)$^3_{\rm RC}$, NP affects the Wilson coefficient C_9^{bs} but not C_{10}^{bs}.

- Explaining the B physics anomalies implies the presence of a narrow neutral vector resonance around $1\,{\rm TeV}$ with a sizable branching ratio into $t\bar{t}$ or dijets with a production cross section just below what has been excluded in LHC run 1.

- Various excesses in diboson events at a mass of roughly $2\,{\rm TeV}$ observed by ATLAS and CMS can be explained in all three models as well by the decay of a $2\,{\rm TeV}$ vector resonance, see figures 18 and 19. The solution possibly, but not necessarily, predicts a signal in dilepton events around the same mass as well, see figure 20.

While we have limited ourselves to a single model with four different flavour structures in this work, there are several ways how our analysis could be generalized, such as studying non-minimal cosets, non-minimal couplings, different fermion representations, or different flavour structures, including more radical changes like disposing of partial compositeness for the first two generation quarks [57, 58]. It would also be interesting to include a more realistic lepton sector. Finally, a more accurate treatment of the top quark mass, of loop corrections to the $Zb_L\bar{b}_L$ coupling, of renormalization group effects on FCNC operators, and of LHC constraints on singly produced fermion resonances would be very interesting to further scrutinize composite Higgs models in the future.

Acknowledgments

A SO(5) conventions

For concreteness, we will present the conventions for SO(5) generators and embeddings used by us.

The group SO(5) can locally be expressed as $\text{SO}(5) \cong \text{SU}(2)_L \times \text{SU}(2)_R \times \text{SO}(5)/\text{SO}(4)$. Therefore, its 10 generators can be grouped into "left", "right" and "coset":

$$\left(\mathsf{T}^{a_L}\right)_{ij} = -\frac{i}{2}\left(\frac{1}{2}\epsilon^{a_L bc}\left(\delta_i^b \delta_j^c - \delta_j^b \delta_i^c\right) + \left(\delta_i^{a_L}\delta_j^4 - \delta_j^{a_L}\delta_i^4\right)\right), \tag{A.1}$$

$$\left(\mathsf{T}^{a_R}\right)_{ij} = -\frac{i}{2}\left(\frac{1}{2}\epsilon^{a_R bc}\left(\delta_i^b \delta_j^c - \delta_j^b \delta_i^c\right) - \left(\delta_i^{a_R}\delta_j^4 - \delta_j^{a_R}\delta_i^4\right)\right), \tag{A.2}$$

$$\left(\mathsf{T}^{\hat{a}}\right)_{ij} = -\frac{i}{\sqrt{2}}\left(\delta_i^{\hat{a}}\delta_j^5 - \delta_j^{\hat{a}}\delta_i^5\right), \tag{A.3}$$

Then, SO(4) singlets S and bidoublets Q^{n_1,n_2} (with $\text{SU}(2)_L \times \text{SU}(3)_R$ quantum numbers (n_1, n_2)) can be embedded into SO(5) fundamentals via

$$\begin{pmatrix} Q^1 \\ Q^2 \\ Q^3 \\ Q^4 \\ Q^5 \end{pmatrix} = \frac{1}{\sqrt{2}}\begin{pmatrix} Q^{++} + Q^{--} \\ iQ^{++} - iQ^{--} \\ Q^{+-} - Q^{-+} \\ iQ^{+-} + iQ^{-+} \\ \sqrt{2}\,S \end{pmatrix}. \tag{A.4}$$

B Mass matrices

In this appendix we give the expressions for the mass mixing matrices that were obtained in the M4DCHM5.

B.1 Boson sector

The pNGB structure of the M4DCHM Lagrangian leads to mixings between the elementary and composite vector bosons of equal charge. In particular, the composite triplets ρ_L^μ and ρ_R^μ as well as the axial resonances $\mathfrak{a}^\mu$ will have neutral and charged components mixing with the elementary $W^{0\mu}$ and $B^{0\mu}$ gauge bosons. In addition, the neutral components will also mix with the $\text{U}(1)_X$ resonance ρ_X^μ.

For the neutral and charged vector bosons one finds the following mass matrices given in table 4.

By the explicit mixing introduced in the Lagrangian one finds the following mass matrices for the gluon and their composite resonances. By construction this does not spoil invariance under the SM $\text{SU}(3)_c$, which survives as a linear combination of the elementary and composite SU(3) symmetries as can be seen from the fact that the gluon mass matrices exhibit a massless eigenvalue.

$$M^2_{\text{Boson,Gluon}} = \left(\begin{array}{c|cc} & G^0{}_\mu & \rho_{G\,\mu} \\ \hline G^{0\mu} & \frac{1}{2}g_{03}^2 f_G^2 & -\frac{1}{2}g_{03}g_G f_G^2 \\ \rho_G^\mu & & \frac{1}{2}g_{\rho_3}^2 f_G^2 \end{array}\right)$$

B.2 Fermion sector

After EWSB the elementary quarks mix with all resonances carrying the same electric charge. By using the embedding (A.4) we express the components of the bidou-

$$M^2_{\text{Boson,neutral}} =$$

$$
\begin{array}{c|ccccccc}
 & W^{03}_\mu & B^0_\mu & \rho_{L\mu} & \rho_{R\mu} & \mathbf{a}^3_\mu & \rho_{X\mu} & \mathbf{a}^4_\mu \\
\hline
W^{03\,\mu} & \frac{1}{2}g_0 f_1^2 & 0 & -\frac{1}{2}g_0 g_\rho f_1^2 \cos^2\!\left(\frac{h}{2f}\right) & -\frac{1}{2}g_0 g_\rho f_1^2 \sin^2\!\left(\frac{h}{2f}\right) & -\frac{1}{2\sqrt{2}}g_0 g_\rho f_1^2 \sin\!\left(\frac{h}{f}\right) & 0 & 0 \\
B^{0\,\mu} & & \frac{1}{2}g_0'^{\,2}\left(f_1^2+f_X^2\right) & -\frac{1}{2}g_0' g_\rho f_1^2 \sin^2\!\left(\frac{h}{2f}\right) & -\frac{1}{2}g_0' g_\rho f_1^2 \cos^2\!\left(\frac{h}{2f}\right) & \frac{1}{2\sqrt{2}}g_0' g_\rho f_1^2 \sin\!\left(\frac{h}{f}\right) & -\frac{1}{2}g_0' g_X f_X^2 & 0 \\
\rho_L^{\mu} & & & \frac{1}{2}g_\rho^2 f_1^2 & 0 & 0 & 0 & 0 \\
\rho_R^{\mu} & & & & \frac{1}{2}g_\rho^2 f_1^2 & 0 & 0 & 0 \\
\mathbf{a}^{3\,\mu} & & & & & \frac{1}{2}g_\rho^2 \frac{f_1^4}{f_1^2-f^2} & 0 & 0 \\
\rho_X^{\mu} & & & & & & \frac{1}{2}g_X^2 f_X^2 & 0 \\
\mathbf{a}^{4\,\mu} & & & & & & & \frac{1}{2}g_\rho^2 \frac{f_1^4}{f_1^2-f^2}
\end{array}
$$

$$M^2_{\text{Boson,charged}} =$$

$$
\begin{array}{c|cccc}
 & W^{0+}_\mu & \rho^+_{L\mu} & \rho^+_{R\mu} & \mathbf{a}^+_\mu \\
\hline
W^{0-\,\mu} & \frac{1}{2}g_0^2 f_1^2 & -\frac{1}{2}g_0 g_\rho f_1^2 \cos^2\!\left(\frac{h}{2f}\right) & -\frac{1}{2}g_0 g_\rho f_1^2 \sin^2\!\left(\frac{h}{2f}\right) & -\frac{1}{2\sqrt{2}}g_0 g_\rho f_1^2 \sin\!\left(\frac{h}{f}\right) \\
\rho_L^{-\,\mu} & & \frac{1}{2}g_\rho^2 f_1^2 & 0 & 0 \\
\rho_R^{-\,\mu} & & & \frac{1}{2}g_\rho^2 f_1^2 & 0 \\
\mathbf{a}^{-\,\mu} & & & & \frac{1}{2}g_\rho^2 \frac{f_1^4}{f_1^2-f^2}
\end{array}
$$

Table 4. Mass matrices for the neutral and singly charged bosons in the M4DCHM5.

blet resonances in such a way that they have definite quantum numbers under the $\mathrm{SO}(4) = \mathrm{SU}(2)_L \times \mathrm{SU}(2)_R$ custodial symmetry.[20]

For the up- and down-type quarks we find the mass matrices given in table 5.

For the exotically charged fermion resonances the mass matrices are independent of the Higgs field. Thus, they do not give a contribution to the Higgs potential, which is clear since they do not mix with elementary fields.

$$
M_{\mathrm{fermion}}^{+\frac{5}{3}} = \left(\begin{array}{c|cc} & Q_{uR}^{++} & \widetilde{Q}_{uR}^{++} \\ \hline \overline{Q}_{uL}^{++} & m_U & m_{Y_U} \\ \overline{\widetilde{Q}}_{uL}^{++} & 0 & m_{\widetilde{U}} \end{array}\right), \qquad
M_{\mathrm{fermion}}^{-\frac{4}{3}} = s \left(\begin{array}{c|cc} & Q_{dR}^{--} & \widetilde{Q}_{dR}^{--} \\ \hline \overline{Q}_{dL}^{--} & m_D & m_{Y_D} \\ \overline{\widetilde{Q}}_{dL}^{--} & 0 & m_{\widetilde{D}} \end{array}\right)
$$

Of course, the fields used above still carry flavour indices. As a consequence of this, all the entries tin the fermionic mass matrices actually are 3×3 matrices in flavour space, promoting the up- and down-type mass matrices to 27×27 objects. The explicit form of the entries is model dependent and will be given in appendix C.

Since we took the leptons as purely elementary, their mass matrices are just diagonal taking the SM values.

C Explicit form of the composite-elementary mixings

In this appendix, we give the explicit flavour structure of the composite-elementary mixings in the flavour symmetric models. We use bases where all unphysical parameters have already been rotated away and all phases have been made explicit.

- In $\mathrm{U}(3)_{\mathrm{LC}}^3$,

$$
\Delta_{u_L} = \Delta_{Lt}\, \mathbb{1}\,, \qquad \Delta_{u_R}^\dagger = V^\dagger \begin{pmatrix} \Delta_{Ru} & & \\ & \Delta_{Rc} & \\ & & \Delta_{Rt} \end{pmatrix}, \tag{C.1}
$$

$$
\Delta_{d_L} = \Delta_{Lb}\, \mathbb{1}\,, \qquad \Delta_{d_R}^\dagger = \begin{pmatrix} \Delta_{Rd} & & \\ & \Delta_{Rs} & \\ & & \Delta_{Rb} \end{pmatrix}. \tag{C.2}
$$

Here, V is the CKM matrix with 3 angles and 1 phase.

- In $\mathrm{U}(3)_{\mathrm{RC}}^3$,

$$
\Delta_{u_L} = V^\dagger \begin{pmatrix} \Delta_{Lu} & & \\ & \Delta_{Lc} & \\ & & \Delta_{Lt} \end{pmatrix}, \qquad \Delta_{u_R}^\dagger = \Delta_{Rt}\, \mathbb{1}\,, \tag{C.3}
$$

$$
\Delta_{d_L} = \begin{pmatrix} \Delta_{Ld} & & \\ & \Delta_{Ls} & \\ & & \Delta_{Lb} \end{pmatrix}, \qquad \Delta_{d_R}^\dagger = \Delta_{Rb}\, \mathbb{1}\,. \tag{C.4}
$$

[20]For example, the field Q_u^{+-} is part of a composite bidoublet resonance with $q_X^{(u)} = \frac{2}{3}$ and it has eigenvalues $+\frac{1}{2}$ and $-\frac{1}{2}$ under T^{3L} and T^{3R}, respectively.

$$
M^{(\mathrm{u})}_{\text{fermion}} =
\left(\begin{array}{c|ccccccccc}
 & u^0_R & Q^{+-}_{uR} & \widetilde{Q}^{+-}_{uR} & Q^{-+}_{uR} & \widetilde{Q}^{-+}_{uR} & Q^{++}_{dR} & \widetilde{Q}^{++}_{dR} & S_{uR} & \widetilde{S}_{uR} \\
\hline
\overline{u^0}_L & 0 & -\Delta_{u_L}\cos^2\!\left(\tfrac{h}{2f}\right) & 0 & \Delta_{u_L}\sin^2\!\left(\tfrac{h}{2f}\right) & 0 & -\Delta_{d_L} & 0 & \tfrac{i}{\sqrt{2}}\Delta_{u_L}\sin\!\left(\tfrac{h}{f}\right) & 0 \\
\overline{Q}^{+-}_{uL} & 0 & m_U & mY_U & 0 & 0 & 0 & 0 & 0 & 0 \\
\overline{\widetilde{Q}}^{+-}_{uL} & -\tfrac{i}{\sqrt{2}}\Delta^\dagger_{u_R}\sin\!\left(\tfrac{h}{f}\right) & 0 & m_{\widetilde{U}} & 0 & 0 & 0 & 0 & 0 & 0 \\
\overline{Q}^{-+}_{uL} & -\tfrac{i}{\sqrt{2}}\Delta^\dagger_{u_R}\sin\!\left(\tfrac{h}{f}\right) & 0 & 0 & m_U & mY_U & 0 & 0 & 0 & 0 \\
\overline{\widetilde{Q}}^{-+}_{uL} & 0 & 0 & 0 & 0 & m_{\widetilde{U}} & 0 & 0 & 0 & 0 \\
\overline{Q}^{++}_{dL} & 0 & 0 & 0 & 0 & 0 & m_D & mY_D & 0 & 0 \\
\overline{\widetilde{Q}}^{++}_{dL} & 0 & 0 & 0 & 0 & 0 & m_{\widetilde{D}} & 0 & 0 & 0 \\
\overline{S}_{uL} & 0 & 0 & 0 & 0 & 0 & 0 & 0 & m_U & mY_U + Y_U \\
\overline{\widetilde{S}}_{uL} & -\Delta^\dagger_{u_R}\cos\!\left(\tfrac{h}{f}\right) & 0 & 0 & 0 & 0 & 0 & 0 & 0 & m_{\widetilde{U}}
\end{array}\right)
$$

$$
M^{(\mathrm{d})}_{\text{fermion}} =
\left(\begin{array}{c|ccccccccc}
 & d^0_R & Q^{+-}_{dR} & \widetilde{Q}^{+-}_{dR} & Q^{-+}_{dR} & \widetilde{Q}^{-+}_{dR} & Q^{--}_{uR} & \widetilde{Q}^{--}_{uR} & S_{dR} & \widetilde{S}_{dR} \\
\hline
\overline{d^0}_L & 0 & \Delta_{d_L}\sin^2\!\left(\tfrac{h}{2f}\right) & 0 & -\Delta_{d_L}\cos^2\!\left(\tfrac{h}{2f}\right) & 0 & -\Delta_{u_L} & 0 & \tfrac{i}{\sqrt{2}}\Delta_{d_L}\sin\!\left(\tfrac{h}{f}\right) & 0 \\
\overline{Q}^{+-}_{dL} & 0 & m_D & mY_D & 0 & 0 & 0 & 0 & 0 & 0 \\
\overline{\widetilde{Q}}^{+-}_{dL} & -\tfrac{i}{\sqrt{2}}\Delta^\dagger_{d_R}\sin\!\left(\tfrac{h}{f}\right) & 0 & m_{\widetilde{D}} & 0 & 0 & 0 & 0 & 0 & 0 \\
\overline{Q}^{-+}_{dL} & -\tfrac{i}{\sqrt{2}}\Delta^\dagger_{d_R}\sin\!\left(\tfrac{h}{f}\right) & 0 & 0 & m_D & mY_D & 0 & 0 & 0 & 0 \\
\overline{\widetilde{Q}}^{-+}_{dL} & 0 & 0 & 0 & 0 & m_{\widetilde{D}} & 0 & 0 & 0 & 0 \\
\overline{Q}^{--}_{uL} & 0 & 0 & 0 & 0 & 0 & m_U & mY_U & 0 & 0 \\
\overline{\widetilde{Q}}^{--}_{uL} & 0 & 0 & 0 & 0 & 0 & m_{\widetilde{U}} & 0 & 0 & 0 \\
\overline{S}_{dL} & 0 & 0 & 0 & 0 & 0 & 0 & 0 & m_D & mY_D + Y_D \\
\overline{\widetilde{S}}_{dL} & -\Delta^\dagger_{d_R}\cos\!\left(\tfrac{h}{f}\right) & 0 & 0 & 0 & 0 & 0 & 0 & 0 & m_{\widetilde{D}}
\end{array}\right)
$$

Table 5. Mass matrices for the up- and down-type fermions in the M4DCHM5.

- In $\mathrm{U}(2)^3_{\mathrm{LC}}$,

$$\Delta_{u_L} = \begin{pmatrix} \Delta_{Lu} & & \\ & \Delta_{Lu} & \\ & & \Delta_{Lt} \end{pmatrix}, \quad \Delta_{u_R}^\dagger = \begin{pmatrix} c_u\Delta_{Ru} & -s_u\Delta_{Rc}e^{i\alpha_u} & \\ s_u\Delta_{Ru}e^{-i\alpha_u} & c_u\Delta_{Rc} & \epsilon_u\Delta_{Rt}e^{i\phi_t} \\ & & \Delta_{Rt} \end{pmatrix}, \quad \text{(C.5)}$$

$$\Delta_{d_L} = \begin{pmatrix} \Delta_{Ld} & & \\ & \Delta_{Ld} & \\ & & \Delta_{Lb} \end{pmatrix}, \quad \Delta_{d_R}^\dagger = \begin{pmatrix} c_d\Delta_{Rd} & -s_d\Delta_{Rs}e^{i\alpha_d} & \\ s_d\Delta_{Rd}e^{-i\alpha_d} & c_d\Delta_{Rs} & \epsilon_d\Delta_{Rb}e^{i\phi_b} \\ & & \Delta_{Rb} \end{pmatrix}.$$

$$\text{(C.6)}$$

- In $\mathrm{U}(2)^3_{\mathrm{RC}}$,

$$\Delta_{u_L} = \begin{pmatrix} c_u\Delta_{Lu} & -s_u\Delta_{Lc}e^{i\alpha_u} & \\ s_u\Delta_{Lu}e^{-i\alpha_u} & c_u\Delta_{Lc} & \epsilon_u\Delta_{Lt}e^{i\phi_t} \\ & & \Delta_{Lt} \end{pmatrix}, \quad \Delta_{u_R}^\dagger = \begin{pmatrix} \Delta_{Ru} & & \\ & \Delta_{Ru} & \\ & & \Delta_{Rt} \end{pmatrix}, \quad \text{(C.7)}$$

$$\Delta_{d_L} = \begin{pmatrix} c_d\Delta_{Ld} & -s_d\Delta_{Ls}e^{i\alpha_d} & \\ s_d\Delta_{Ld}e^{-i\alpha_d} & c_d\Delta_{Ls} & \epsilon_d\Delta_{Lb}e^{i\phi_b} \\ & & \Delta_{Lb} \end{pmatrix}, \quad \Delta_{d_R}^\dagger = \begin{pmatrix} \Delta_{Rd} & & \\ & \Delta_{Rd} & \\ & & \Delta_{Rb} \end{pmatrix}. \quad \text{(C.8)}$$

D   Constraints from the dijet angular distribution

As discussed in section 3.2.6, experimental analyses of contact interactions typically only quote constraints on a single operator — or for individual operators, but only allowing one at a time. To correctly treat the case with simultaneous contributions from multiple operators, we follow the procedure outlined in [119]. In this paper, analytical expressions are given for the dijet cross section in bins of the dijet mass m_{jj} and the rapidity χ. The most recent ATLAS and CMS analyses use multivariate techniques rather than considering only a ratio of bins. In our numerical analysis, we have thus adopted the following procedure:

1. We identify the most sensitive bin in the experimental analysis;

2. We compute the numerical coefficients $\vec{\mathcal{P}}$ and $\vec{\mathcal{Q}}$ defined as in [119] for the 8 TeV LHC in the respective bin.

3. We compute the NP contribution of all operators to the cross section in this bin;

4. We multiply our result by an overall factor to exactly reproduce the 95% C.L. bound on the Wilson coefficient $c_{qq}^{(1)}$ quoted in the experimental paper.

In this way, our approximation of computing the cross section analytically and pretending that only a single bin is relevant is only used for the relative contributions of the individual operators, while any overall change (such as k-factors) cancels out since we normalize to the bound obtained for the $c_{qq}^{(1)}$ coefficient by the experimentalists. We have checked that the relative contributions are not very sensitive to changes in the bin chosen in the first step.

In our numerical analysis, we use the bound from the most recent ATLAS analysis [178]. We assume the most sensitive bin to be the one with $\chi < 3.32$, $m_{jj} > 3.2\,\mathrm{TeV}$. We can then write the new physics contribution to the dijet cross section in this bin,

$$\sigma_{jj}^\chi = \int_1^{3.32} d\chi \left. \frac{d\sigma(pp \to jj)}{d\chi}\right|_{m_{jj} > 3.2\,\mathrm{TeV}}^{\mathrm{NP}} \tag{D.1}$$

normalized to the 95% C.L. cross section on this quantity extracted by reproducing the bound on $c_{qq}^{(1)}$ quoted in [178], as

$$\frac{\sigma_{jj}^\chi}{(\sigma_{jj}^\chi)_{95\%\ \mathrm{C.L.}}} = -\frac{1}{\Lambda^2}\vec{A}\cdot\vec{\mathcal{P}}' + \frac{1}{\Lambda^4}\vec{B}\cdot\vec{\mathcal{Q}}', \tag{D.2}$$

where $\vec{A}$ and $\vec{B}$ are given in eq. (16) of [119] and $\vec{\mathcal{P}}'$, $\vec{\mathcal{Q}}'$ are equal up to normalization to $\vec{\mathcal{P}}$, $\vec{\mathcal{Q}}$ defined in [119]. Numerically, we find

$$\vec{\mathcal{P}}' = \left(0.36 P'_{uu}, 0.12 P'_{uu}, 0.36 P'_{dd}, 0.12 P'_{dd}, 0.17 P'_{ud}, 0.74 P'_{ud}\right), \tag{D.3}$$

$$\vec{\mathcal{Q}}' = \left(0.013 Q'_{uu}, 0.0069 Q'_{uu}, 0.013 Q'_{dd}, 0.0069 Q'_{dd}, 0.0024 Q'_{ud}, 0.00097 Q'_{ud}\right), \tag{D.4}$$

where

$$P'_{uu} = (4.93\,\mathrm{TeV})^2, \qquad P'_{dd} = (1.46\,\mathrm{TeV})^2, \qquad P'_{ud} = (3.82\,\mathrm{TeV})^2. \tag{D.5}$$

$$Q'_{uu} = (7.93\,\mathrm{TeV})^4, \qquad Q'_{dd} = (4.28\,\mathrm{TeV})^4, \qquad Q'_{ud} = (6.95\,\mathrm{TeV})^4. \tag{D.6}$$

References

[1] D.B. Kaplan and H. Georgi, SU(2) × U(1) *breaking by vacuum misalignment*, *Phys. Lett.* **B 136** (1984) 183 [INSPIRE].

[2] M.J. Dugan, H. Georgi and D.B. Kaplan, *Anatomy of a composite Higgs model*, *Nucl. Phys.* **B 254** (1985) 299 [INSPIRE].

[3] D.B. Kaplan, *Flavor at SSC energies: a new mechanism for dynamically generated fermion masses*, *Nucl. Phys.* **B 365** (1991) 259 [INSPIRE].

[4] Y. Grossman and M. Neubert, *Neutrino masses and mixings in nonfactorizable geometry*, *Phys. Lett.* **B 474** (2000) 361 [hep-ph/9912408] [INSPIRE].

[5] T. Gherghetta and A. Pomarol, *Bulk fields and supersymmetry in a slice of AdS*, *Nucl. Phys.* **B 586** (2000) 141 [hep-ph/0003129] [INSPIRE].

[6] S.J. Huber and Q. Shafi, *Fermion masses, mixings and proton decay in a Randall-Sundrum model*, *Phys. Lett.* **B 498** (2001) 256 [hep-ph/0010195] [INSPIRE].

[7] C. Csáki, C. Grojean, J. Hubisz, Y. Shirman and J. Terning, *Fermions on an interval: quark and lepton masses without a Higgs*, *Phys. Rev.* **D 70** (2004) 015012 [hep-ph/0310355] [INSPIRE].

[8] R. Contino, Y. Nomura and A. Pomarol, *Higgs as a holographic pseudo-Goldstone boson*, *Nucl. Phys.* **B 671** (2003) 148 [hep-ph/0306259] [INSPIRE].

[9] K. Agashe, R. Contino and A. Pomarol, *The minimal composite Higgs model*, *Nucl. Phys.* **B 719** (2005) 165 [hep-ph/0412089] [INSPIRE].

[10] G. Panico and A. Wulzer, *Effective action and holography in 5D gauge theories*, *JHEP* **05** (2007) 060 [hep-th/0703287] [INSPIRE].

[11] S. De Curtis, M. Redi and A. Tesi, *The 4D composite Higgs*, *JHEP* **04** (2012) 042 [arXiv:1110.1613] [INSPIRE].

[12] G. Panico and A. Wulzer, *The discrete composite Higgs model*, *JHEP* **09** (2011) 135 [arXiv:1106.2719] [INSPIRE].

[13] D. Marzocca, M. Serone and J. Shu, *General composite Higgs models*, *JHEP* **08** (2012) 013 [arXiv:1205.0770] [INSPIRE].

[14] B. Bellazzini, C. Csáki and J. Serra, *Composite higgses*, *Eur. Phys. J.* **C 74** (2014) 2766 [arXiv:1401.2457] [INSPIRE].

[15] G. Panico and A. Wulzer, *The composite Nambu-Goldstone Higgs*, *Lect. Notes Phys.* **913** (2016) 1 [arXiv:1506.01961] [INSPIRE].

[16] C. Grojean, O. Matsedonskyi and G. Panico, *Light top partners and precision physics*, *JHEP* **10** (2013) 160 [arXiv:1306.4655] [INSPIRE].

[17] R. Contino and M. Salvarezza, *One-loop effects from spin-1 resonances in Composite Higgs models*, *JHEP* **07** (2015) 065 [arXiv:1504.02750] [INSPIRE].

[18] R. Barbieri, D. Buttazzo, F. Sala, D.M. Straub and A. Tesi, *A 125 GeV composite Higgs boson versus flavour and electroweak precision tests*, *JHEP* **05** (2013) 069 [arXiv:1211.5085] [INSPIRE].

[19] M. König, M. Neubert and D.M. Straub, *Dipole operator constraints on composite Higgs models*, *Eur. Phys. J.* **C 74** (2014) 2945 [arXiv:1403.2756] [INSPIRE].

[20] A. Azatov, G. Panico, G. Perez and Y. Soreq, *On the flavor structure of natural composite Higgs models & top flavor violation*, *JHEP* **12** (2014) 082 [arXiv:1408.4525] [INSPIRE].

[21] C. Csáki, A. Falkowski and A. Weiler, *The flavor of the composite pseudo-Goldstone Higgs*, *JHEP* **09** (2008) 008 [arXiv:0804.1954] [INSPIRE].

[22] I. Low and A. Vichi, *On the production of a composite Higgs boson*, *Phys. Rev.* **D 84** (2011) 045019 [arXiv:1010.2753] [INSPIRE].

[23] M. Gillioz, R. Grober, C. Grojean, M. Muhlleitner and E. Salvioni, *Higgs low-energy theorem (and its corrections) in composite models*, *JHEP* **10** (2012) 004 [arXiv:1206.7120] [INSPIRE].

[24] M. Montull, F. Riva, E. Salvioni and R. Torre, *Higgs couplings in composite models*, *Phys. Rev.* **D 88** (2013) 095006 [arXiv:1308.0559] [INSPIRE].

[25] M. Carena, L. Da Rold and E. Pontón, *Minimal composite Higgs models at the LHC*, *JHEP* **06** (2014) 159 [arXiv:1402.2987] [INSPIRE].

[26] A. De Simone, O. Matsedonskyi, R. Rattazzi and A. Wulzer, *A first top partner hunter's guide*, *JHEP* **04** (2013) 004 [arXiv:1211.5663] [INSPIRE].

[27] M. Redi, V. Sanz, M. de Vries and A. Weiler, *Strong signatures of right-handed compositeness*, *JHEP* **08** (2013) 008 [arXiv:1305.3818] [inSPIRE].

[28] J. Li, D. Liu and J. Shu, *Towards the fate of natural composite Higgs model through single t′ search at the 8 TeV LHC*, *JHEP* **11** (2013) 047 [arXiv:1306.5841] [inSPIRE].

[29] A. Azatov, M. Salvarezza, M. Son and M. Spannowsky, *Boosting top partner searches in composite Higgs models*, *Phys. Rev.* **D 89** (2014) 075001 [arXiv:1308.6601] [inSPIRE].

[30] C. Delaunay, T. Flacke, J. Gonzalez-Fraile, S.J. Lee, G. Panico and G. Perez, *Light non-degenerate composite partners at the LHC*, *JHEP* **02** (2014) 055 [arXiv:1311.2072] [inSPIRE].

[31] J. Reuter and M. Tonini, *Top partner discovery in the $T \to tZ$ channel at the LHC*, *JHEP* **01** (2015) 088 [arXiv:1409.6962] [inSPIRE].

[32] B. Gripaios, T. Müller, M.A. Parker and D. Sutherland, *Search strategies for top partners in composite Higgs models*, *JHEP* **08** (2014) 171 [arXiv:1406.5957] [inSPIRE].

[33] O. Matsedonskyi, G. Panico and A. Wulzer, *On the interpretation of top partners searches*, *JHEP* **12** (2014) 097 [arXiv:1409.0100] [inSPIRE].

[34] M. Backovic, T. Flacke, J.H. Kim and S.J. Lee, *Search strategies for TeV scale fermionic top partners with charge 2/3*, arXiv:1507.06568 [inSPIRE].

[35] K. Agashe, A. Azatov, T. Han, Y. Li, Z.-G. Si and L. Zhu, *LHC signals for coset electroweak gauge bosons in warped/composite PGB Higgs models*, *Phys. Rev.* **D 81** (2010) 096002 [arXiv:0911.0059] [inSPIRE].

[36] D. Pappadopulo, A. Thamm, R. Torre and A. Wulzer, *Heavy vector triplets: bridging theory and data*, *JHEP* **09** (2014) 060 [arXiv:1402.4431] [inSPIRE].

[37] K. Lane, *A composite Higgs model with minimal fine-tuning: The large-N and weak-technicolor limit*, *Phys. Rev.* **D 90** (2014) 095025 [arXiv:1407.2270] [inSPIRE].

[38] A. Thamm, R. Torre and A. Wulzer, *Future tests of Higgs compositeness: direct vs indirect*, *JHEP* **07** (2015) 100 [arXiv:1502.01701] [inSPIRE].

[39] A. Kaminska, *Improving LHC searches for strong EW symmetry breaking resonances*, arXiv:1505.04645 [inSPIRE].

[40] S. Casagrande, F. Goertz, U. Haisch, M. Neubert and T. Pfoh, *Flavor physics in the Randall-Sundrum model: I. Theoretical setup and electroweak precision tests*, *JHEP* **10** (2008) 094 [arXiv:0807.4937] [inSPIRE].

[41] M. Blanke, A.J. Buras, B. Duling, S. Gori and A. Weiler, *$\Delta F = 2$ observables and fine-tuning in a warped extra dimension with custodial protection*, *JHEP* **03** (2009) 001 [arXiv:0809.1073] [inSPIRE].

[42] M. Blanke, A.J. Buras, B. Duling, K. Gemmler and S. Gori, *Rare K and B decays in a warped extra dimension with custodial protection*, *JHEP* **03** (2009) 108 [arXiv:0812.3803] [inSPIRE].

[43] M.E. Albrecht, M. Blanke, A.J. Buras, B. Duling and K. Gemmler, *Electroweak and flavour structure of a warped extra dimension with custodial protection*, *JHEP* **09** (2009) 064 [arXiv:0903.2415] [inSPIRE].

[44] M. Bauer, S. Casagrande, U. Haisch and M. Neubert, *Flavor physics in the*

Randall-Sundrum model: II. Tree-level weak-interaction processes, *JHEP* **09** (2010) 017 [arXiv:0912.1625] [inSPIRE].

[45] S. Casagrande, F. Goertz, U. Haisch, M. Neubert and T. Pfoh, *The custodial Randall-Sundrum model: from precision tests to Higgs physics*, *JHEP* **09** (2010) 014 [arXiv:1005.4315] [inSPIRE].

[46] D.M. Straub, *Anatomy of flavour-changing Z couplings in models with partial compositeness*, *JHEP* **08** (2013) 108 [arXiv:1302.4651] [inSPIRE].

[47] K. Agashe, R. Contino, L. Da Rold and A. Pomarol, *A custodial symmetry for Zbb̄*, *Phys. Lett.* **B 641** (2006) 62 [hep-ph/0605341] [inSPIRE].

[48] R. Contino, L. Da Rold and A. Pomarol, *Light custodians in natural composite Higgs models*, *Phys. Rev.* **D 75** (2007) 055014 [hep-ph/0612048] [inSPIRE].

[49] A. Pomarol and F. Riva, *The composite Higgs and light resonance connection*, *JHEP* **08** (2012) 135 [arXiv:1205.6434] [inSPIRE].

[50] O. Matsedonskyi, G. Panico and A. Wulzer, *Light top partners for a light composite Higgs*, *JHEP* **01** (2013) 164 [arXiv:1204.6333] [inSPIRE].

[51] A.L. Fitzpatrick, G. Perez and L. Randall, *Flavor anarchy in a Randall-Sundrum model with 5D minimal flavor violation and a low Kaluza-Klein scale*, *Phys. Rev. Lett.* **100** (2008) 171604 [arXiv:0710.1869] [inSPIRE].

[52] C. Csáki, A. Falkowski and A. Weiler, *A simple flavor protection for RS*, *Phys. Rev.* **D 80** (2009) 016001 [arXiv:0806.3757] [inSPIRE].

[53] J. Santiago, *Minimal flavor protection: a new flavor paradigm in warped models*, *JHEP* **12** (2008) 046 [arXiv:0806.1230] [inSPIRE].

[54] C. Csáki, G. Perez, Z. Surujon and A. Weiler, *Flavor alignment via shining in RS*, *Phys. Rev.* **D 81** (2010) 075025 [arXiv:0907.0474] [inSPIRE].

[55] C. Delaunay, O. Gedalia, S.J. Lee, G. Perez and E. Ponton, *Ultra visible warped model from flavor triviality and improved naturalness*, *Phys. Rev.* **D 83** (2011) 115003 [arXiv:1007.0243] [inSPIRE].

[56] M. Redi, *Composite MFV and beyond*, *Eur. Phys. J.* **C 72** (2012) 2030 [arXiv:1203.4220] [inSPIRE].

[57] O. Matsedonskyi, *On flavour and naturalness of composite Higgs models*, *JHEP* **02** (2015) 154 [arXiv:1411.4638] [inSPIRE].

[58] G. Cacciapaglia et al., *Anarchic Yukawas and top partial compositeness: the flavour of a successful marriage*, *JHEP* **06** (2015) 085 [arXiv:1501.03818] [inSPIRE].

[59] G. Cacciapaglia et al., *A GIM mechanism from extra dimensions*, *JHEP* **04** (2008) 006 [arXiv:0709.1714] [inSPIRE].

[60] M. Redi and A. Weiler, *Flavor and CP invariant composite Higgs models*, *JHEP* **11** (2011) 108 [arXiv:1106.6357] [inSPIRE].

[61] R. Barbieri, D. Buttazzo, F. Sala and D.M. Straub, *Flavour physics from an approximate U(2)³ symmetry*, *JHEP* **07** (2012) 181 [arXiv:1203.4218] [inSPIRE].

[62] A. Carmona and F. Goertz, *A naturally light Higgs without light top partners*, *JHEP* **05** (2015) 002 [arXiv:1410.8555] [inSPIRE].

[63] C. Niehoff, P. Stangl and D.M. Straub, *Violation of lepton flavour universality in composite Higgs models*, *Phys. Lett.* **B 747** (2015) 182 [arXiv:1503.03865] [INSPIRE].

[64] S.R. Coleman and E.J. Weinberg, *Radiative corrections as the origin of spontaneous symmetry breaking*, *Phys. Rev.* **D 7** (1973) 1888 [INSPIRE].

[65] K.G. Chetyrkin, J.H. Kuhn and M. Steinhauser, *RunDec: a Mathematica package for running and decoupling of the strong coupling and quark masses*, *Comput. Phys. Commun.* **133** (2000) 43 [hep-ph/0004189] [INSPIRE].

[66] PARTICLE DATA GROUP collaboration, K.A. Olive et al., *Review of particle physics*, *Chin. Phys.* **C 38** (2014) 090001 [INSPIRE].

[67] SLD ELECTROWEAK GROUP, DELPHI, ALEPH, SLD, SLD HEAVY FLAVOUR GROUP, OPAL, LEP ELECTROWEAK WORKING GROUP, L3 collaboration, S. Schael et al., *Precision electroweak measurements on the Z resonance*, *Phys. Rept.* **427** (2006) 257 [hep-ex/0509008] [INSPIRE].

[68] J.C. Hardy and I.S. Towner, *Superallowed $0^+ \to 0^+$ nuclear β decays: 2014 critical survey, with precise results for V_{ud} and CKM unitarity*, *Phys. Rev.* **C 91** (2015) 025501 [arXiv:1411.5987] [INSPIRE].

[69] S. Aoki et al., *Review of lattice results concerning low-energy particle physics*, *Eur. Phys. J.* **C 74** (2014) 2890 [arXiv:1310.8555] [INSPIRE].

[70] FERMILAB LATTICE, MILC collaboration, J.A. Bailey et al., *$|V_{ub}|$ from $B \to \pi\ell\nu$ decays and $(2+1)$-flavor lattice QCD*, *Phys. Rev.* **D 92** (2015) 014024 [arXiv:1503.07839] [INSPIRE].

[71] CMS collaboration, *Precise determination of the mass of the Higgs boson and tests of compatibility of its couplings with the standard model predictions using proton collisions at 7 and 8 TeV*, *Eur. Phys. J.* **C 75** (2015) 212 [arXiv:1412.8662] [INSPIRE].

[72] ATLAS collaboration, *Measurements of the Higgs boson production and decay rates and coupling strengths using pp collision data at $\sqrt{s} = 7$ and 8 TeV in the ATLAS experiment*, arXiv:1507.04548.

[73] BABAR collaboration, J.P. Lees et al., *Study of $\bar{B} \to X_u\ell\bar{\nu}$ decays in $B\bar{B}$ events tagged by a fully reconstructed B-meson decay and determination of $|V_{ub}|$*, *Phys. Rev.* **D 86** (2012) 032004 [arXiv:1112.0702] [INSPIRE].

[74] FERMILAB LATTICE, MILC collaboration, J.A. Bailey et al., *Update of $|V_{cb}|$ from the $\bar{B} \to D^*\ell\bar{\nu}$ form factor at zero recoil with three-flavor lattice QCD*, *Phys. Rev.* **D 89** (2014) 114504 [arXiv:1403.0635] [INSPIRE].

[75] A. Alberti, P. Gambino, K.J. Healey and S. Nandi, *Precision determination of the Cabibbo-Kobayashi-Maskawa element V_{cb}*, *Phys. Rev. Lett.* **114** (2015) 061802 [arXiv:1411.6560] [INSPIRE].

[76] CMS collaboration, *Measurement of the t-channel single-top-quark production cross section and of the $|V_{tb}|$ CKM matrix element in pp collisions at $\sqrt{s} = 8$ TeV*, *JHEP* **06** (2014) 090 [arXiv:1403.7366] [INSPIRE].

[77] HEAVY FLAVOR AVERAGING GROUP (HFAG) collaboration, Y. Amhis et al., *Averages of b-hadron, c-hadron and τ-lepton properties as of summer 2014*, arXiv:1412.7515 [INSPIRE].

[78] LHCb collaboration, *Precision measurement of CP violation in $B_s^0 \to J/\psi K^+ K^-$ decays*, *Phys. Rev. Lett.* **114** (2015) 041801 [arXiv:1411.3104] [INSPIRE].

[79] GFITTER GROUP collaboration, M. Baak et al., *The global electroweak fit at NNLO and prospects for the LHC and ILC*, *Eur. Phys. J.* **C 74** (2014) 3046 [arXiv:1407.3792] [INSPIRE].

[80] J. Charles et al., *Current status of the standard model CKM fit and constraints on $\Delta F = 2$ new physics*, *Phys. Rev.* **D 91** (2015) 073007 [arXiv:1501.05013] [INSPIRE].

[81] R. Barbieri, B. Bellazzini, V.S. Rychkov and A. Varagnolo, *The Higgs boson from an extended symmetry*, *Phys. Rev.* **D 76** (2007) 115008 [arXiv:0706.0432] [INSPIRE].

[82] A. Orgogozo and S. Rychkov, *The S parameter for a light composite Higgs: a dispersion relation approach*, *JHEP* **06** (2013) 014 [arXiv:1211.5543] [INSPIRE].

[83] T. Hahn and M. Pérez-Victoria, *Automatized one loop calculations in four-dimensions and D-dimensions*, *Comput. Phys. Commun.* **118** (1999) 153 [hep-ph/9807565] [INSPIRE].

[84] D.M. Pierce, J.A. Bagger, K.T. Matchev and R.-j. Zhang, *Precision corrections in the minimal supersymmetric standard model*, *Nucl. Phys.* **B 491** (1997) 3 [hep-ph/9606211] [INSPIRE].

[85] A. Freitas, *Higher-order electroweak corrections to the partial widths and branching ratios of the Z boson*, *JHEP* **04** (2014) 070 [arXiv:1401.2447] [INSPIRE].

[86] M. Carena, E. Ponton, J. Santiago and C.E.M. Wagner, *Electroweak constraints on warped models with custodial symmetry*, *Phys. Rev.* **D 76** (2007) 035006 [hep-ph/0701055] [INSPIRE].

[87] C. Anastasiou, E. Furlan and J. Santiago, *Realistic composite Higgs models*, *Phys. Rev.* **D 79** (2009) 075003 [arXiv:0901.2117] [INSPIRE].

[88] B. Grzadkowski, M. Iskrzynski, M. Misiak and J. Rosiek, *Dimension-six terms in the standard model lagrangian*, *JHEP* **10** (2010) 085 [arXiv:1008.4884] [INSPIRE].

[89] E.E. Jenkins, A.V. Manohar and M. Trott, *Renormalization group evolution of the standard model dimension six operators II: Yukawa dependence*, *JHEP* **01** (2014) 035 [arXiv:1310.4838] [INSPIRE].

[90] R. Alonso, E.E. Jenkins, A.V. Manohar and M. Trott, *Renormalization group evolution of the standard model dimension six operators III: gauge coupling dependence and phenomenology*, *JHEP* **04** (2014) 159 [arXiv:1312.2014] [INSPIRE].

[91] J. Brod, A. Greljo, E. Stamou and P. Uttayarat, *Probing anomalous $t\bar{t}Z$ interactions with rare meson decays*, *JHEP* **02** (2015) 141 [arXiv:1408.0792] [INSPIRE].

[92] A.J. Buras, *Weak Hamiltonian, CP-violation and rare decays*, in the proceedings of the *Summer School in Theoretical Physics*, 68th session, July 28–September 5, Les Houches, France (1997), hep-ph/9806471 [INSPIRE].

[93] A.J. Buras, S. Jager and J. Urban, *Master formulae for $\Delta F = 2$ NLO QCD factors in the standard model and beyond*, *Nucl. Phys.* **B 605** (2001) 600 [hep-ph/0102316] [INSPIRE].

[94] ETM collaboration, V. Bertone et al., *Kaon mixing beyond the SM from $N_f = 2$ tmQCD and model independent constraints from the UTA*, *JHEP* **03** (2013) 089 [*Erratum ibid.* **1307** (2013) 143] [arXiv:1207.1287] [INSPIRE].

[95] N. Carrasco et al., *D^0-$\bar{D}^0$ mixing in the standard model and beyond from $N_f = 2$ twisted mass QCD*, *Phys. Rev.* **D 90** (2014) 014502 [arXiv:1403.7302] [INSPIRE].

[96] P. Frings, U. Nierste and M. Wiebusch, *Penguin contributions to CP phases in $B_{d,s}$ decays to charmonium*, *Phys. Rev. Lett.* **115** (2015) 061802 [arXiv:1503.00859] [INSPIRE].

[97] CMS collaboration, *Measurement of the CP-violating weak phase ϕ_s and the decay width difference $\Delta\Gamma_s$ using the $B_s^0 \to J/\psi\phi(1020)$ decay channel in pp collisions at $\sqrt{s} = 8$ TeV*, arXiv:1507.07527 [INSPIRE].

[98] ATLAS collaboration, *Flavor tagged time-dependent angular analysis of the $B_s \to J/\psi\phi$ decay and extraction of $\Delta\Gamma_s$ and the weak phase ϕ_s in ATLAS*, *Phys. Rev.* **D 90** (2014) 052007 [arXiv:1407.1796] [INSPIRE].

[99] Z. Bai, N.H. Christ, T. Izubuchi, C.T. Sachrajda, A. Soni and J. Yu, *K_L-K_S mass difference from lattice QCD*, *Phys. Rev. Lett.* **113** (2014) 112003 [arXiv:1406.0916] [INSPIRE].

[100] M. Misiak et al., *Updated NNLO QCD predictions for the weak radiative B-meson decays*, *Phys. Rev. Lett.* **114** (2015) 221801 [arXiv:1503.01789] [INSPIRE].

[101] A.J. Buras, L. Merlo and E. Stamou, *The impact of flavour changing neutral gauge bosons on $\bar{B} \to X_s\gamma$*, *JHEP* **08** (2011) 124 [arXiv:1105.5146] [INSPIRE].

[102] K. Agashe et al., *LHC signals for warped electroweak neutral gauge bosons*, *Phys. Rev.* **D 76** (2007) 115015 [arXiv:0709.0007] [INSPIRE].

[103] LHCb collaboration, *Angular analysis of the $B^0 \to K^{*0}\mu^+\mu^-$ decay*, arXiv:1512.04442.

[104] S. Descotes-Genon, L. Hofer, J. Matias and J. Virto, *On the impact of power corrections in the prediction of $B \to K^*\mu^+\mu^-$ observables*, *JHEP* **12** (2014) 125 [arXiv:1407.8526] [INSPIRE].

[105] A. Bharucha, D.M. Straub and R. Zwicky, *$B \to V\ell^+\ell^-$ in the standard model from light-cone sum rules*, arXiv:1503.05534 [INSPIRE].

[106] LHCb collaboration, *Angular analysis and differential branching fraction of the decay $B_s^0 \to \phi\mu^+\mu^-$*, *JHEP* **09** (2015) 179 [arXiv:1506.08777] [INSPIRE].

[107] LHCb collaboration, *Test of lepton universality using $B^+ \to K^+\ell^+\ell^-$ decays*, *Phys. Rev. Lett.* **113** (2014) 151601 [arXiv:1406.6482] [INSPIRE].

[108] J. Lyon and R. Zwicky, *Resonances gone topsy turvy — The charm of QCD or new physics in $b \to s\ell^+\ell^-$?*, arXiv:1406.0566 [INSPIRE].

[109] S. Jäger and J. Martin Camalich, *Reassessing the discovery potential of the $B \to K^*\ell^+\ell^-$ decays in the large-recoil region: SM challenges and BSM opportunities*, arXiv:1412.3183 [INSPIRE].

[110] S. Descotes-Genon, J. Matias and J. Virto, *Understanding the $B \to K^*\mu^+\mu^-$ anomaly*, *Phys. Rev.* **D 88** (2013) 074002 [arXiv:1307.5683] [INSPIRE].

[111] W. Altmannshofer and D.M. Straub, *New physics in $B \to K^*\mu\mu$?*, *Eur. Phys. J.* **C 73** (2013) 2646 [arXiv:1308.1501] [INSPIRE].

[112] F. Beaujean, C. Bobeth and D. van Dyk, *Comprehensive bayesian analysis of rare (semi)leptonic and radiative B decays*, *Eur. Phys. J.* **C 74** (2014) 2897 [*Erratum ibid.* **C 74** (2014) 3179] [arXiv:1310.2478] [INSPIRE].

[113] G. Hiller and M. Schmaltz, *R_K and future $b \to s\ell\ell$ physics beyond the standard model opportunities*, *Phys. Rev.* **D 90** (2014) 054014 [arXiv:1408.1627] [INSPIRE].

[114] D. Ghosh, M. Nardecchia and S.A. Renner, *Hint of lepton flavour non-universality in B meson decays*, *JHEP* **12** (2014) 131 [arXiv:1408.4097] [INSPIRE].

[115] W. Altmannshofer and D.M. Straub, *New physics in* $b \to s$ *transitions after LHC run 1*, *Eur. Phys. J.* **C 75** (2015) 382 [arXiv:1411.3161] [ɪɴSPIRE].

[116] B. Gripaios, M. Nardecchia and S.A. Renner, *Composite leptoquarks and anomalies in B-meson decays*, *JHEP* **05** (2015) 006 [arXiv:1412.1791] [ɪɴSPIRE].

[117] LHCʙ, CMS collaboration, V. Khachatryan et al., *Observation of the rare* $B_s^0 \to \mu^+\mu^-$ *decay from the combined analysis of CMS and LHCb data*, *Nature* **522** (2015) 68 [arXiv:1411.4413] [ɪɴSPIRE].

[118] C. Bobeth, M. Gorbahn, T. Hermann, M. Misiak, E. Stamou and M. Steinhauser, $B_{s,d} \to \ell^+\ell^-$ *in the standard model with reduced theoretical uncertainty*, *Phys. Rev. Lett.* **112** (2014) 101801 [arXiv:1311.0903] [ɪɴSPIRE].

[119] O. Domenech, A. Pomarol and J. Serra, *Probing the SM with dijets at the LHC*, *Phys. Rev.* **D 85** (2012) 074030 [arXiv:1201.6510] [ɪɴSPIRE].

[120] M. de Vries, *Four-quark effective operators at hadron colliders*, *JHEP* **03** (2015) 095 [arXiv:1409.4657] [ɪɴSPIRE].

[121] CMS collaboration, *Search for heavy quarks decaying into a top quark and a W or Z boson using lepton + jets events in pp collisions at* $\sqrt{s} = 7$ *TeV*, *JHEP* **01** (2013) 154 [arXiv:1210.7471] [ɪɴSPIRE].

[122] ATLAS collaboration, *Search for pair-produced heavy quarks decaying to Wq in the two-lepton channel at* $\sqrt{s} = 7$ *TeV with the ATLAS detector*, *Phys. Rev.* **D 86** (2012) 012007 [arXiv:1202.3389] [ɪɴSPIRE].

[123] CDF collaboration, *Search for heavy top* $t' \to Wq$ *in lepton plus jets events in* $\int \mathcal{L}dt = 4.6$ fb^{-1}, CDF-PUB-TOP-PUBLIC-10110 (2010).

[124] CMS collaboration, *Search for vector-like quarks in final states with a single lepton and jets in pp collisions at* $\sqrt{s} = 8$ *TeV*, CMS-PAS-B2G-12-017 (2012).

[125] CDF collaboration, *Search for new particles decaying to* Z^0 *+jets*, CDF note 85900 (2006).

[126] CMS collaboration, *Search for a vector-like quark with charge 2/3 in t + Z events from pp collisions at* $\sqrt{s} = 7$ *TeV*, *Phys. Rev. Lett.* **107** (2011) 271802 [arXiv:1109.4985] [ɪɴSPIRE].

[127] ATLAS collaboration, *Search for production of vector-like quark pairs and of four top quarks in the lepton plus jets final state in pp collisions at* $\sqrt{s} = 8$ *TeV with the ATLAS detector*, *JHEP* **08** (2015) 015 [arXiv:1505.04306].

[128] CMS collaboration, *Search for pair-produced vector-like quarks of charge* $-1/3$ *in lepton+jets final state in pp collisions at* $\sqrt{s} = 8$ *TeV*, CMS-PAS-B2G-12-019 (2012).

[129] CMS collaboration, *Search for vector-like* b' *pair production with multilepton final states in pp collisions at* $\sqrt{s} = 8$ *TeV*, CMS-PAS-B2G-13-003 (2013).

[130] CMS collaboration, *Search for pair-produced vector-like quarks of charge* $-1/3$ *decaying to bH using boosted Higgs jet-tagging in pp collisions at* $\sqrt{s} = 8$ *TeV*, CMS-PAS-B2G-14-001 (2014).

[131] CMS collaboration, *Search for a vector-like quark of charge* $-1/3$ *and decaying to bZ in pp collisions at* $\sqrt{s} = 7$ *TeV*, CMS-PAS-EXO-11-066 (2011).

[132] CMS collaboration, *Search for pair-produced vector-like quarks of charge* $-1/3$ *in dilepton+jets final state in pp collisions at* $\sqrt{s} = 8$ *TeV*, CMS-PAS-B2G-12-021 (2012).

[133] ATLAS collaboration, *Analysis of events with b-jets and a pair of leptons of the same charge in pp collisions at $\sqrt{s} = 8$ TeV with the ATLAS detector*, *JHEP* **10** (2015) 150 [arXiv:1504.04605] [InSPIRE].

[134] CDF collaboration, T. Aaltonen et al., *Search for new bottomlike quark pair decays $Q\bar{Q} \rightarrow (tW^{\mp})(\bar{t}W^{\pm})$ in same-charge dilepton events*, *Phys. Rev. Lett.* **104** (2010) 091801 [arXiv:0912.1057] [InSPIRE].

[135] CMS collaboration, *Search for heavy, top-like quark pair production in the dilepton final state in pp collisions at $\sqrt{s} = 7$ TeV*, *Phys. Lett.* **B 716** (2012) 103 [arXiv:1203.5410] [InSPIRE].

[136] CMS collaboration, *Search for pair produced fourth-generation up-type quarks in pp collisions at $\sqrt{s} = 7$ TeV with a lepton in the final state*, *Phys. Lett.* **B 718** (2012) 307 [arXiv:1209.0471] [InSPIRE].

[137] ATLAS collaboration, *Search for pair production of heavy top-like quarks decaying to a high-p_T W boson and a b quark in the lepton plus jets final state at $\sqrt{s} = 7$ TeV with the ATLAS detector*, *Phys. Lett.* **B 718** (2013) 1284 [arXiv:1210.5468] [InSPIRE].

[138] ATLAS collaboration, *Search for vectorlike B quarks in events with one isolated lepton, missing transverse momentum and jets at $\sqrt{s} = 8$ TeV with the ATLAS detector*, *Phys. Rev.* **D 91** (2015) 112011 [arXiv:1503.05425] [InSPIRE].

[139] CMS collaboration, *Search for top partners with charge 5e/3 in the same-sign dilepton final state*, CMS-PAS-B2G-12-012 (2012).

[140] CMS collaboration, *Search for vector-like top quark partners produced in association with Higgs bosons in the diphoton final state*, CMS-PAS-B2G-14-003 (2014).

[141] M. Aliev, H. Lacker, U. Langenfeld, S. Moch, P. Uwer and M. Wiedermann, *HATHOR: HAdronic Top and Heavy quarks crOss section calculatoR*, *Comput. Phys. Commun.* **182** (2011) 1034 [arXiv:1007.1327] [InSPIRE].

[142] M. Backović, T. Flacke, S.J. Lee and G. Perez, *LHC top partner searches beyond the 2 TeV mass region*, *JHEP* **09** (2015) 022 [arXiv:1409.0409] [InSPIRE].

[143] A. Azatov, D. Chowdhury, D. Ghosh and T.S. Ray, *Same sign di-lepton candles of the composite gluons*, *JHEP* **08** (2015) 140 [arXiv:1505.01506] [InSPIRE].

[144] J.P. Araque, N.F. Castro and J. Santiago, *Interpretation of vector-like quark searches: heavy gluons in composite Higgs models*, *JHEP* **11** (2015) 120 [arXiv:1507.05628] [InSPIRE].

[145] A. Anandakrishnan, J.H. Collins, M. Farina, E. Kuflik and M. Perelstein, *Odd top partners at the LHC*, arXiv:1506.05130 [InSPIRE].

[146] ATLAS collaboration, *ATLAS search for a heavy gauge boson decaying to a charged lepton and a neutrino in pp collisions at $\sqrt{s} = 7$ TeV*, *Eur. Phys. J.* **C 72** (2012) 2241 [arXiv:1209.4446] [InSPIRE].

[147] ATLAS collaboration, *Search for a new resonance decaying to a W or Z boson and a Higgs boson in the $\ell\ell/\ell\nu/\nu\nu + b\bar{b}$ final states with the ATLAS detector*, *Eur. Phys. J.* **C 75** (2015) 263 [arXiv:1503.08089] [InSPIRE].

[148] CMS collaboration, *Search for massive WH resonances decaying to $\ell\nu b\bar{b}$ final state in the boosted regime at $\sqrt{s} = 8$ TeV*, CMS-PAS-EXO-14-010 (2014).

[149] ATLAS collaboration, *Search for production of WW/WZ resonances decaying to a lepton, neutrino and jets in pp collisions at* $\sqrt{s} = 8\,TeV$ *with the ATLAS detector*, *Eur. Phys. J.* **C 75** (2015) 209 [*Erratum ibid.* **C 75** (2015) 370] [arXiv:1503.04677] [ɪɴSPIRE].

[150] ATLAS collaboration, *Search for WZ resonances in the fully leptonic channel using pp collisions at* $\sqrt{s} = 8\,TeV$ *with the ATLAS detector*, *Phys. Lett.* **B 737** (2014) 223 [arXiv:1406.4456] [ɪɴSPIRE].

[151] ATLAS collaboration, *Search for high-mass diboson resonances with boson-tagged jets in proton-proton collisions at* $\sqrt{s} = 8\ TeV$ *with the ATLAS detector*, *JHEP* **12** (2015) 055 [arXiv:1506.00962] [ɪɴSPIRE].

[152] CMS collaboration, *Search for massive resonances in dijet systems containing jets tagged as W or Z boson decays in pp collisions at* $\sqrt{s} = 8\ TeV$, *JHEP* **08** (2014) 173 [arXiv:1405.1994] [ɪɴSPIRE].

[153] CMS collaboration, *Search for* $W' \to tb$ *decays in the lepton + jets final state in pp collisions at* $\sqrt{s} = 8\ TeV$, *JHEP* **05** (2014) 108 [arXiv:1402.2176] [ɪɴSPIRE].

[154] CMS collaboration, *Search for massive resonances decaying into pairs of boosted bosons in semi-leptonic final states at* $\sqrt{s} = 8\ TeV$, *JHEP* **08** (2014) 174 [arXiv:1405.3447] [ɪɴSPIRE].

[155] CMS collaboration, *Search for narrow high-mass resonances in proton-proton collisions at* $\sqrt{s} = 8\ TeV$ *decaying to a Z and a Higgs boson*, *Phys. Lett.* **B 748** (2015) 255 [arXiv:1502.04994] [ɪɴSPIRE].

[156] ATLAS collaboration, *Search for high-mass dilepton resonances in pp collisions at* $\sqrt{s} = 8$ *TeV with the ATLAS detector*, *Phys. Rev.* **D 90** (2014) 052005 [arXiv:1405.4123] [ɪɴSPIRE].

[157] CMS collaboration, *Search for physics beyond the standard model in dilepton mass spectra in proton-proton collisions at* $\sqrt{s} = 8\ TeV$, *JHEP* **04** (2015) 025 [arXiv:1412.6302] [ɪɴSPIRE].

[158] ATLAS collaboration, *A search for* $t\bar{t}$ *resonances using lepton plus jets events in proton-proton collisions at* $\sqrt{s} = 8\ TeV$ *with the ATLAS detector*, arXiv:1505.07018.

[159] CMS collaboration, *Search for pair production of resonances decaying to a top quark plus a jet in final states with two leptons*, CMS-PAS-B2G-12-008 (2012).

[160] A. Thamm, R. Torre and A. Wulzer, *Composite heavy vector triplet in the ATLAS diboson excess*, *Phys. Rev. Lett.* **115** (2015) 221802 [arXiv:1506.08688] [ɪɴSPIRE].

[161] A. Carmona, A. Delgado, M. Quirós and J. Santiago, *Diboson resonant production in non-custodial composite Higgs models*, *JHEP* **09** (2015) 186 [arXiv:1507.01914] [ɪɴSPIRE].

[162] L. Bian, D. Liu and J. Shu, *Low scale composite Higgs model and* $1.8 \sim 2\ TeV$ *diboson excess*, arXiv:1507.06018 [ɪɴSPIRE].

[163] K. Lane and L. Prichett, *Heavy vector partners of the light composite Higgs*, *Phys. Lett.* **B 753** (2016) 211 [arXiv:1507.07102] [ɪɴSPIRE].

[164] M. Low, A. Tesi and L.-T. Wang, *Composite spin-1 resonances at the LHC*, *Phys. Rev.* **D 92** (2015) 085019 [arXiv:1507.07557] [ɪɴSPIRE].

[165] S.G. Johnson, *The nlopt nonlinear-optimization package*, http://ab-initio.mit.edu/nlopt (2011).

[166] F. Beaujean and S. Jahn, *pypmc version 1.0*, see website (2015).

[167] R. Barbieri and G.F. Giudice, *Upper bounds on supersymmetric particle masses*, *Nucl. Phys.* **B 306** (1988) 63 [INSPIRE].

[168] G. Panico, M. Redi, A. Tesi and A. Wulzer, *On the tuning and the mass of the composite Higgs*, *JHEP* **03** (2013) 051 [arXiv:1210.7114] [INSPIRE].

[169] J. Barnard and M. White, *Collider constraints on tuning in composite Higgs models*, *JHEP* **10** (2015) 072 [arXiv:1507.02332] [INSPIRE].

[170] G.F. Giudice, C. Grojean, A. Pomarol and R. Rattazzi, *The strongly-interacting light Higgs*, *JHEP* **06** (2007) 045 [hep-ph/0703164] [INSPIRE].

[171] C. Delaunay, C. Grojean and G. Perez, *Modified Higgs physics from composite light flavors*, *JHEP* **09** (2013) 090 [arXiv:1303.5701] [INSPIRE].

[172] R. Barbieri, D. Buttazzo, F. Sala and D.M. Straub, *Flavour physics and flavour symmetries after the first LHC phase*, *JHEP* **05** (2014) 105 [arXiv:1402.6677] [INSPIRE].

[173] A. Bevan et al., *Standard model updates and new physics analysis with the unitarity triangle fit*, arXiv:1411.7233 [INSPIRE].

[174] UTFIT collaboration, A.J. Bevan et al., *The UTfit collaboration average of D meson mixing data: Winter 2014*, *JHEP* **03** (2014) 123 [arXiv:1402.1664] [INSPIRE].

[175] M. Blanke, A.J. Buras and S. Recksiegel, *Quark flavour observables in the littlest Higgs model with T-parity after LHC Run 1*, arXiv:1507.06316 [INSPIRE].

[176] TOP QUARK WORKING GROUP collaboration, K. Agashe et al., *Working group report: top quark*, arXiv:1311.2028 [INSPIRE].

[177] K. Mohan and N. Vignaroli, *Vector resonances in weak-boson-fusion at future pp colliders*, *JHEP* **10** (2015) 031 [arXiv:1507.03940] [INSPIRE].

[178] ATLAS collaboration, *Search for new phenomena in dijet angular distributions in proton-proton collisions at $\sqrt{s} = 8$ TeV measured with the ATLAS detector*, *Phys. Rev. Lett.* **114** (2015) 221802 [arXiv:1504.00357] [INSPIRE].